Radiation-Induced Defects in Quartz and Stishovite: Studies of ESR, OSL, TL and MO Theory

By
Atsushi TANI

A thesis submitted in partial fulfillment of the requirements for the degree of

Ph. D. (Science)

Osaka University
Graduate School of Science
Department of Earth and Space Science
Toyonaka, Osaka, JAPAN

March 2000

ABSTRACT

Quartz, a common and basic silica mineral in the earth, has been used for geological and archaeological surveys because of its chemical stability and wide distribution. Electron spin resonance (ESR), thermoluminescence (TL) and optically stimulated luminescence (OSL) of quartz have been studied to develop chronology and thermometry mainly for Quaternary sample. In this thesis, two types of silica crystals, ordinary quartz and a high-pressure polymorph stishovite that can be found around meteor craters, were investigated for further developments in chronology and thermometry using paramagnetic centers like radiation-induced centers. First, the unidentified electron center having an orthorhombic g-tensor ($g_1 = 1.9764$, $g_2 = 1.9527$ and $g_3 = 1.9370$) was found in synthetic stishovite and identified as a trapped electron around the impurity of titanium ion due to the relatively large g-shift. Electronic structures of the paramagnetic impurity centers in stishovite were calculated by the discrete variational (DV)-Xα method to investigate the models of the substitutional impurity centers; the Ti, Al and Ge centers. The obtained g-factors showed good qualitative agreement with the experimental results. Secondly, the OSL of synthetic stishovite was measured for the first time under infrared laser (830 nm) or blue light emitting diodes (470 nm) to establish a direct dating technique of meteor craters because the Al and Ti centers measured by ESR were not stable at room temperature. As the blue light stimulated luminescence (BLSL) was still measurable after TL measurement up to 450 °C, the centers related to BLSL are very stable and may be useful for geochronology. Thirdly, mechanical process like crushing, cutting, pressing *etc.* should give strain to minerals and affect ESR signals. The g-shift changes of the E' center in strain-introduced quartz were evaluated by semi-empirical molecular orbital calculation with MOPAC. It is confirmed that the changes of molecular orbital caused the distribution of g-factors in crushed quartz rather than the distribution of energy splitting. Similar broad E'-like center ($g_{//} = 2.00181$ and $g_{\perp} = 2.00062$) and the isotropic center ($g = 2.00305$) were found in stishovite produced by the sudden pressure drop after synthesis. Last, the quartz samples of the drilling cores were investigated to reveal thermometry and to assess the cooling rate and denudation rate in Quaternary. The obtained cooling and denudation rates were 170 °C/Ma and 2.5 mm/Ma for mountainside of the intrusive Eldzhurtinskiy granite in Grate Caucasus, Russia. The GSJ Nojima core analysis revealed no high thermal event around the fault gauge during the Kobe earthquake in 1995 but Quaternary thermal evernt around the depth of 200-300 m in the host rock, the Nojima granodiorite.

TABLE OF CONTENTS

LIST OF FIGURES

LIST OF TABLES

ACKNOWLEDGEMENTS

First of all, I wish to express my sincere gratitude to my supervisor and promoter, Prof. Dr. Motoji Ikeya (Osaka University) for introducing me to this field of research and for many valuable suggestions and discussions for the whole studies. I also express my gratitude to Prof. Dr. Rainer Grün (ANU: Australian National University, Australia) for giving me a chance to stay in Canberra, Australia for wonderful collaborative works and to go to really nice field trip in the Great Caucasus, Russia.

I thank Dr. Chihiro Yamanaka (Osaka University), Dr. Jens Bartoll (McMaster University, Canada), Dr. Shin Toyoda (Okayama University of Science), Dr. H. Kohno (Osaka University), Dr. H. Sasaoka (Yamaguchi University) and Dr. S. Takaki (Daiichi Kigenso Kagaku Kogyo Co., Ltd.) for many worthwhile discussions on experiments.

Dr. E. Ito, Dr. T. Katsura (ISEI, Okayama University), Dr. K. Ogoh (Miyazaki Prefectural Nursing University), Dr. O. Ohtaka and Mr. Okita (Osaka University) helped me synthesize stishovite. Dr. H. Adachi (Kyoto University), the other members in the society for DV-Xα and Dr. T. Tsuchiya (Osaka University) gave me helpful advice for DV-Xα calculations. Dr. M. Takada (Nara Woman University) offered me to use the RISO set for OSL & TL measurements. Dr. A. Gurbanov (Institute of Geology of Ore Deposits, Russia), Dr. D. Koshchug (Moscow State University, Russia), members in Quaternary Dating Research Center (ANU), Dr. H. Ito, Dr. K. Fujimoto, Dr. T. Ohtani (GSJ; Geological Survey of Japan) and Dr. H. Tanaka (Ehime University) gave me an opportunity to study the two drilling cores of the Eldzhurtinskiy intrusive granite in Russia and the GSJ Nojima core in Japan. Dr. H. Kajiwara (Tohoku Fukushi University), Dr. K. Komura (Kanazawa University), Dr. S. Fujimura, Dr. T. Kamada and Dr. Y. Yokoyama (Tohoku Paleolithic Institute) offered the valuable ancient lithic tool from the Kami-takamori site and measured natural isotope concentration in the lithic tool. Dr. T. Ikeda (Osaka University), Dr. T. Nagatomo (Nara University of Education), Dr. Oshima (University of Osaka Prefecture) and CSIRO in Canberra, Australia helped me for γ-ray irradiation. I am very grateful to all mentioned above and all members in Ikeya laboratory (Osaka University), especially Dr. H. Furuta, Dr. K. Kanosue, Mr. H. Matsumoto and Mr. K. Norizawa.

At last, I wish to express my appreciate to Dr. Makoto Hirai (Osaka University) for a lots and lots discussions and encouraging advice day and night, and also Prof. Dr. Fujio Masuda (Kyoto University) for leading me to earth science (especially geology) through his lecture and several short field trips in the undergraduate course.

This work was supported by the grant from Research Fellowships of the Japan Society for the Promotion of Science for Young Scientists (No. 5083, 1997-2000) and I greatly appreciate it to concentrate in my work completely for these three years.

CHAPTER 1

Introduction

1.1 General introduction

Silica is a name for silicon dioxide SiO_2. The most famous silica crystal, quartz has a beautiful transparent figure of a hexagonal rod. The varieties of quartz are available because of impurities like transition metal elements. For example, the transparent crystal quartz is called rock crystal, the violet one is amethyst and the yellow one is citrine. They have been very popular and widely used for decoration, jewelry, lucky stone and fortune telling for a long time. The synthetic quartz is used for electronic devices like crystal oscillator. The mysterious crystal has attracted many scientists to studies of crystal structure, crystal growth, optical and electric properties, deformation, weathering *etc.* (*e.g.* Akizuki 1993).

One of the big interests on natural quartz is the history; when and where it was formed and what have happened on it up to now. Nowadays, several dating methods are available (*e.g.* Aitken 1990; Kaneoka 1998). One of the major techniques is isotope dating like K-Ar, $^{40}Ar/^{39}Ar$, U-Pb or ^{14}C method, which is based on the constant decay time as a time counter (the details in the book like Faure 1986). Another method is fission track (FT) dating. The track is made by the fission fragments in spontaneous nuclear fission of ^{238}U. Such tracks were first observed in mica irradiated by thermal neutron using electron microscope (Silk & Barnes 1959) and later in natural mica samples under an optical microscope by etching technique to enlarge the tracks (Price & Walker 1962). These methods can be useful to estimate the thermal history, too. Increase of temperature induces diffusion of molecule in solid or shortening of the fission tracks, which can affect the storage isotopes or the tracks.

The method used in this thesis is based on another type of radiation damages. Radiation like γ-rays and β-rays can produce secondary electrons and holes in minerals through the interaction with materials. Most of the charges are recombined but some of them are trapped in intrinsic defects or impurity elements (Figure 1-1-a). Those trapped electrons and holes in natural minerals were summarized in the book by Marfunin (1979). As the radiation-induced centers are accumulated in minerals for a geological or archaeological time, the age started at the accumulation of the centers can be estimated from the intensity of natural sample. Measurement methods and a brief history are described in next section. The radiation-induced centers are unstable at high temperature, so that these methods can be used for thermometry as well. In order to know the defects themselves and to reveal geological and archaeological history, I

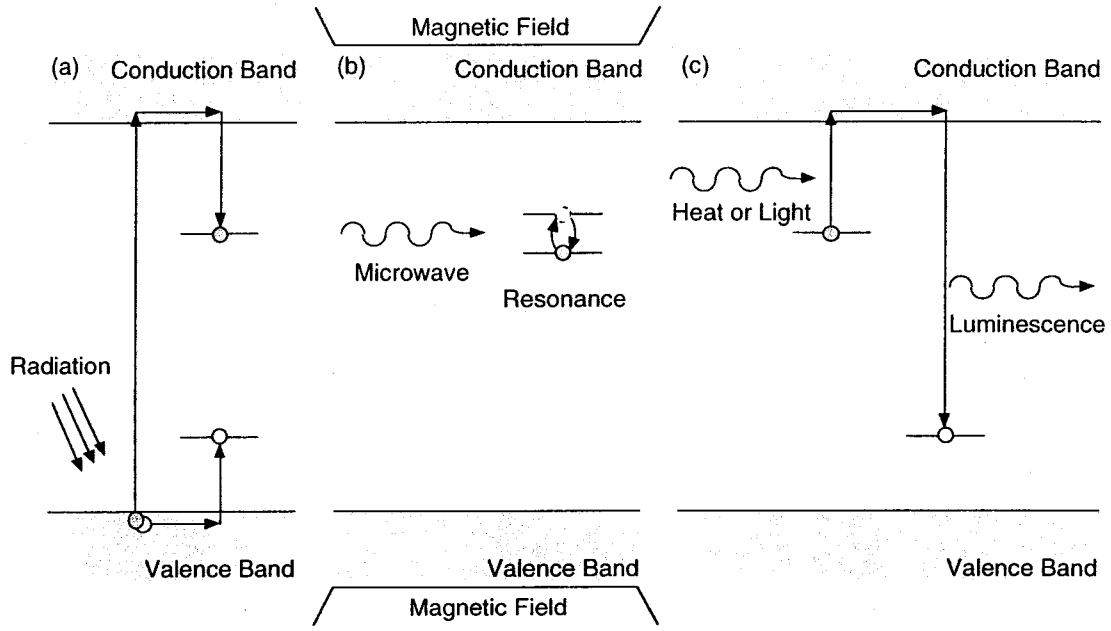

Figure 1-1. ESR, TL & OSL.

(a) Radiation ionizes the material and produces electrons and holes inside. Some of them are trapped by intrinsic defects or impurities without recombination. (b) ESR occurs under electromagnetic waves (usually microwave) whose energy is equal to the difference of energy levels split by external magnetic field. (c) TL or OSL can be observed by activating trapped charges by heat or light.

decided to study the radiation-induced centers in silica.

1.2 Experimental methods

(i) Principles and a brief history

Trapped electrons or holes can be studied by electron spin resonance (ESR), thermoluminescence (TL) and optically stimulated luminescence (OSL). The ESR can be measured under high magnetic field and a microwave (Figure 1-1-b). Magnetic field forces to split energy levels of electrons due to the interaction between magnetic field and electron spin (Zeeman effect). Microwave absorption can be observed under magnetic resonance where energy of microwave is equal to the difference between two energy levels of the singly occupied orbital. ESR does not follow any recombination of trapped electrons and holes and can be detected repeatedly but needs unpaired electrons or holes. In TL and OSL, heat or light excites trapped charges to conduction band or higher energy levels of trapping centers. Luminescence can be emitted by recombination of such excited charges with the appropriate centers (Figure 1-1-c).

ESR dating was proposed by Zellar [1967] and successfully reported on a study of stalactite by Ikeya (1975). This have been applied to not only quartz but also carbonates like coral, fossil shells and eggs ($CaCO_3$), various evaporates like barite ($BaSO_4$), gypsum ($CaSO_4$), halite (NaCl) *etc.*, bone and tooth (apatite), the other silicates and iced material. The detail descriptions and list of papers are written in the book

(Ikeya 1993) and the reviews (Grun 1989; Rink 1997). ESR dating of quartz was proposed by McMorris (1971) and Moiseyev & Rakov (1977) but the sensitivity of the ESR spectrometer was not sufficient at that time to get meaningful ages. ESR dating applications to quartz or SiO_2 material were reported on flint by Garrison *et al.* (1981), geological fault by Ikeya (1982) and volcanic material by Imai (1985) in the early stage. ESR dating with slow production of the oxygen vacancy was studied for much larger scale geochronology up to a few Ga by Odom & Rink (1988).

TL dating was proposed by Daniels (1953) and has been developed for applications to archaeological materials such as ceramics, glass, bones, shells, flint, potteries *etc.* as well as geological materials like quartz and feldspar (Aitken 1985; McKeever 1985). TL color imaging was also studied by Hashimoto *et al.* (1986) which could resolve spatial distribution of the signals with the color information.

OSL dating was attempted by Ugumori & Ikeya (1980) using ultraviolet nitrogen laser and later demonstrated with success on sedimentary soil with green argon ion laser (Huntley *et al.* 1985) and on feldspar with infrared laser (Hutt *et al.* 1988). This technique has been developed to estimate a burial age of sedimentary soil like eolian sand and archaeological relics because OSL is based on measurement of more or less light-sensitive signals. Recently, Bøtter-Jensen *et al.* (1999) showed that the blue light emitting diodes (LED) had enough power to stimulate trapped charges and could be used for dating and retrospective dosimetry. The book about optical dating was recently published by Aitken (1998) and also many review papers about it can be found in journals (*e.g.* Wintle 1990).

ESR measurement needs about 10^{12} spins of a center in recent ESR spectrometer. This is less sensitive than luminescence measurement due to photon counting technique in luminescence measurements.

(ii) Thermal stability and production of radiation-induced centers

Trapped electrons or holes are in metastable state and decay thermally in the manner of the kinetics. The first order decay is a case that a trapped electron can recombine with the correlated hole, while the second order decay is a case that a trapped electron can recombine with one of any holes in material. The decay can be represented for both the kinetics by the following differential equations,

$$\frac{dn}{dt} = -\nu n \quad \text{(for the first order)}, \tag{1-1}$$

$$\frac{dn}{dt} = -\lambda n^2 \quad \text{(for the second order)}, \tag{1-2}$$

where ν and λ are called rate constant. The rate constants depend on temperature T and can be described as

$$\nu = \frac{1}{\tau} = \nu_0 \exp\left(-\frac{E_a}{k_B T}\right), \tag{1-3}$$

$$\lambda = \lambda_0 \exp\left(-\frac{E_a}{k_B T}\right), \tag{1-4}$$

where E_a is activation energy for the center, k_B is Boltzman constant and ν_0 and λ_0 are called pre-exponential factors for the first and second kinetics. So that thermal stability of the center can be represented with activation energy and pre-exponential factor. Some of the center decays through both kinds of decays. The equation must be the mixture of them for that case.

Natural radiation α-rays, β-rays and γ-rays are emitted from isotope elements like ^{238}U, ^{232}Th, ^{40}K or cosmic ray comes out of the earth. They can make interaction with material and produce secondary electrons and holes, which can be trapped by intrinsic defects or impurity atoms. As the center cannot increase more than lattice sites or impurity atoms, the limitation must be considered. The following idea is called interaction volume and used for the defects in ionic crystal (Itoh, 1972). Assuming a for a production efficiency of radiation-induced defects, $\dot{D}$ for an annual dose and b for interact volume, the following equation can be obtained.

$$\frac{dn}{dt} = a\dot{D}\left(\frac{N_0 - bn}{N_0}\right) = a\dot{D} - \frac{n}{\tau_s}, \tag{1-5}$$

where $\tau_s = N_0 / ab\dot{D}$ is called saturation lifetime. Now we can describe the differential equation of the signal growth curve including two decay terms of thermal stability and saturation,

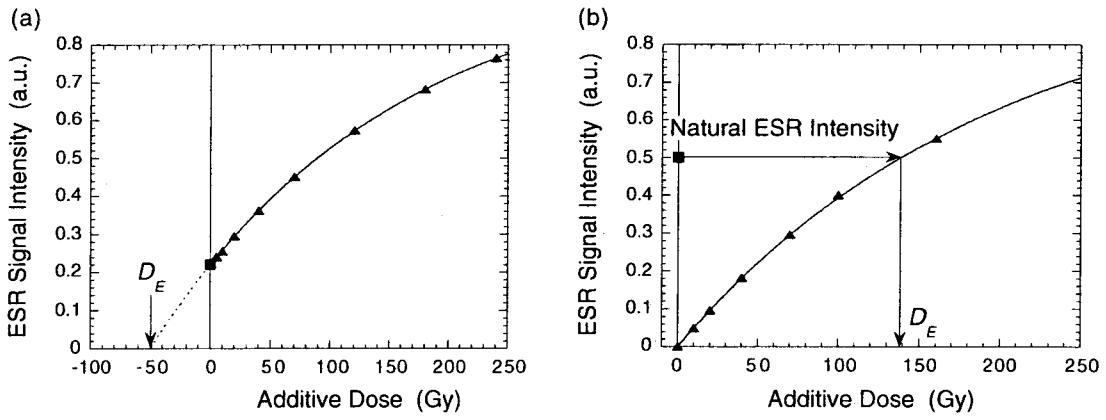

Figure 1-2. Additive dose method and regeneration method.
(a) Equivalent dose D_E can be estimated by extrapolating the dose response curve (DRC) obtained by artificial additive irradiation. (b) Once the signal intensity is zeroed by heat at a particular temperature or light exposure, the DRC is regenerated by artificial irradiation to estimate equivalent dose D_E with the ESR intensity before zeroing.

$$\frac{dn}{dt} = a\dot{D} - \frac{n}{\tau} - \frac{n}{\tau_s} \quad \text{(for the first order),} \tag{1-6}$$

$$\frac{dn}{dt} = a\dot{D} - \lambda n^2 - \frac{n}{\tau_s} \quad \text{(for the second order).} \tag{1-7}$$

(iii) Additive dose method and regeneration method

Those radiation-induced centers are accumulated in minerals for a long time if they are stable at storage temperature. As the accumulating rate of the centers is dependent on environmental natural radiation rate, we can estimate how long the material (sample) were stored at a particular place from the total intensity of the accumulated signal.

Figure 1-2 shows two ways to estimate equivalent dose, D_E that is equivalent to the dose of airtifial irradiation by α-rays, β-rays or γ-rays. The additive dose method needs artificial irradiation to increase the signal intensity and to see the production efficiency of the signals. Equivalent dose can be estimated by extrapolating the dose response curve (growth curve) to zero signal intensity. Another method is called regeneration method where the growth curve is reproduced by artificial irradiation after the signal is zeroed. It can be reduce the error coming from fitting the dose response curve but it should be careful to check a change of production efficiency before and after heating.

1.3 Theoretical calculation methods

The calculation of electronic structures in material is concerned with the approximate solution of the quantum-mechanical equation of motion, the Schrödinger equation. Models and methods are summarized in Figure 1-3. Our interest is local electronic structure of impurity centers or radiation-induced centers, so that localized electronic structure calculation must be considered. In this section, all equations were written in atomic unit as usually used in this field. More accurate or detailed discussions are found in many books (*e.g.* Szabo & Ostlund 1982; Foresman & Frisch 1996; Adachi 1991)

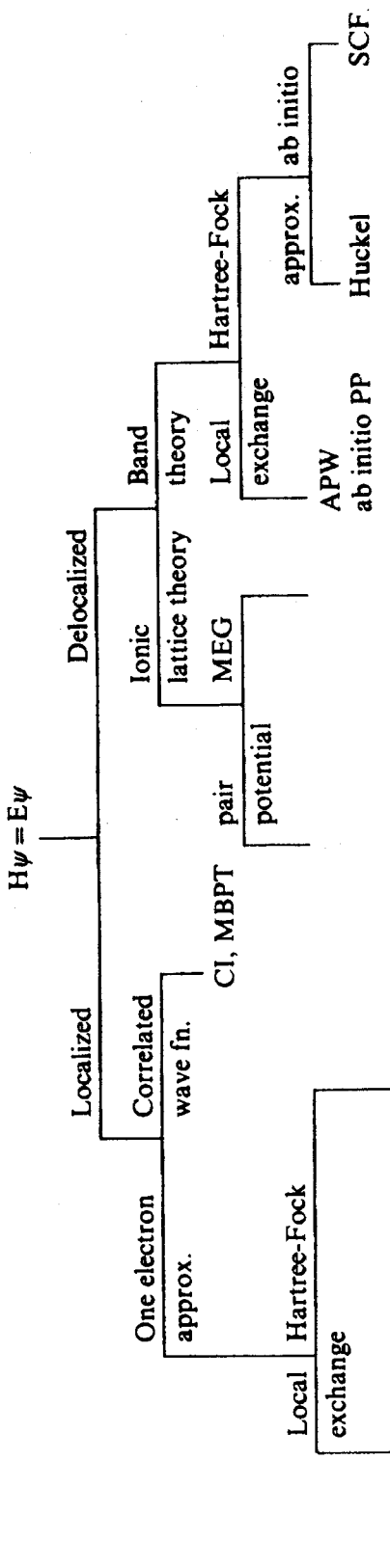

Figure 1-3. Model and method of theoretical calculation (Tossell & Vaughan 1992).

(i) Hartree-Fock (HF) method

The motion of electrons can be considered under the Born-Oppenheimer approximation meaning that only electrons can move in the static field created by heavy atomic nuclei. The Hamiltonian $\mathcal{H}$ for N-electron system can be defined as

$$\mathcal{H} = -\sum_i \frac{1}{2}\nabla_i^2 - \sum_i \sum_A \frac{Z_A}{r_{iA}} + \sum_i \sum_{i>j} \frac{1}{r_{ij}}, \tag{1-8}$$

where Z_A is atomic number for Ath nucleus, r_{iA} is a distance between ith electron and Ath nucleus and r_{ij} is a distance between ith and jth electrons. The first term on the right side is kinetic energy of electrons. The second and third ones are Coulomb potentials by nucleus and electrons, respectively. This Hamiltonian $\mathcal{H}$ should satisfy the Schrödinger equation,

$$\mathcal{H}\Phi = E\Phi, \tag{1-9}$$

where Φ is a wave function for all N electrons and E is an eigenvalue for the system.

The wave function Φ can be represented as the Slater determinant due to a requirement of antisymmetry principle (Pauli exclusion principle).

$$\begin{aligned}\Phi(r_1, r_2, \cdots, r_n) &= (n!)^{-1/2}\begin{vmatrix} \phi_1(r_1) & \phi_1(r_2) & \cdots & \phi_1(r_n) \\ \phi_2(r_1) & \phi_2(r_2) & \cdots & \phi_2(r_n) \\ \vdots & \vdots & \ddots & \vdots \\ \phi_n(r_1) & \phi_n(r_2) & \cdots & \phi_n(r_n) \end{vmatrix}, \\ &\equiv |\phi_1, \phi_2, \cdots \phi_n\rangle\end{aligned} \tag{1-10}$$

where ϕ_i is ith orbital function occupied by two degenerated electrons and called molecular orbital. In Hartree-Fock approximation (one-electron approximation), motion of each electron is considered under mean Coulomb field by the other electrons. As the potential is dependent on the orbitals of the other electrons, the Hartree-Fock equation should be solved by self-consistent-field (SCF) method. Each orbital ϕ_i satisfies one-electron Schrödinger equation called Hartree-Fock equation,

$$f_i\phi_i = \varepsilon\phi_i. \tag{1-11}$$

The eigenvalue ε is the energy level of the molecular orbital. The f_i is an effective one-electron operator called the Fock operator and described as

$$f_i = -\frac{1}{2}\nabla_i^2 - \sum_A \frac{Z_A}{r_{iA}} + \sum_l \int \frac{\rho_l(r_2)}{r_{12}} dr_2 + V_i^{ex}. \tag{1-12}$$

The potential V_i^{ex} is the term due to the exchange interaction for parallel spin electrons. However, it does not include correlation interaction for anti-parallel spin electrons.

(ii) Hartree-Fock-Slater (HFS) and DV-Xα methods

In order to include the correlation interaction between two electrons of different spins and to reduce computational works on calculating many complex integrals in the

HF method, Slater (1963) suggested the Xα potential for interaction among electrons. The revised Xα potential is expressed with a parameter α and electron density $\rho(r)$ as

$$V_i^{ex}(r) = -3\alpha\left[\frac{3}{4\pi}\rho(r)\right]^{1/3}. \quad (1\text{-}13)$$

The α is 2/3 for free electron gas, 0.978 for hydrogen, 0.773 for helium and 0.781 for lithium. The value gradually decreases and gets close to 2/3 for heavy atoms. For ordinary molecular orbital calculations, it can be assumed as 0.70 for any atoms without significant errors.

(iii) Linear combination of atomic orbitals (LCAO)

The molecular orbital ϕ_i is an unknown function but can be approximated to be linear combination of atomic orbitals χ_k (LCAO),

$$\phi_i = \sum_i c_{ik}\chi_k. \quad (1\text{-}14)$$

The type of the atomic orbitals must be selected to enable us to solve the equations easily. Slater-type orbitals (STO) and gaussian-type orbitals (GTO) were proposed and have been used extensively in *ab-initio* methods. On the other hand, numerically generated atomic orbitals are used in the discrete variational (DV)-Xα method instead of functions. They are generated by solving the Schrödinger equation for 'atom in molecule', meaning that the basis functions are renewed for each SCF iteration taking a modification of charge density into account (Adachi *et al.* 1978; 1991). The another characteristic of the DV-Xα method is weighted numerical integration at discrete sampling points that can reduce a lot of tasks on computer.

(iv) ESR parameters: g-tensors

ESR analysis can start with spin Hamiltonian derived from Hamiltonian with perturbation theory. The spin Hamiltonian is expressed using tensors as

$$\mathrm{H} = \beta\mathbf{S}\cdot\mathbf{g}\cdot\mathbf{H} + \mathbf{S}\cdot\mathbf{D}\cdot\mathbf{S} + \mathbf{S}\cdot\mathbf{A}\cdot\mathbf{I}. \quad (1\text{-}15)$$

The first term is the Zeeman split for an electron with spin **S** under magnetic field **H**, the second one is spin-spin interaction, the third one is hyperfine interaction with nuclear spin **I**. The β is Bohr magneton and the others **g**, **D**, **A**, are ESR parameters.

The matrix element of the g-tensor g_{pq} in a cluster is described with LCAO χ_i as

$$g_{pq} = g_e\left\{\delta_{pq} - \sum_{m\neq t}\sum_k\sum_{k'}\frac{\zeta_{k'}\langle\chi_k^{(t)}|l_p^{(k)}|\chi_k^{(m)}\rangle\langle\chi_{k'}^{(m)}|l_q^{(k')}|\chi_{k'}^{(t)}\rangle}{\varepsilon_t - \varepsilon_m}\right\}, \quad (1\text{-}16)$$

where ζ_k is a spin-orbital coupling constant on the kth nucleus and $l_p^{(k)}$ is an angular moment at the origin of kth nucleus (Stone,1963). The second term is called g-shift meaning the difference from g-factor of free electron $g_e = 2.0023$. Suffix t stands for the SOMO orbital.

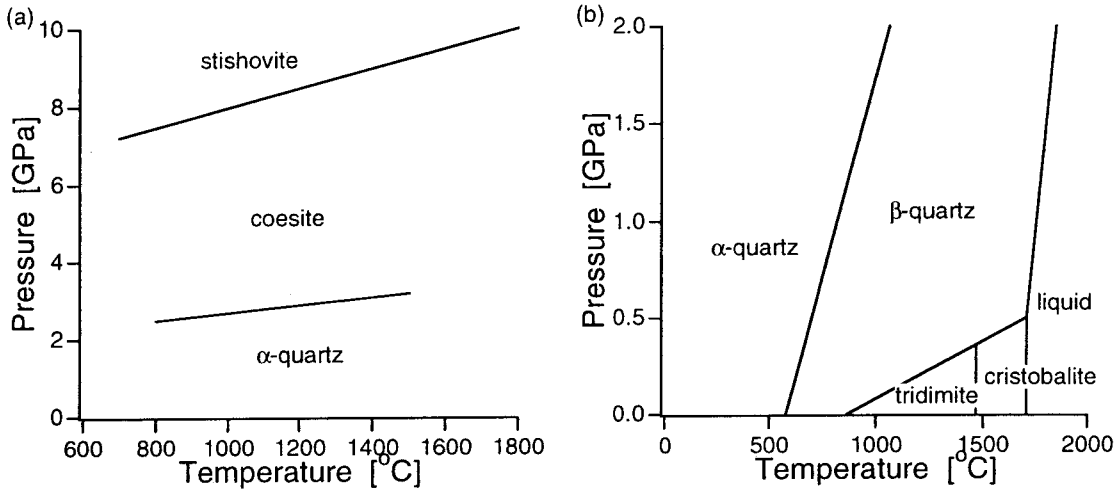

Figure 1-4. Phase diagram of silica crystals.
(a) The phase boundaries of α-quartz-coesite and coesite-stishovite transitions were calculated with thermodynamic data (Akaogi *et al.* 1995). The both lines are concordant with the experimental results by Bohlen & Boettcher (1982) for the α-quartz-coesite transition and Zhang et al. (1996) for the coesite-stishovite transition. (b) The other phase boundaries of silica for high temperature and low pressure are shown.

1.4 Crystal chemistry of silica

(i) Silica

Quartz, one of silica crystals, is the most thermodynamically stable at room temperature and under atmosphere, but the structure changes under high-pressure or high-temperature condition. The phase diagram of crystalline silica is shown in Figure 1-4.

The famous crystal structures of the type AX_2 are quartz, fluorite and rutile types. The fluorite structure generally forms for very ionic compounds with cations significantly larger than anions like CaF_2 but does not occur in silica polymorphs. Stishovite has the rutile structure providing octahedral coordination for cations. Quartz and the other crystalline silica polymorphs have a ring structure made with a tetrahedron of SiO_4. In addition, amorphous silica and silica glass can be found in nature. Most crystalline silica polymorphs are summarized in Table 1-1. High-pressure polymorphs, coesite and stishovite, are denser than α-quartz. High-temperature polymorphs, β-quartz, tridymite and cristobalite, have higher symmetrical structures than α-quartz.

Natural quartz and synthetic stishovite were specified for the study of this thesis. Quartz is one of the most important minerals in the world and can be found in many geological and archaeological places. Stishovite found naturally in meteor craters has not been studied well yet.

(ii) Quartz

The structure of α-quartz has a ring structure grouped to trigonal symmetry. The two types of quartz (left-hand and right-hand) are available and distinguished by observation of the surface after etching. Some of quartz crystal called twin are made with both types of quartz. The unit cell and the projection on (001) are shown in Figure 1-5-a and b. This model is left-hand α-quartz. The structure is based on tetrahedron SiO_4 but not regular. The bond length of silicon and oxygen is 1.605 Å for two bonds and 1.613 Å for the other two. This causes the lower symmetry rather than β-quartz that is hexagonal symmetry. The density is 2.65 g/cm^3 and the hardness number is 7 as standard. Igneous rock usually includes quartz and larger quartz can be found in pegmatite. It also occurs in sedimentary rock due to its chemical stability and sometimes happens to quartzite.

(iii) Stishovite

Stishovite, a high-dense and high-pressure polymorph, was first synthesized by Stishov & Popova (1961). Naturally formed stishovite was found first in Arizona meteor impact crater (Chao *et al.* 1962). The meteor impact produced high pressure and high temperature, causing the formation of stishovite. The unit component is not SiO_4 tetrahedron but SiO_6 octahedron providing octahedral coordination for a silicon ion (Figure 1-5-d). The crystal structure is called rutile-type structure that consists of edge-sharing chains of SiO_6 octahedra running parallel to the c-axis. The octahedra in adjacent chains are joined at their corners. Figure 1-5-f shows the projection of the structure onto (001). The density is 4.287 g/cm^3. It is about 60 % higher than that of α-quartz and the highest density among known silica polymorphs. The rutile structure transformed into $CaCl_2$ structure (a distorted rutile structure) above 100 GPa but this transformation is reversible on release of pressure (Tsuchida & Yagi 1989).

Table 1-1. Silica polymorphs.
The table was modified from Navrotsky (1994).

Polymorph	Symmetry Space group	Molar volume (cm^3/mol) at 298 K	Structural features	Enthalpy relative to Qz (kJ/mol)
α-quartz	trigonal $P3_121$	22.67	6 rings	0
β-quartz	hexagonal $P6_222$		6 rings	0.3
β-cristobalite	cubic $Fd3m$	25.78	6 rings	2.8
β-tridymite	hexagonal $P6_3/mmc$	26.53	6 rings	3.2
coesite	monoclinic $C2/c$	20.64	4 & 8 rings	2.9
stishovite	tetragonal $P4_2/mnm$	14.01	rutile structure	51.9

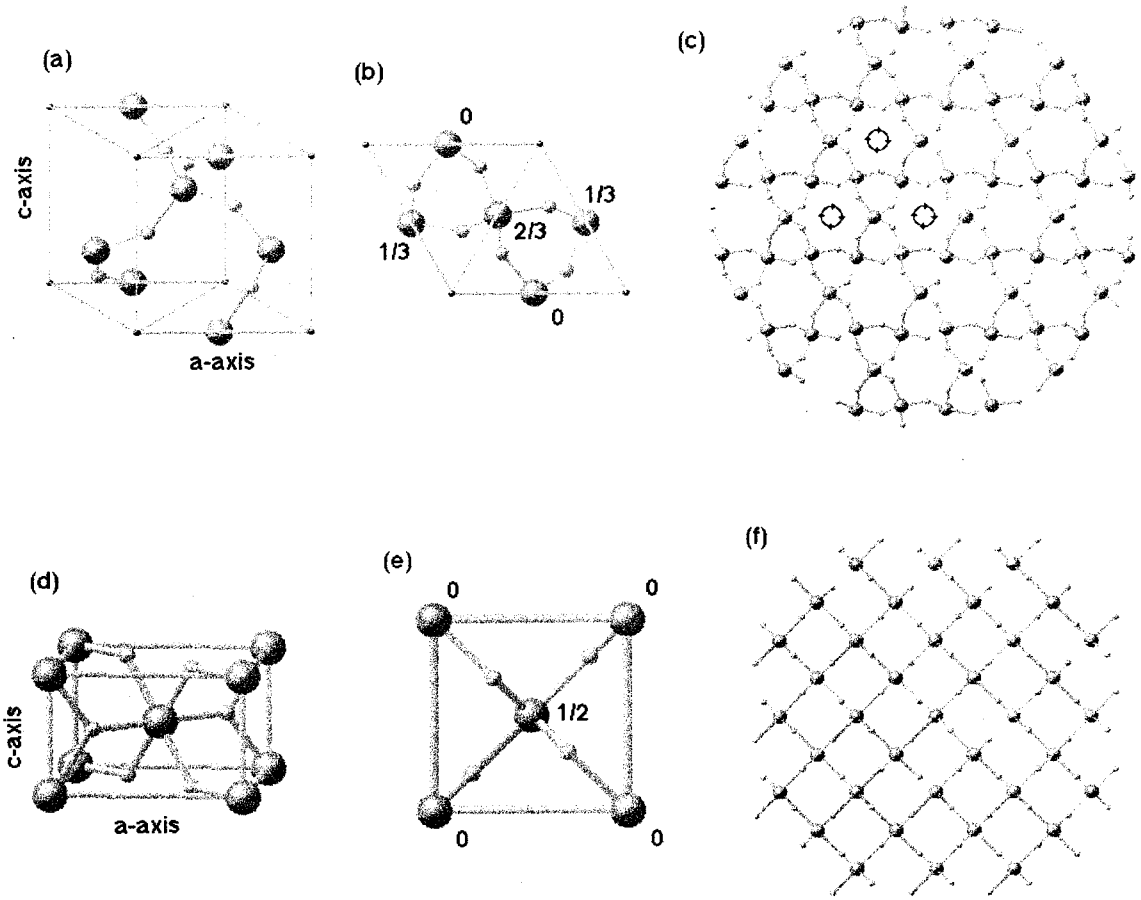

Figure 1-5. Unit cells and crystal structures of α-quartz and stishovite. Unit cells of left-hand α-quartz and stishovite are shown in (a) and (d) and their projections on (001) are (b) and (e), respectively. The numbers in (b) and (e) are the height of the silicon atoms in unit of c-axis. The projections of crystals on (001) are shown in (c) and (f), too. A larger atom (red) is silicon and a smaller one (green) is oxygen. The bonds between oxygen and silicon are drawn together.

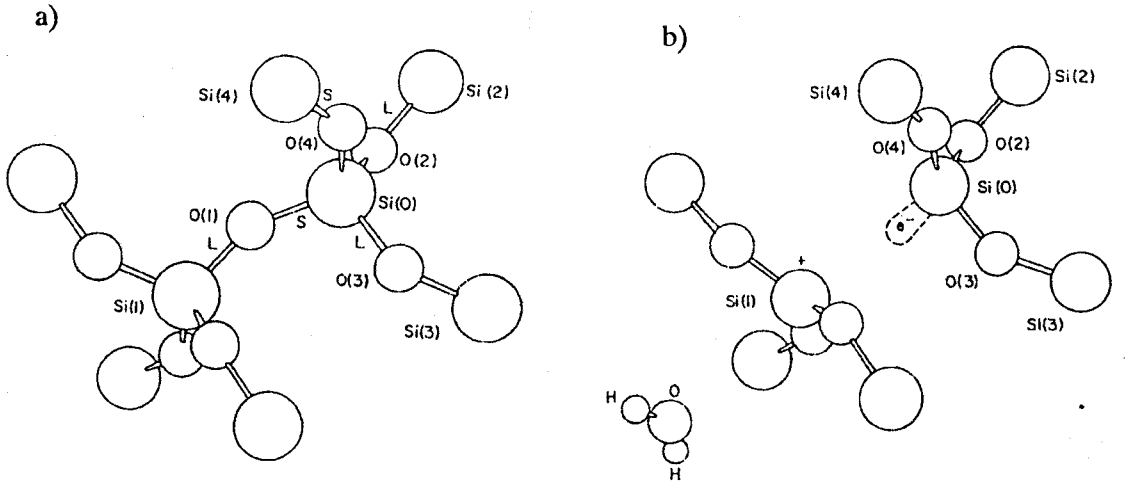

Figure 1-6. A model of the E′ center.
(a) This is a cluster of α-quartz. (b) An electron is trapped in oxygen vacancy. It is localized to near silicon atom (Rudra & Fowler 1987).

1.5 Paramagnetic centers in silica

(i) Quartz

Many studies revealed the radiation-induced centers in quartz. The E′ center, peroxy center, the Al, Ti and Ge centers among them are usually considered for geological applications (e.g. Jani *et al.* 1983; Stapelbroek *et al.* 1979; Griscom 1980; Isoya *et al.* 1988; Rinneberg & Weil 1972; Weil 1971; Nuttall & Weil 1981). The E′ center is an electron at an oxygen vacancy and a kind of dangling bond (Figure 1-6). The model of the peroxy center is a hole-trapped interstitial oxygen ion bonding with oxygen at the normal site. The impurity centers are associated with substitutional impurities like aluminum, titanium and germanium. The Al center is a hole center while the Ti and Ge centers are electron centers. ESR spectra of those centers were shown in the following chapters. Thermal stability of quartz taken from granite is shown in Figure 1-7 for a reference.

(ii) Stishovite

ESR study of stishovite and coesite is of interest due to a potential for applying to dating meteor impacts (Ikeya 1993). First ESR study of stishovite was made on natural occurring sample by Devine & Hübner (1989). They found naturally formed ESR signals around $g = 2.0030$. Subsequent studies have identified radiation-induced centers as the E' center, oxygen hole center, the Al center and atomic hydrogen center (Ogoh *et al.* 1994; 1995a; 1996a; 1996b). The Al center is detectable at low temperature like 77 K because the center is not stable at room temperature. The other centers can be measured at room temperature and would give an age of meteor impact.

1.6 The outline and purpose of the thesis

The scope of this thesis is to study radiation-induced centers themselves as well

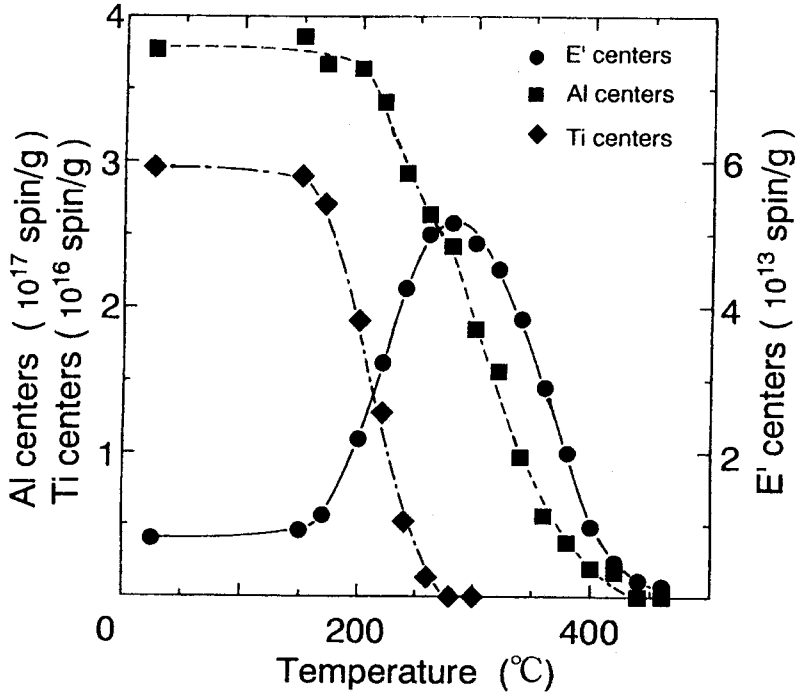

Figure 1-7. Typical isochronal annealing experiments on quartz. The Ti and Al center decreased monotonically but the E′ center increased about 180 °C and decreased above about 300 °C (Toyoda 1992).

as geological and archaeological applications. Radiation-induced defects can be accumulated for a long time and the number of them increases during the geological time scale, which means that this information can imply some geological data. However, those centers are quite sensitive for the change of thermal and mechanical environment. It is a disadvantage to know the simple age of the material but an advantage to know the whole story during ages. In order to use this technique for geology and archaeology, I should know the physical and chemical properties of the centers. This area has not been explored well and there are many interesting topics inside.

The studies of this thesis can be divided to two parts, basic and application. In chapter 2 and 3, synthetic stishovite was studied to know the radiation-induced defects themselves and to develop a dating method using stishovite. Chapter 4 is also basic study of the effect of strain to ESR spectra of the E′ center in α-quartz. Chapter 5 is a geological application to estimate cooling rate and denudation rate from drilling core samples and to survey unknown thermal events in the granite penetrating the Nojima fault at the depth of 625 m, which caused the Kobe earthquake in 1995. In addition, two appendixes are attached at the end of the thesis.

CHAPTER 2

The Titanium Center & Molecular Orbital Calculations in Stishovite

A new unidentified electron center was found in synthetic stishovite on ESR measurements. A model of the center was proposed to be the titanium electron center because a common substitutional titanium ion Ti^{3+} trapping an electron in 3*d*-orbital will give a relatively large *g*-shift while a germanium ion Ge^{3+} trapping an electron in 4*s*-orbital will give almost no *g*-shift. The possibility of geochronological applications with this center was discussed. In addition, electronic structures of three impurity-related centers (the Al, Ti and Ge centers) in stishovite were calculated with the DV-Xα method to compare the tendency of the *g*-shift with experimental data.

2.1 First observation of an electron center in stishovite by ESR

(i) Sample synthesis & experimental

Sample was synthesized at 1200 °C and 13 GPa using uniaxial split-sphere anvil apparatus (USSA-1000) at Institute for Study of the Earth's Interior, Okayama University and confirmed as stishovite by X-ray diffraction analysis. The starting material was natural quartz including aluminum and titanium impurities, which was confirmed by ESR. These procedures were done by Ogoh and the more details are in his thesis (Ogoh 1996c). The obtained powder sample was irradiated at 77 K with a pen-type γ-ray source of ^{60}Co and the amount of the artificial dose was about 10 kGy.

The irradiated powdered stishovite was measured with a finger Dewar vessel at 77 K with ESR spectrometer (JEOL RE-1X) using 100 kHz modulation field of 0.1 mT and microwave power of 1 mW except experiments of microwave power dependence of the signal intensities. In isochronal annealing experiments, the sample was annealed at a particular temperature from 120 to 300 K for 15 minutes using a nitrogen-gas flow unit.

(ii) The ESR spectrum and the characteristics of the electron center

ESR signals of an unidentified electron center, the aluminum hole center and atomic hydrogen center were detected at 77 K. The new center shown in Figure 2-1-a appeared between fourth and fifth of Mn^{2+} sextet signals. Figure 2-1-b shows the ESR spectrum after subtraction of broad background signals. In the comparison with the simulated spectrum shown in Figure 2-1-c, these three signals can be due to one center. This was also indicated by the same characteristics of microwave power dependence and thermal decay discussed in later. The center had an anisotropic *g*-tensor of

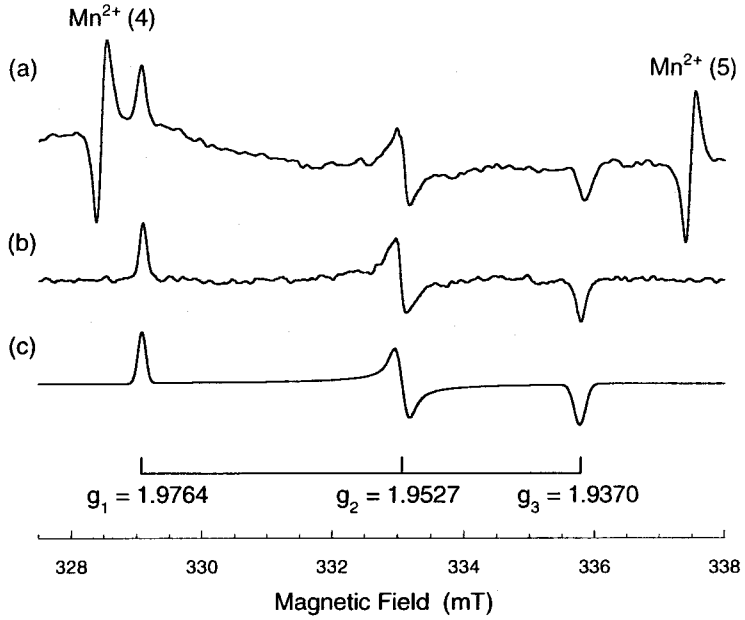

Figure 2-1. ESR spectra of the electron center in stishovite.
(a) This is the original spectrum with two of Mn^{2+} sextet signals. (b) The spectrum without Mn^{2+} signals was obtained after background signal subtraction. (c) The spectrum of an orthorhombic signal was simulated.

orthorhombic symmetry ($g_1 = 1.9764$, $g_2 = 1.9527$ and $g_3 = 1.9370$) calibrated with manganese standard maker signals, which indicates that the center is an electron-trapped center in a sense that the g-shifts are minus.

Figure 2-2 shows microwave power dependence of the signal intensities of the electron center together with those of the E' and Al centers in stishovite (Ogoh *et al.* 1995a; 1996a). Only one series of data was plotted because all three signals of the electron center had the same saturation behavior that was different from that of the

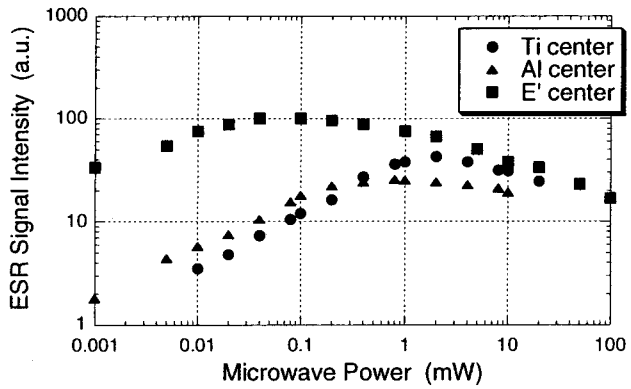

Figure 2-2. Microwave power dependence of the electron center.
The electron center was labeled as the Ti center. All signals at g_1, g_2 and g_3 showed the same dependence. The results of the Al and E' centers were shown as well (Ogoh *et al.* 1995a; 1996a).

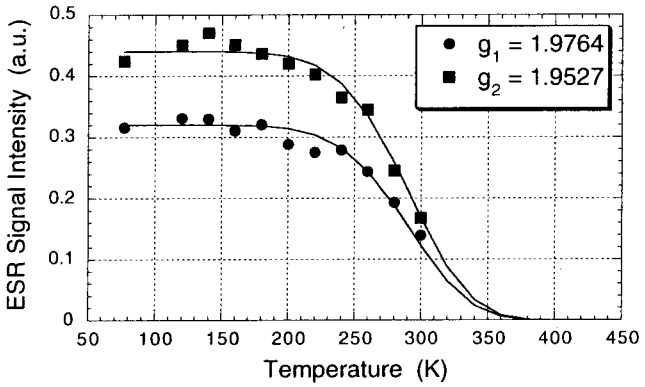

Figure 2-3. Isochronal annealing experiments of the electron center. Each marker showed signal intensity after heating the sample at a particular temperature. Solid lines were obtained by calculation based on the first order decay kinetics.

other centers.

Isochronal annealing experiments revealed that the center was annealed out around 280 K and unstable at room temperature as shown in Figure 2-3. The same signals were not detected in the samples irradiated at room temperature. This center can not be used for chronology and dosimetry at room temperature, though it is a little more stable than the Al center in stishovite (Ogoh *et al.* 1996a). The isochronal annealing curves calculated on assumption of the first-order decay kinetics were also shown in Figure 2-3 as solid lines. Best-fitted activation energy and frequency factor were 0.18 eV and 0.5 s^{-1}, respectively. The frequency factor is too small in comparison with that of the other impurity centers in quartz; *e.g.* 2.9 x 10^{7} s^{-1} (Fukuchi 1992) and 4.1 x 10^{11} s^{-1} (Toyoda & Ikeya 1991) for the Ti center in quartz. Presumably, migration of atomic hydrogen would be involved for decrease of the electron center. Similar activation energies and very low frequency factors of the radiation-induced defects were observed in the other solid oxides like SO_2 and CO_2 (Kanosue *et al.* 1996; Norizawa *et al.* 2000).

(iii) A proposed model of the center

The Ti and Ge centers were found in α-quartz as electron centers and their *g*-factors are summarized in Table 2-1. A substitutional impurity Ti or Ge atom in quartz can trap an unpaired electron produced by radiation and also trap an alkali cation like Li^+ or Na^+ or a proton as a charge compensator (Weil 1984). Those charge compensator ions can be confirmed on ESR spectra by hyperfine structure due to an interaction between a trapped electron and magnetic moment of nuclear spin. This model can be applied to the stishovite because Ti and Ge atoms could be easily substituted in the position of Si atoms in stishovite as well.

A Ti or Ge atom locates in the center of octahedron whose form is written as $[TiO_6]^0$ or $[GeO_6]^0$. That can trap an electron at low temperature irradiation to form

$[TiO_6]^-$ or $[GeO_6]^-$ that may be detectable by ESR. In this case, an alkali ion, Li^+ or Na^+, or a proton might not migrate to the vicinity of the electron-trapped center at 77 K to compensate the charge because of no hyperfine signals of protons which could move in solid more easily at low temperature than alkali cations. An ion of titanium, Ti^{3+} has one electron in 3*d*-orbital and the Ti center has a relatively larger *g*-shift due to interaction with the other molecular orbitals than the Ge center having an electron in 4*s*-orbital of Ge^{3+} ion. It may indicate that the observed center may be ascribed to the Ti center.

Two types of the Ti center can be considered in stishovite; one is interstitial and the other is substitutional. Both sites are located at the octahedral coordination of oxygen atoms as shown in Figure 2-4. The another ESR signals were recently obtained in the other synthetic stishovite after γ-ray irradiation. The *g*-factors were $g_1 = 1.9749$, $g_2 = 1.9572$ and $g_3 = 1.9331$ which were quite similar to the above Ti center. The *g*-factors of the electron center in rutile TiO_2 (the same crystal structure as stishovite) were reported as $g_1 = 1.977$, $g_2 = 1.974$ and $g_3 = 1.941$ (Chester 1961) and assigned to the interstitial Ti center (e.g. Kingsbury *et al.* 1968). The *g*-shift of the Ti center in stishovite and rutile were close each other but the symmetry was different. The Ti center in stishovite was orthorhombic but that in rutile was almost axial. This might be caused by structural difference of the octahedra as well as different host materials. Although it is not easy to specify which signal is the interstitial Ti center or the substitutional Ti center, the latter center might be the interstitial because the lower *g*-factors g_1 and g_2 are closer than the higher ones, which is concordant with those of the interstitial Ti center in rutile.

Table 2-1. The Ti and Ge center in quartz and stishovite.
The *g*-factors of Al and E′ centers in stishovite were shown as well.

Material	Center	g_1	g_2	g_3	Reference
Quartz	$[TiO_4/Li^+]^0_A$	1.97887	1.93094	1.91193	(Isoya *et al.* 1988)
	$[TiO_4/Na^+]^0_A$	1.9675	1.9536	1.8994	(Okada *et al.* 1971)
	$[TiO_4/H^+]^0_A$	1.9856	1.9310	1.9151	(Rinneberg & Weil 1972)
	$[GeO_4/Li^+]^0_A$	2.0014	1.99965	1.9913	(Weil 1971)
	$[GeO_4/Li^+]^0_C$	2.0000	1.9973	1.9962	(Weil 1971)
Stishovite	Ti center	1.9764	1.9527	1.9370	this thesis
		1.9749	1.9572	1.9331	this thesis
	Al center	2.0155	2.0094	2.0033	(Ogoh *et al.* 1996a)
	E' center	2.0055	2.0044	2.0023	(Ogoh *et al.* 1995a)
Rutile	Ti center	1.977	1.974	1.941	(Chester 1961)

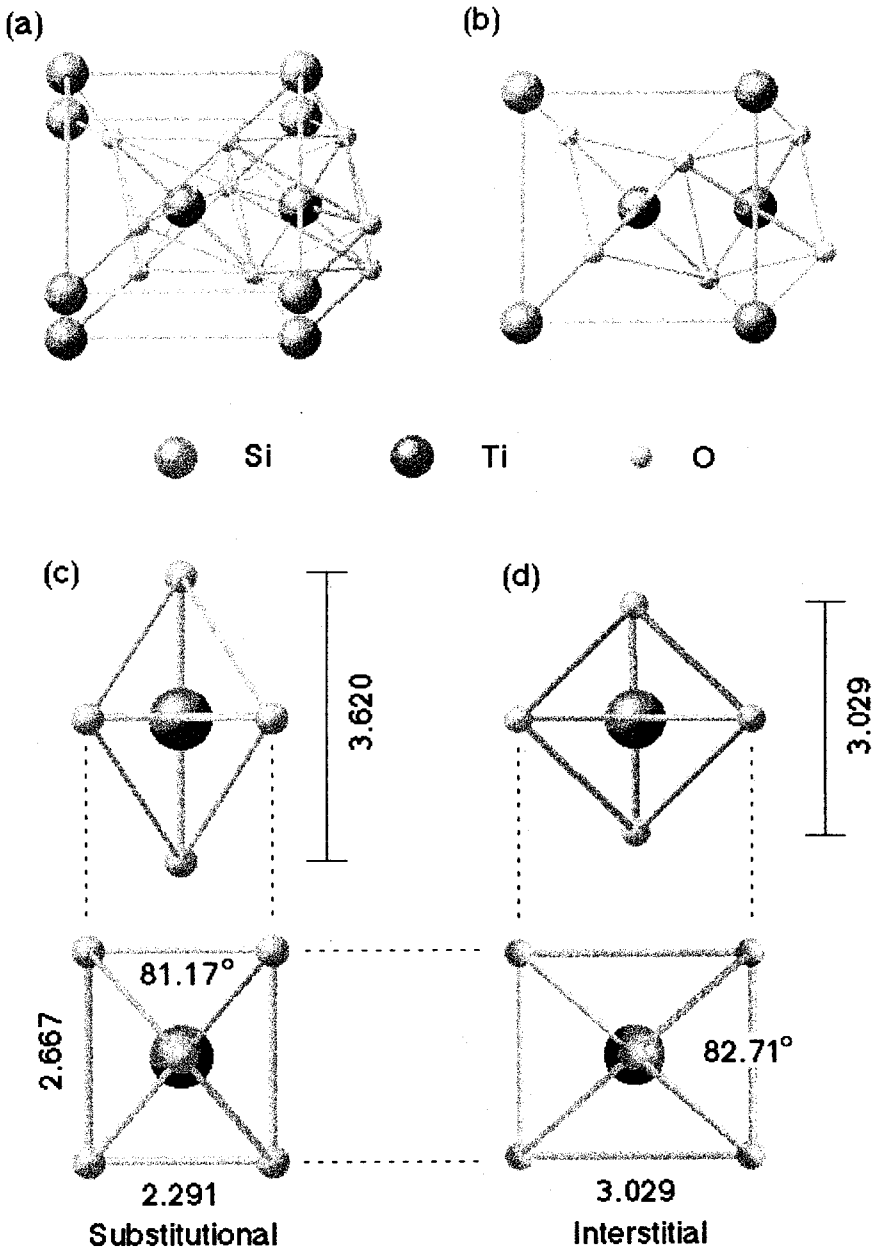

Figure 2-4. Two models of the Ti center in stishovite.
(a) The model of the Ti center can be substitutional or interstitial. (b) This is a projection on (001). The interstitial atom can occupy the center of the (100) or (010) plane. The substitutional model is in (c) and the interstitial model in (d).

2.2 Molecular orbital calculations by the DV-Xα method

(i) The method of molecular orbital calculations

The following calculations were carried out to confirm that the above model of the electron center was the Ti center as well as to know electronic structures of the paramagnetic centers in stishovite. The MOPAC, a semi-empirical method, does not support titanium at the moment and also is not good at calculating molecular orbital of ionic crystal. *Ab-initio* method like Gaussian98 package was tested but it needs quite large memory device and fast computer if several unit cells are involved and larger basis set is selected. Molecular orbital calculation by the discrete variational (DV)-Xα method has been done in this study to know electronic structures and to estimate *g*-factors of the impurity centers in stishovite, though geometry of the clusters cannot be optimized on the DV-Xα calculation. This is the reason why only substitutional impurity centers were considered. The DV-Xα method can manage a large cluster up to about a hundred atoms on personal computer with a few hundred MB memories.

(ii) Models of the stishovite clusters

Clusters of stishovite were constructed with a unit of SiO_6 octahedron that was a basic component of the rutile-type crystal structure. As the unit cell had D_{2h} symmetry (Appendix B) if the origin was at the silicon site of the octahedron, all clusters were made to have the same symmetry. Several sizes of clusters were tested to study the size effect to electronic structure (Figure 2-5). Minimum cluster is a SiO_6 octahedron and next two smaller clusters are Si_3O_{14} and Si_5O_{22} made by sharing edges of SiO_6 octahedron along c-axis. $Si_{11}O_{44}$ and larger clusters seem to be close to crystalline stishovite because a rutile structure was included in the clusters. The cluster $Si_{45}O_{146}$ was the maximum cluster in this study. Clusters including an impurity atom were made by substituting a silicon atom at the center of clusters with aluminum, titanium or germanium atom. Crystal structure at 300 K and 1 atm was used for constructing unit cell (Ross *et al.* 1990).

(iii) Conditions of DV-Xα calculations

The material of interest is not a cluster of about a hundred atoms but crystal. When molecular orbital of a cluster is calculated to demonstrate electronic structure in crystal, it should be considered to put point charges around the cluster to reproduce the crystal field especially for ionic crystal. This Coulomb field is called Madelung potential. Another matter is the initial number of charges on each atom. For example, ionic crystal needs ions rather than atoms and many point charges around the cluster. As stishovite has ionic property (e.g. Li & Ching 1985), a starting cluster was made with ions of silicon and oxygen and set in relatively large Madelung potential in this study.

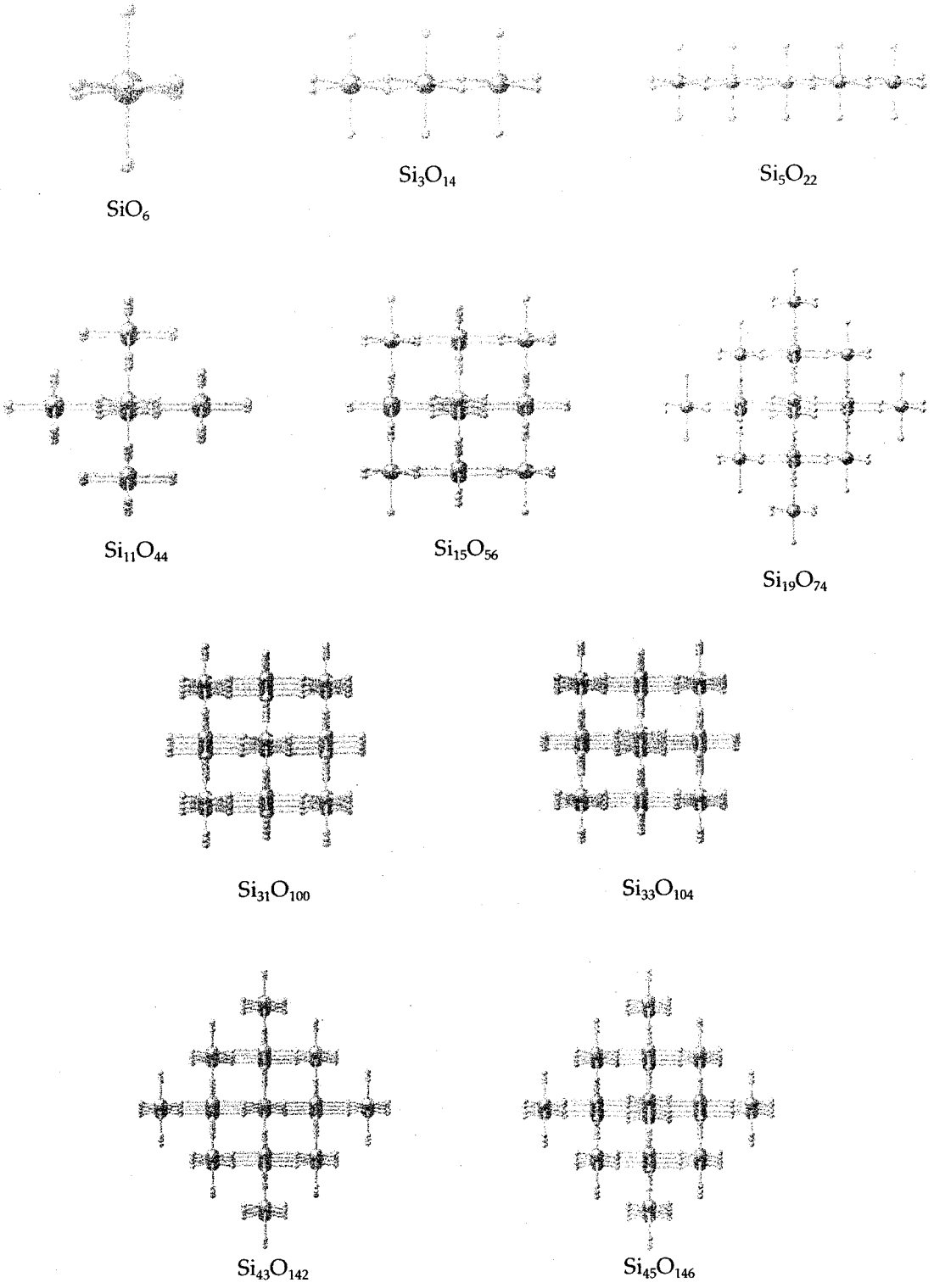

Figure 2-5. Various cluster models used on the DV-Xα calculations.

This model has another advantage to avoid the boundary problem of the cluster. In molecular orbital calculations, a hydrogen atom is often used for termination of each bond because hydrogen has one electron and makes only one bond to any atom ideally. In silica crystals based on SiO_4 tetrahedra like quartz, each bond between silicon and oxygen atoms is made by one electron from silicon and one from oxygen in a viewpoint of covalent crystal. Thus, it is easy to terminate ends of a cluster by hydrogen atoms. On the other hand, stishovite is not simple because each bond shares 4/3 electrons; 4/6 electrons from silicon and 2/3 from oxygen. If a hydrogen atom is used for termination instead of an oxygen atom, total numbers of electron for the bond exceed 4/3 electrons. If ionic crystal with Madelung potential is considered as the initial cluster model, this problem can be avoided because there are initially no bonds between cations and anions.

In this study, more than a few thousands of point charges that were equivalent to about 700 unit cells were distributed around the cluster as Madelung potential. 500 sampling points for discrete numerical integration were taken around each atom. Symmetric molecular orbital (D_{2h}) was also considered to simplify calculations and to save time. The spec of the computer is 500 MHz Pentium III® CPU with about 1 GB memories and 6 GB hard disk drive working on Windows 98. The package of DV-Xα calculation is called 'dvscat' program for IBM-PC, distributed with the introductory textbook about the DV-Xα method (Adachi *et al.* 1998).

(iv) Effects of cluster and Madelung potential size to electronic properties

When number of atoms increases, electronic structure at the center of a cluster should get close to crystal. In order to check the cluster size effects of molecular orbital calculations to electronic structures, net charges and bond overlap populations (BOP's) were calculated on different size of clusters shown in Figure 2-5. As only the center part of the cluster was of interest, net charges of the silicon atom 'Si' and the six surrounding oxygen atoms 'O(6)' in the central SiO_6 octahedron were shown in Figure 2-6-a. The initial net charges were 4 electrons for silicon and –2 electrons for oxygen due to ionic cluster. The results of smaller clusters still showed a strong ionic property while the larger clusters had similar net charges for both of them and the ionic property became lower. Figure 2-6-b shows the BOP's between central silicon and the nearest equivalent four oxygen 'Si-O(4)' or the next nearest two oxygen 'Si-O(2)' as well as between the oxygen atoms 'O(4)-O(2)'. The results were quite similar to the previous one and showed that the SiO_6 octahedron and the smaller clusters were not enough to reproduce crystalline stishovite in the central SiO_6.

The cluster size must affect to the whole electronic properties like band gap and bandwidth, too. Calculated energy band gap between the highest occupied molecular orbital (HOMO) and the lowest unoccupied molecular orbital (LUMO) was shown in Figure 2-6-c. Two widths of oxygen 2*s* and 2*p* bands, which were the highest and next highest valence band of stishovite, were also evaluated (Figure 2-6-d). The unit cell cluster had a large energy gap of about 11 eV but the energy gap gradually decreased

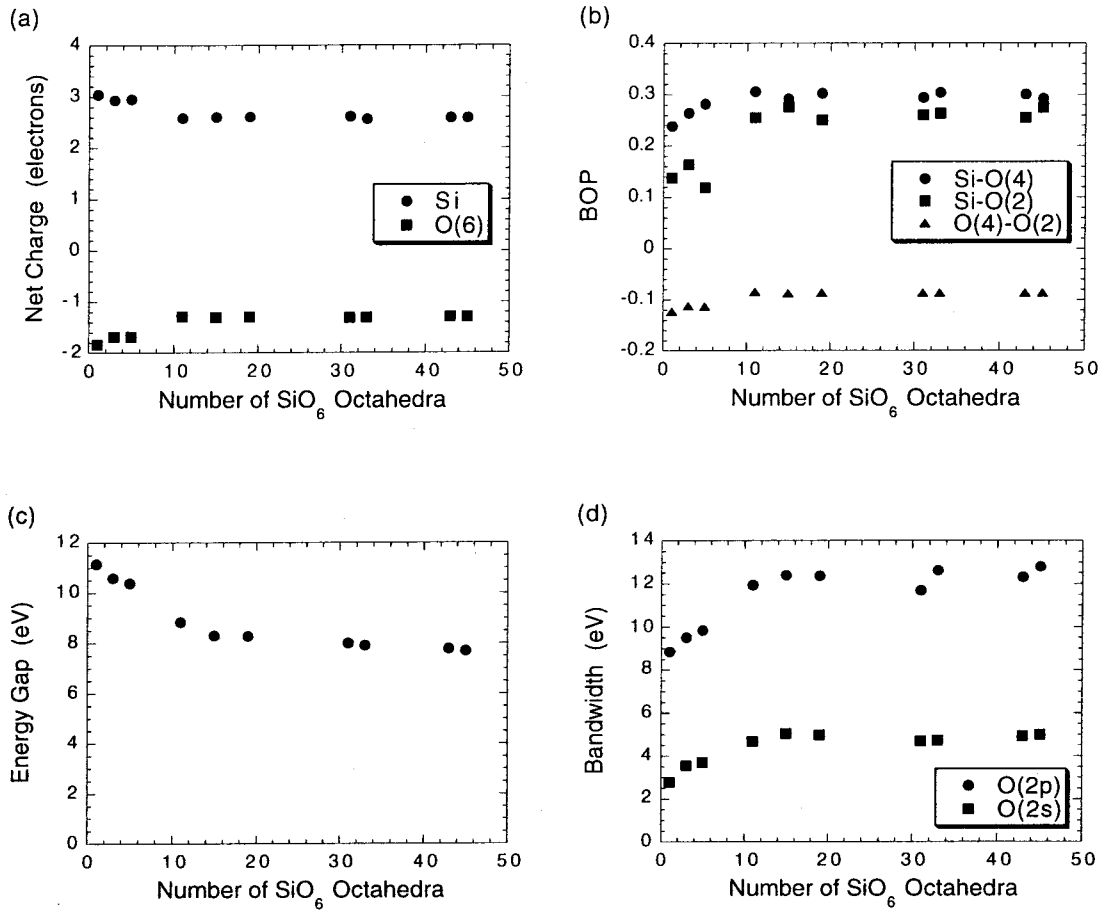

Figure 2-6. Electronic property changes on various size of the clusters. (a) Net charge on the central silicon atom 'Si' and average of net charge on the six oxygen atoms surrounding the central silicon 'O(6)'. (b) Bond overlap population (BOP) of the silicon orbital and the orbital of four equivalent oxygen atoms 'Si-O(4)' and the other two next nearest oxygen atoms 'Si-O(2)' as well as the BOP of the two kinds of oxygen orbital 'O(4)-O(2)'. (c) Energy gap between HOMO and LUMO. (d) Bandwidth of two bands formed by oxygen 2*p*-orbital 'O(2p)'and 2*s*-orbital 'O(2s)'.

for the larger clusters. Similarly, the bandwidths in the smaller clusters gave too small values in comparison with the results for the larger ones.

These results indicate that the SiO_6 octahedron, Si_3O_{14} and Si_5O_{22} clusters are not sufficient. As the $Si_{11}O_{44}$ and larger clusters have similar electronic properties, they can reproduce crystalline stishovite on the DV-Xα calculation. The $Si_{11}O_{44}$ cluster was used on the later calculations.

Figure 2-7 shows the other results calculated on the $Si_{11}O_{44}$ cluster with different sizes of Madelung potential. Net charges and BOP's were not affected but energy levels without Madelung potential were totally different, which indicated that at least some of Madelung potential was necessary to calculate the electronic structure of the

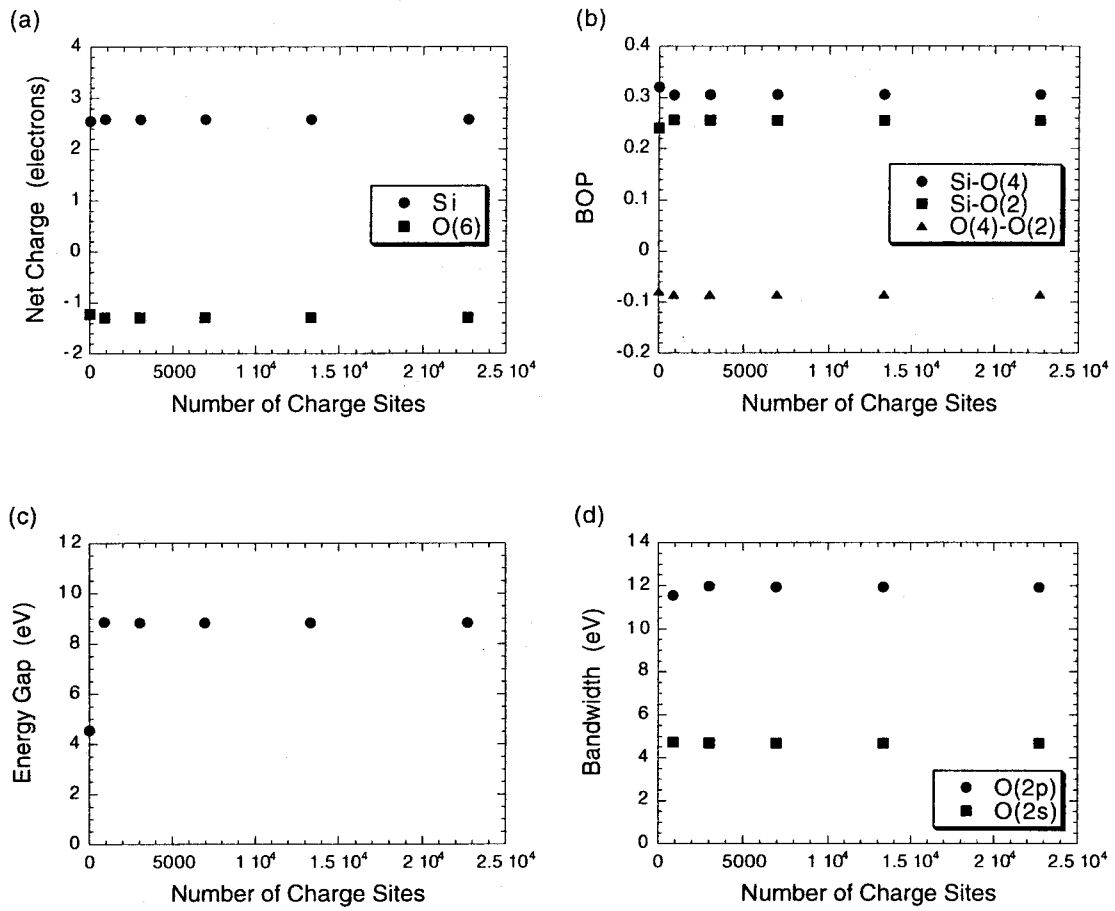

Figure 2-7. Electronic property changes under different size of Madelung potential. Legends are the same as those in the previous figure.

central SiO_6 properly. The Madelung potential created by about 3000 charge sites was used on the later calculations.

(v) Molecular orbital calculations of impurity centers and g-tensors

Aluminum, titanium and germanium are common impurities in silicon dioxides because the ionic sizes and electron configurations are similar to those of silicon. A trapped electron or hole is necessary to observe ESR signals. Titanium or germanium ion can trap one electron while aluminum ion can be related to a hole center. In order to produce a hole or electron trapped center, Al^{4+}, Ti^{3+} or Ge^{3+} ion was used in an initial cluster instead of Al^{3+}, Ti^{4+} or Ge^{4+} ion.

The obtained energy levels for those impurity centers were shown in Figure 2-8. The singly occupied molecular orbital (SOMO) was indicated with a marker. The top valence band was produced by 2*p*-orbital of oxygen as described before. The bottom conduction band was contributed by 2*s*-orbital of silicon. The energy levels mainly given by orbital of the impurity atoms were pointed out in the Figure 2-8. Figure 2-9 shows the cross sections of the SOMO for the impurity centers on xy-plane, yz-plane

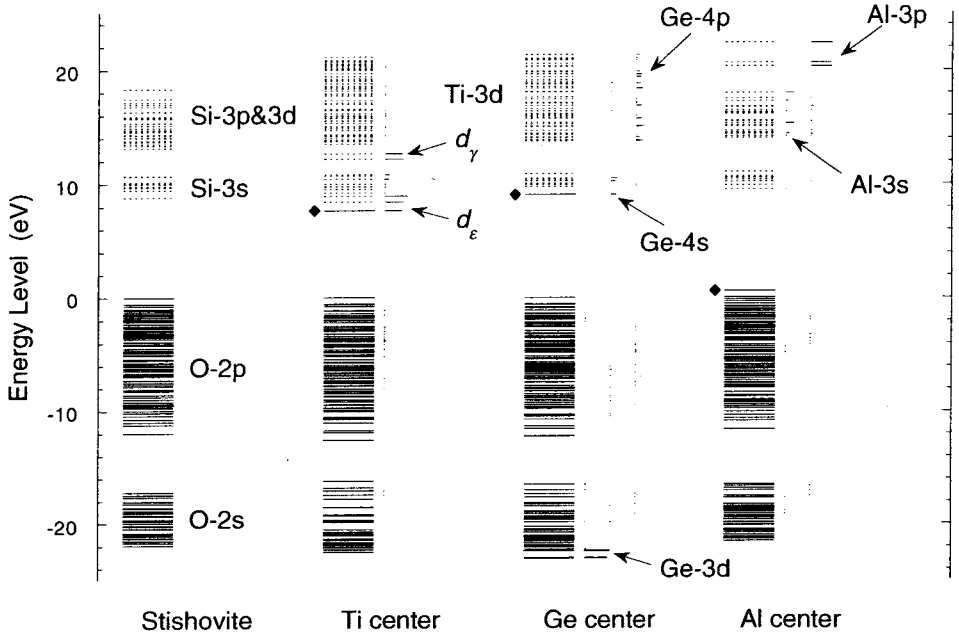

Figure 2-8. Energy levels of the pure cluster and the impurity centers. Energy levels of occupied molecular orbital were shown in solid line and those of unoccupied molecular orbital were in dotted line. Solid markers beside the levels indicated the energy level of the SOMO. The molecular orbitals constructing band structure of stishovite were shown on the right side of the 'Stishovite'. The *d*-orbital of titanium were split mainly into two parts; 'd_ε' and 'd_γ'

and zx-plane. The results indicated clearly that the electron was trapped in the 3*d*-orbital for the Ti center and in the 4*s*-orbital for the Ge center. The Al center looked somewhat different from those electron centers because a trapped hole did not occupy any orbitals in aluminum atom but the oxygen 2*p*-orbitals surrounding the aluminum. This model is concordant with the proposed model by Ogoh (Ogoh *et al.* 1996a) as well as the Al center model in quartz (Nuttall & Weil 1981).

After the molecular orbital calculations, ESR parameter *g*-shift was evaluated for each center and the results were shown in Figure 2-10 with the experimental data. Only the tendency was in agreement with the experimental results. It might be mainly due to two reasons; no geometry optimization and overestimation of energy levels of unoccupied molecular orbitals. Once one could optimize the sites of silicon and oxygen atoms especially the six oxygen atoms surrounding the impurity atom, the anisotropy of *g*-tensor might get larger due to relaxation of the lattice. The energy gap calculated by the DV-Xα method was larger than the other result of 5.15 eV by Xu and Ching (1991) and 5.7 by Cohen (1991) obtained by band theory. This may cause the smaller *g*-shift contribution from unoccupied molecular orbital, so that the *g*-factors would be shifted to the left side on the Figure 2-10. However, these calculations can be used as qualitative study of the center and the results indicate that the obtained electron center is not the Ge center but can be ascribed to the Ti center.

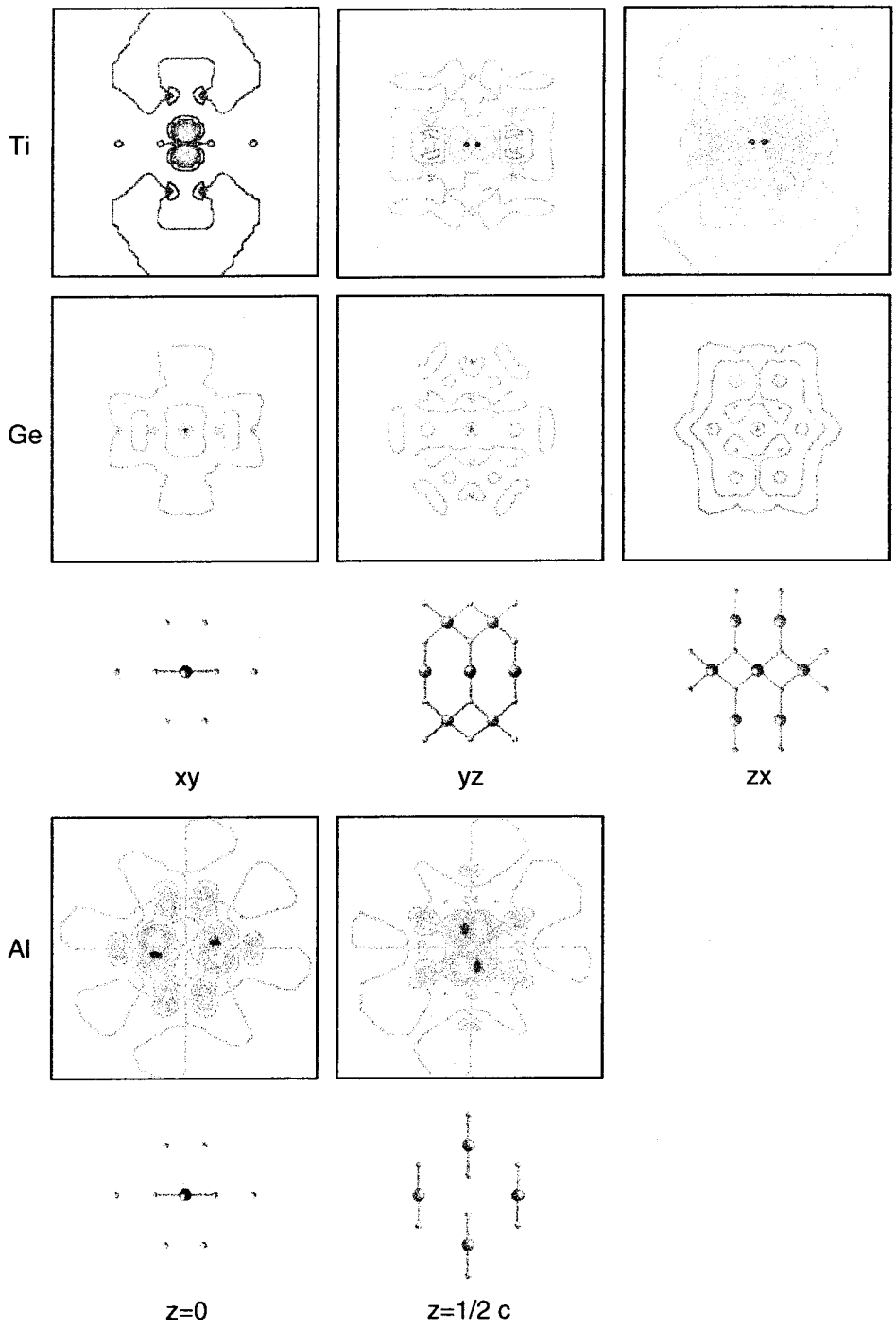

Figure 2-9. The contour images of SOMO for the impurity centers. (1st row) In the Ti center, an electron trapped in 3*d*-orbital is very localized. (2nd row) In the Ge center, a trapped electron occupies mainly 4*s*-orbital of germanium atom but also shared with 3*s*-orbitals of silicon atoms. (4th row) In the Al center, the upper valence band consisting of 2*p*-orbital of oxygen atoms traps a hole. The hole is not localized but shared with surrounding oxygen atoms. (3rd & 5th row) This indicates which atoms appear on the plane. The meaning of the column was shown in the figure.

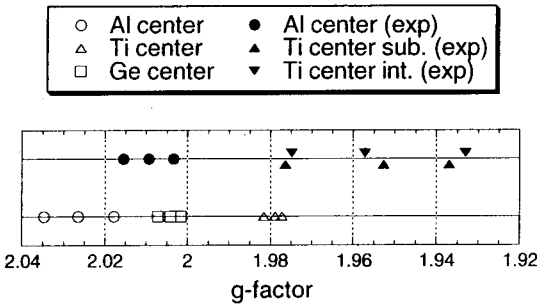

Figure 2-10. Calculated g-factors with experimental data.
Solid markers were obtained experimentally. The data of the Al center was reported by Ogoh (1996a). The Ge center has not been reported yet.

2.3 Summary

A new electron center having an orthorhombic g-tensor of $g_1 = 1.9764$, $g_2 = 1.9527$ and $g_3 = 1.9370$ was detected at 77 K in synthetic stishovite irradiated by γ-rays at 77 K. The signal intensity of the center was saturated at microwave power of 2 mW and the center was annealed out around 280 K. Unfortunately, the center was thermally unstable at room temperature and can not be used for dating and dosimetry on the earth. The center could be used for a geochronological application of impact craters found in much cold places like the other planets.

The model of the center was suggested to be the Ti electron center because the trapped electron in Ti^{3+} ion occupied 3*d*-orbital and it would give a relatively large g-shift rather than a model of the Ge center. Similar center was found in another synthetic stishovite after γ-ray irradiation at 77 K and had a g-factor of $g_1 = 1.9749$, $g_2 = 1.9572$ and $g_3 = 1.9331$. The substitutional and interstitial Ti center could be considered in the rutile-type crystal structure and the latter center is more probable for the interstitial one because the anisotropy of g-tensor was closer to that of the interstitial Ti center found in rutile TiO_2. Further study is necessary to determine these centers more clearly. No hyperfine signals resulting from charge compensator like hydrogen or alkali ion could be observed at 77 K in this study.

The molecular orbital calculations by the DV-Xα method revealed the electronic structures of stishovite clusters and the substitutional impurity Al, Ti and Ge centers. The cluster $Si_{11}O_{44}$ or larger ones satisfied to represent the crystalline electronic properties in the center of the cluster. The SOMO of the impurity centers are summarized below.

- Al center: Oxygen atoms surrounding aluminum atom share a trapped hole in oxygen 2*p*-orbital. The SOMO relatively spreads out to the whole cluster.
- Ti center: The SOMO is contributed by mainly titanium 3*d*-orbital and very locally restricted.
- Ge center: The SOMO is contributed by mainly germanium 4*s*-orbital but has a

probability on silicon atoms as well because germanium 4s-orbital is overlapped with silicon 3s-orbital constructing conduction band.

The calculated g-factors were qualitatively concordant with the experimental results. Further quantitative discussion of the g-factor calculations needs the better calculating method like modern density functional theory (DFT) or ab-initio method to optimize geometry taking lattice relaxation into account.

CHAPTER 3

Optically Stimulated Luminescence of Stishovite

Optically stimulated luminescence (OSL) dating is getting popular in geology and archaeology to date a burial age of sedimentary soil or archaeological relics because light exposure can stimulate trapped charges and reset a burial age to zero. The sensitive optical detection technique can avoid collecting a lot of rare dating material like stishovite to improve signal to noise ratio. On the other hand, mineral separation should be careful because contamination sometimes disturbs OSL signals by contamination. This study is the first observation of the OSL signals of γ-ray irradiated synthetic stishovite under infrared or blue stimulating lights in order to develop direct dating technique of meteor impact craters. Thermoluminescence (TL) of stishovite was also measured before and after OSL measurements to study light effects on TL glow-curves. In addition, two ESR signals, quite similar to those in crushed quartz, were found in unirradiated stishovite synthesized under sudden stress drop. They could be indicators of meter impacts where very high and sudden pressure occurred.

3.1 Sample & Experimental

The starting material was natural quartz picked up from granite because naturally found stishovite could be formed with natural quartz containing many impurities like aluminum, titanium and germanium atoms. The sample covered by tantalum foil heater was fixed in the center of cylindrical heat insulator (zirconia) that was set in the hole of octahedral pressure medium of magnesium oxide (Figure 3-1). This octahedron was kept under about 10 GPa and 900 °C for 5 hours in uniaxial split-sphere anvil apparatus (USSA-1000) at Institute for Study of the Earth's Interior, Okayama University. The tantalum foil was carefully removed using a hand drill with diamond-plated points. Irradiation of 500 Gy from the γ-ray source of ^{60}Co was carried out for each sample at room temperature. Synthetic samples were confirmed as stishovite by powder X-ray diffraction analysis. For comparison, the starting material and mixed sample of quartz and feldspar taken from sedimentary soil were irradiated by γ-rays, too.

Luminescence experiments were made on RISO-set (TL-DA-15) at Nara Women's University using stimulating lights of infrared laser (830 nm) and blue light emitting diodes (LED's) (470 nm). Power of the infrared laser and blue LED's on the sample stage were 500 mW/cm^2 and 18 mW/cm^2 for a setting of 90 % on the program panel, respectively. An optical filter (340 nm) for luminescence was used to cut the stimulating lights in OSL measurements. The same filter was used for TL. The order

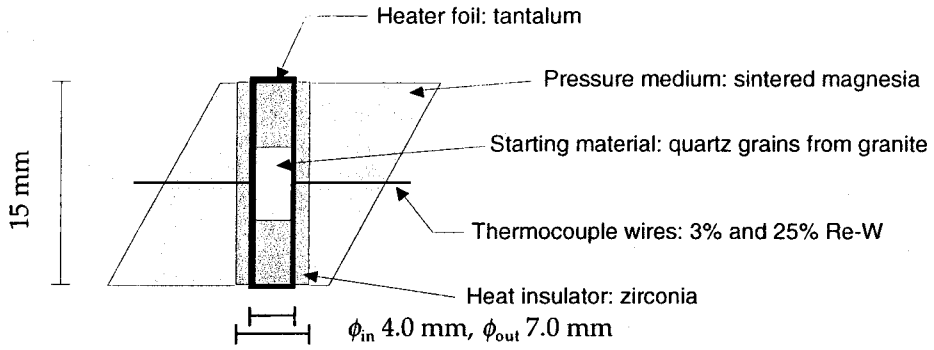

Figure 3-1. The schematic cross section of the assembly.

of OSL measurements was first infrared stimulated luminescence (IRSL) and then blue light stimulated luminescence (BLSL). In this paper, no preheat was carried out and the sample stage was not heated in OSL measurements. The heating rate in TL was 2 °C/s. The sample was also measured by ESR (JEOL RE-2X) at room temperature using 100 kHz field modulation of 0.1 mT.

3.2 OSL of stishovite

(i) IRSL and BLSL of stishovite

A shine-down curve of IRSL of the γ-ray irradiated stishovite was shown in

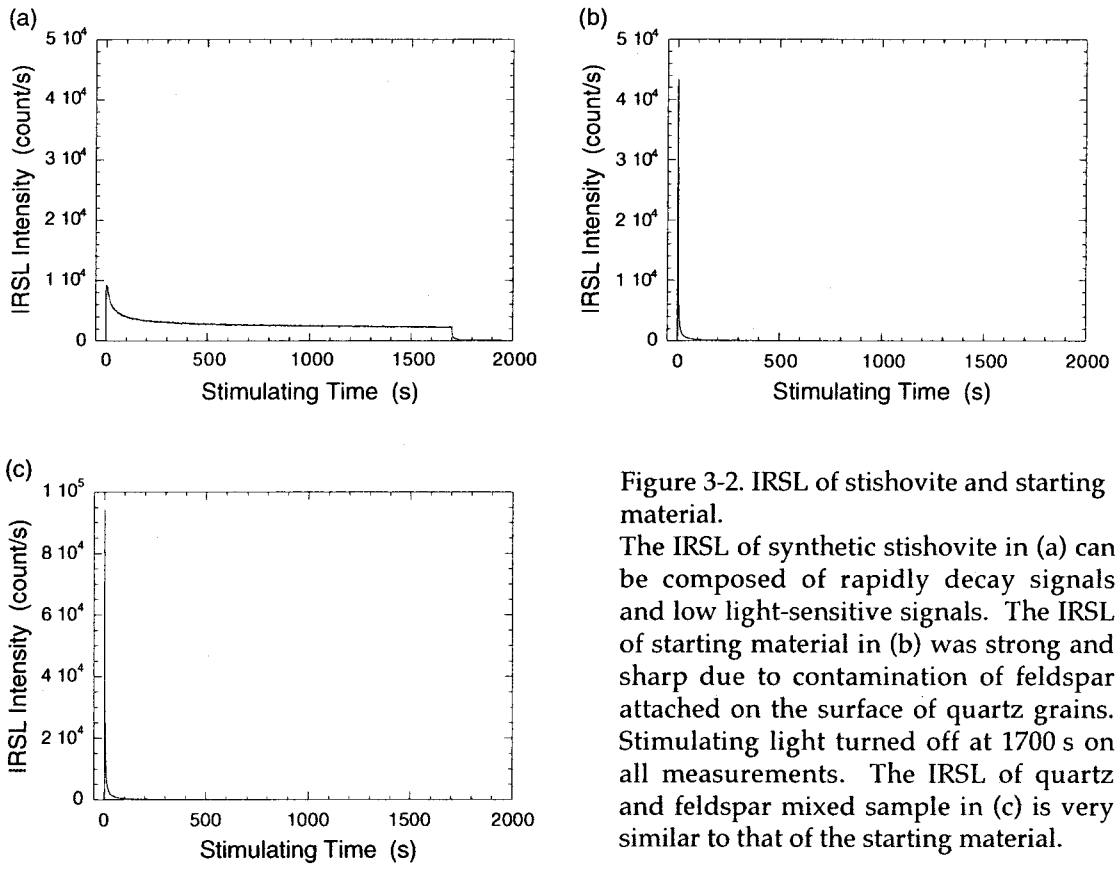

Figure 3-2. IRSL of stishovite and starting material.
The IRSL of synthetic stishovite in (a) can be composed of rapidly decay signals and low light-sensitive signals. The IRSL of starting material in (b) was strong and sharp due to contamination of feldspar attached on the surface of quartz grains. Stimulating light turned off at 1700 s on all measurements. The IRSL of quartz and feldspar mixed sample in (c) is very similar to that of the starting material.

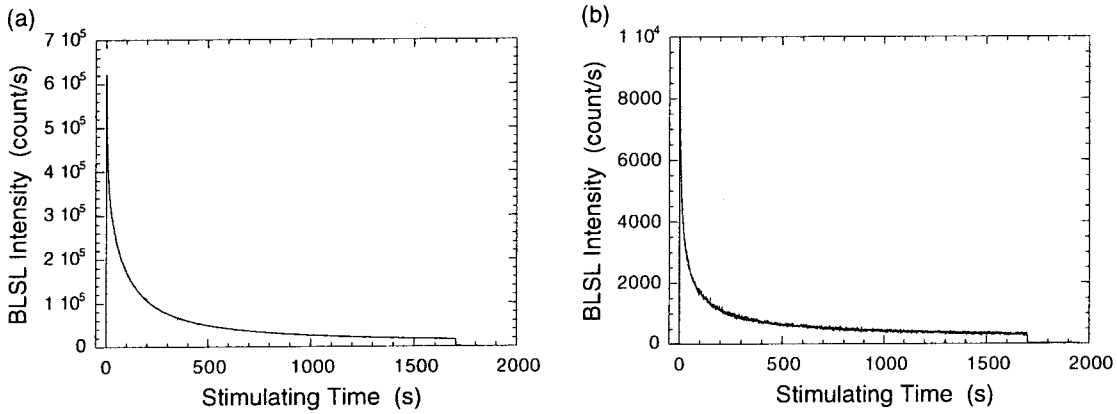

Figure 3-3. BLSL of stishovite and starting material.
The BLSL of synthetic stishovite in (a) is about sixty times larger than the BLSL of starting material in (b). Both the shine-down curves are similar.

Figure 3-2-a. The curve could be a mixture of several types of charge recombination processes and some of them had very low sensitivity for infrared at 830 nm. The decay constant of the low light-sensitive part was about 4000 second, which was obtained by least square fitting of a single exponential curve to the data from 1000 to 1700 second. The IRSL of the starting material was also detected and shown in Figure 3-2-b. As the intense signal and shine-down curve of the IRSL was quite similar to those of the soil sample containing quartz and feldspar (Figure 3-2-c), the signal of the starting material might be caused by contamination of feldspar attached on the surfaces of the quartz grains. The IRSL of feldspar had almost no low light-sensitive part. Therefore, low light-sensitive OSL resulted from stishovite in this experiments, though some of feldspar have a part of low light-sensitive OSL (Rodes 1999).

Both of the stishovite and the starting material emitted BLSL as well (Figure 3-3-a and b). Although the shapes of the shine-down curves were quite similar, the intensity of the stishovite was about sixty times larger than that of the starting material for the same dose irradiation. These IRSL and BLSL were due to radiation-induced centers because those of the unirradiated stishovite could not be detected.

(ii) TL of stishovite before and after OSL measurements

Blue TL glow-curves of the stishovite were detected before and after the OSL measurements in the same system (Figure 3-4). Light-sensitive trapped charges could be optically transferred to shallow traps (100-200 °C) as well as traps around 250 °C. On the other hand, TL intensity around 400 °C decreased after the OSL. The two TL peaks related to atomic hydrogen centers were reported by Ogoh *et al.* (1996b) and those TL parameter were determined as 1.20 eV and 1.32 eV at the same frequency factor of 1.3×10^{12} Hz. The largest TL peak at 220 °C before the OSL was corresponded to the peak of 1.32 eV but no peak related to the other peak was found in the glow-

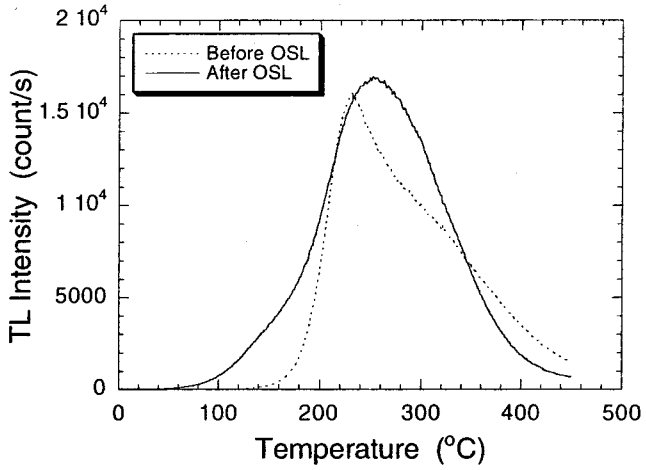

Figure 3-4. TL of stishovite before and after the OSL measurements. Peaks of lower temperature increased but those around 400 °C decreased by light exposure.

curve before the OSL.

(iii) OSL after TL measurements

After the OSL and TL measurements, IRSL and BLSL of the same sample were measured again (Figure 3-5). The centers related to IRSL were completely annealed and no IRSL could be detected. However, intense BLSL could be observed. The maximum intensity of the BLSL after heating was about 70000 count/s and about four times larger than the intensity before heating after light exposure for 1700 second. The trapped charges stimulated by blue light were partly recombined with appropriate charges but some of them could be transferred to shallow traps, which were confirmed

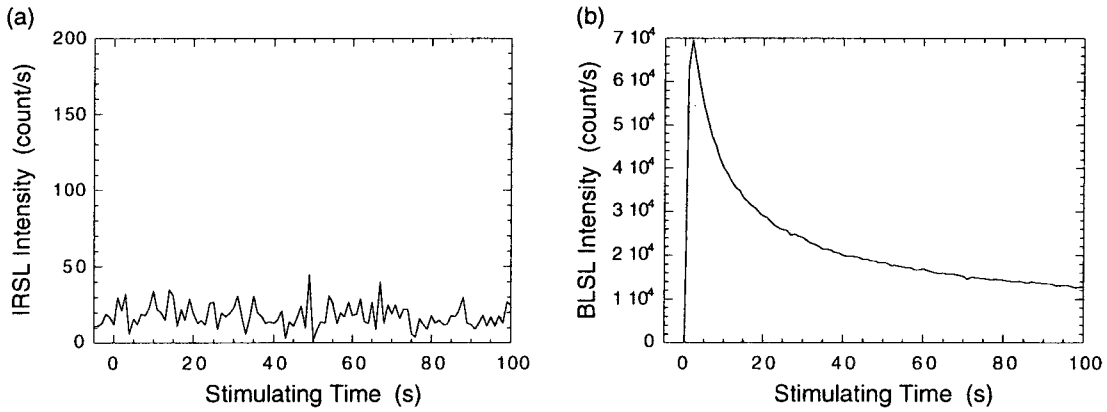

Figure 3-5. OSL after the TL measurements. Heating procedure up to 450 oC completely annealed defects related to IRSL (a). However, the sample showed the intense BLSL (b). Part of thermally stimulated electrons or holes may be re-trapped to the centers related to BLSL.

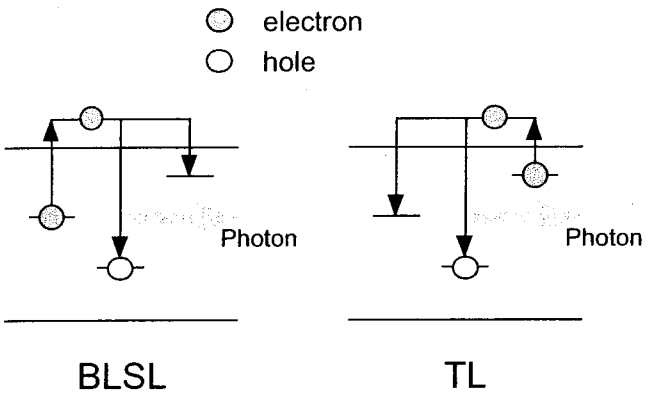

Figure 3-6. Model of recovering BLSL.

in the TL results of the stishovite, Figure 3-4. These charges in shallow traps were partly re-transferred to the original site by heating up to 450 °C in TL (Figure 3-6), which indicates that the centers related to BLSL are quite thermally stable and could be used for geological dating.

3.3 E'-like center in stishovite

ESR measurements of the unirradiated stishovite revealed that two kinds of centers were produced by sudden pressure release in synthesis process (Figure 3-7). The center 'B' in higher magnetic field had an axial g-factor ($g_{//} = 2.00181$ and $g_{\perp} = 2.00062$) and was different from the E' center in stishovite ($g_1 = 2.0055$, $g_2 = 2.0044$ and $g_3 = 2.0023$) assigned by Ogoh (1995a). This was close to the E' center in quartz ($g_1 = 2.00179$, $g_2 = 2.00053$, $g_3 = 2.00030$) (Jani *et al.* 1983) but the line width of the center 'B' was much broadened. The other center 'A' has an isotropic g-factor of 2.00305 and might be a kind of oxygen hole center that could be formed from an interstitial oxygen

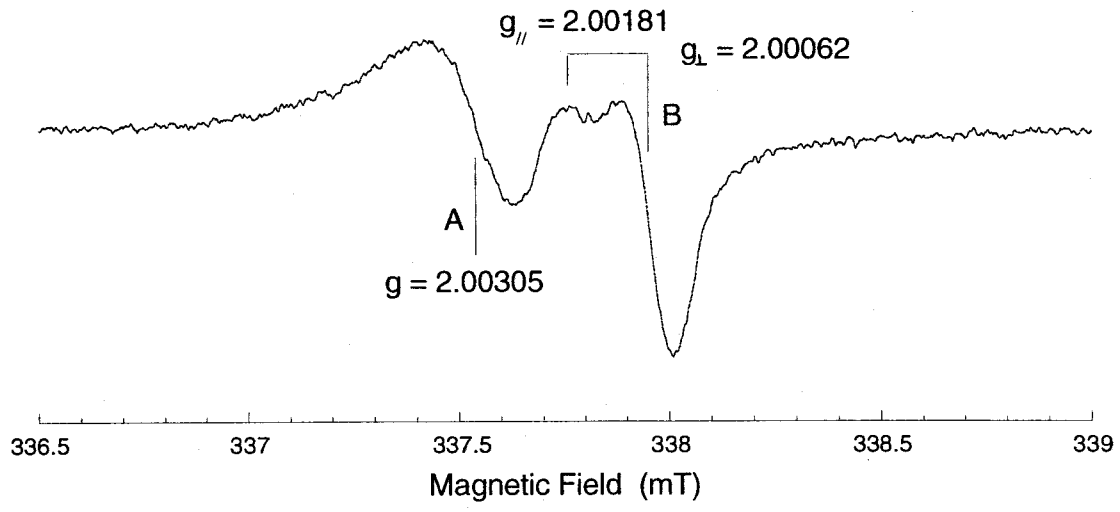

Figure 3-7. ESR powder spectrum of the centers induced by sudden pressure drop. Signal 'A' is isotropic and signal 'B' is axial. These are quite similar to crush-induced centers in crushed quartz (Hirai & Matsumoto 1999). The signal 'B' may have a structure like the E' center in quartz.

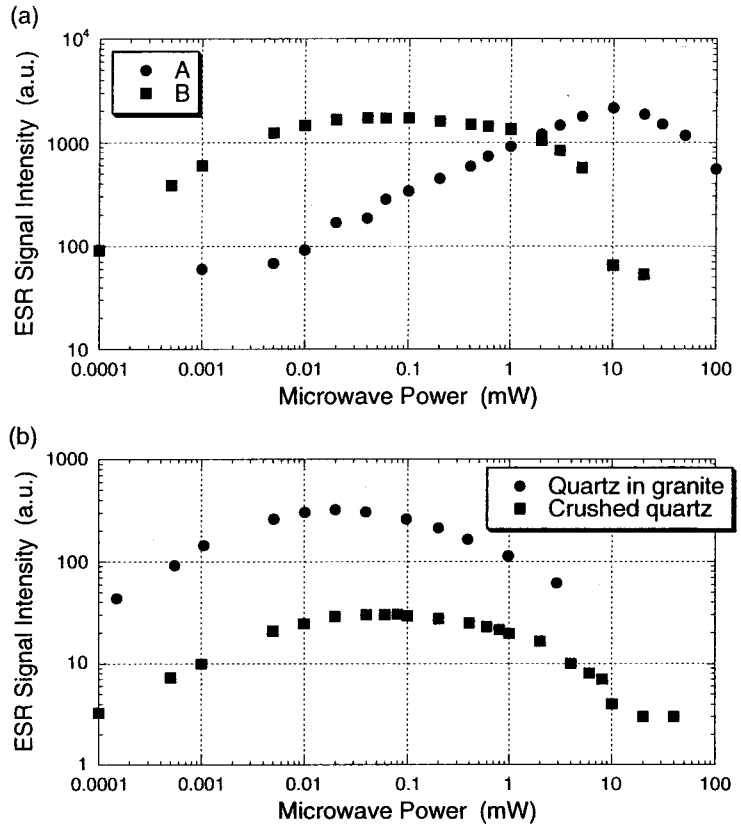

Figure 3-8. Microwave power dependence of the various E′ and isotropic centers. (a) The signal 'A' and signal 'B' have different microwave power dependence (MPD). (b) MPD of the crush-induced E′ center in crushed quartz (Hirai 1997) was quite similar to that of the signal 'B' rather than ordinary E′ center in quartz picked up from the granite (Toyoda 1992).

atom trapped by near oxygen at a normal site. The similar center at g ~ 2.0030 in natural stishovite was obtained by Devine & Hübner (1989). Both the centers could not be found in synthetic stishovite with gradual pressure unload.

Figure 3-8-a is the microwave power dependence (MPD) of those signals. The MPD of the center 'B' was close to the MPD of the E′ center in crushed quartz (Hirai 1997) rather than that in undistorted quartz (Toyoda 1992) shown in Figure 3-8-b. Hirai (1999) got a very similar ESR spectrum of both the centers 'A' and 'B' in quartz crushed with a ball mill. This may indicate that these centers may be produced in amorphous region formed by sudden pressure release in synthesis process where the octahedral coordination (SiO_6) might be locally changed to more stable tetrahedral coordination (SiO_4). As very high and sudden pressure should be applied to soil and produce these centers at a meteor impact, these centers could be used for an evidence of impact events if they are thermally stable.

3.4 Summary

The IRSL and BLSL were discovered for the γ-ray irradiated synthetic stishovite.

The peak intensity of the IRSL was not so different from that of the starting material but part of the IRSL of the stishovite had a long decay constant of about 4000 second, which is concluded to be due to stishovite. The BLSL of the stishovite was sixty times larger than that of the starting material. It may be used for geological dating of impact craters because a part of the centers related to BLSL were not annealed even at 450 °C and may be expected to have a long lifetime. If one can distinguish the luminescence of stishovite from the other minerals (*e.g.* quartz or feldspar) by different wavelength or different sensitivity to stimulating light, this method would be a very useful dating tool of meter impact craters.

Two ESR signals produced by sudden pressure release were found in unirradiated stishovite. One had an isotropic g-factor (2.00305) and the other had an axial g-factor ($g_{//} = 2.00181$ and $g_{\perp} = 2.00062$). The spectrum shape and microwave power dependence of the latter center was quite similar to those of the E′ center in crushed quartz. The former center might be a kind of oxygen hole center. It could be used as an indicator to know the details of an impact, if these centers are stable for a geological time.

CHAPTER 4

The E′ center in Strain-Introduced Quartz

Mechanical process like crush or shock can be another process to produce lattice defects in mineral. It produces an intrinsic defect, oxygen vacancy in quartz. Such oxygen vacancy can be observed by ESR if it traps a hole, which is called the E′ center. The distorted structure surrounding the vacancy affects the ESR signals because the g-tensor is determined with the local electronic structure. In this chapter, the E′ center in strain-introduced quartz was studied by semi-empirical molecular orbital calculation with MOPAC to see the g-shift changes under strain. The reason of the g-shift distribution in crushed quartz was discussed. ESR spectra can be reconstructed using the obtained results. This feature might be used for paleo-pressure analysis of a sample, if the center can be stored for a long time in the same or similar distorted structure that was induced by geological or archaeological events like faulting and glacier grinding.

4.1 Theoretical study of the defects in α-quartz

A computational study on defects is a powerful tool to make a structure model of the centers and to study electronic structures as shown in Chapter 2. The E′ center in quartz has been studied by many scientists for modeling, optical absorption and g-tensor *etc.* (like Rudra & Fowler 1987; Gobsch *et al.* 1978).

The ESR signal of the E′ center was broadened in crushed quartz (Arends *et al.* 1963; Hochstrasser & Antonini 1972; Toyoda *et al.* 1993b). A less broadened E′ center (Figure 4-1) was reported in glassy quartz and discussed with the distribution of the g-shift under the assumption of a Gaussian distribution in energy splitting by Griscom (1979). Hirai (1998) studied crush-induced E′ center in quartz (Figure 4-2) and revealed that the distribution of each principle g-factor was caused not only by the distribution of the energy splitting but also by changes of molecular orbitals. As molecular orbital theory can calculate both of molecular orbitals and energy levels, the changes of g-shift was investigated on the cluster of the E′ center in strain-introduced quartz.

4.2 Cluster model & conditions on calculations

Electronic structures were calculated with a semi-empirical method, MOPAC. It has been developed mainly for organic materials based on covalent bonding and not work well on ionic clusters. However, several papers reported calculations of the electronic properties on small silica clusters by semi-empirical methods (e.g. West *et al.* 1998). In this section, the tendency of the strain effect on g-factors was investigated.

A cluster of the silica $Si_8O_7H_{18}$ was considered. All the outer bonds of silicon atoms are terminated with hydrogen atoms instead of oxygen atoms. The oxygen atom at the center was removed to make an oxygen vacancy and an electron was removed from the cluster to form the E′ center (Figure 4-3). To remain crystalline feature in the cluster, geometry optimization was made for the only inner atoms and hydrogen atoms. For hydrogen, only bond distance between hydrogen and the bonded silicon was optimized but angle to the silicon was fixed. The fixed atoms were marked with '*'. The cluster was distorted by changing not only the length of unit a-, a′- and c-axis but also the primitive angles of α, α' and γ. Here, the a′-axis is defined as the axis perpendicular to a- and c-axis and the angles α, α' and γ are as the angle between a′- & c-axis, c- & a-axis and a- & a′-axis, respectively.

The package of the MOPAC used here was named MOPAC93 though the latest version is the MOPACv2 released by Fujitsu Ltd. The geometry was optimized in the PM3 method (Stewart 1989) under unrestricted Hartree-Fock (UHF) approximation. Then point energy calculation was done on the PM3 under restricted open-shell Hartree-Fock (ROHF) approximation to evaluate energy levels and molecular orbitals. The PM3 is one of refined semi-empirical calculation methods. Restricted Hartree-Fock (RHF) approximation means that each orbital has to be occupied with two electrons of up spin and down spin. The ROHF has the same restriction but can treat with an unpaired electron. In UHF approximation, each molecular orbital has no such a restriction and consists of different spatial wave function for up and down spin electrons. UHF calculation usually gives lower total energy than RHF one so that geometry was optimized in the UHF.

4.3 Computational results

Figure 4-4 shows that the singly occupied molecular orbital (SOMO). The unpaired electron is localized in one of nearest silicon atoms. This model is in agreement with the proposed model (Rudra & Fowler 1987).

Figure 4-5 shows the total energy of the clusters in strain-introduced quartz. The crystal structure of quartz is stable for a strain of extension or pressure. However, the shear strain on the angles α, α' and γ gives the more stable clusters. This might be a characteristic of the E′ center but more calculations with a larger cluster are necessary for further discussion.

Energy level changes can be seen clearly rather than changes of molecular orbitals (Figure 4-6). The 'MO43' is the energy level of the SOMO. MO with higher number stands for the energy level of the unoccupied molecular orbital (UMO) and MO with lower number does for that of the occupied molecular orbital (OMO). The energy level of SOMO changed especially for strain on a- and c-axis; it becomes lower under pressure and higher under extension. If the distance between two silicon atoms over oxygen vacancy decreases, an electron trapped by oxygen vacancy can make bond easily and the E′ center have more characteristics of a hole center. This means the energy level of the SOMO must be lower under pressure. The calculated results are

understood with this model.

The g-shift for each strain-introduced cluster was calculated and shown in Figure 4-7. The g-shift changes drastically for strain in comparison with the results of energy levels. For example in Figure 4-6-c, the biggest change on the inverse of the energy level difference $1/\Delta E$ between strain-introduced quartz and no strain quartz was 26.7 %. However, the g-shift changed much drastically about 80 % for g_1, 800% for g_2 and more for g_3. The UMO of much higher energy levels and OMO of much lower energy levels sometimes gave a big contribution to g-shift but the changes of $1/\Delta E$ under strain may be very small. Therefore, it can conclude that the changes of molecular orbital under strain play an important role in g-shift changes rather than energy level changes.

4.4 Summary

Molecular orbital calculation has been done on the cluster of $Si_8O_6H_{18}$ with an hole added to study g-shift changes of the E′ center in quartz under strain. Griscom explained the g-shift distribution of the E′ center in glassy silica considering a Gaussian distribution in energy splitting. However, in the case of strain-introduced crystalline quartz, the obtained result indicates that change of the molecular orbital is a dominant for g-shift change under strain. This is concordant with the spectral analysis by Hirai.

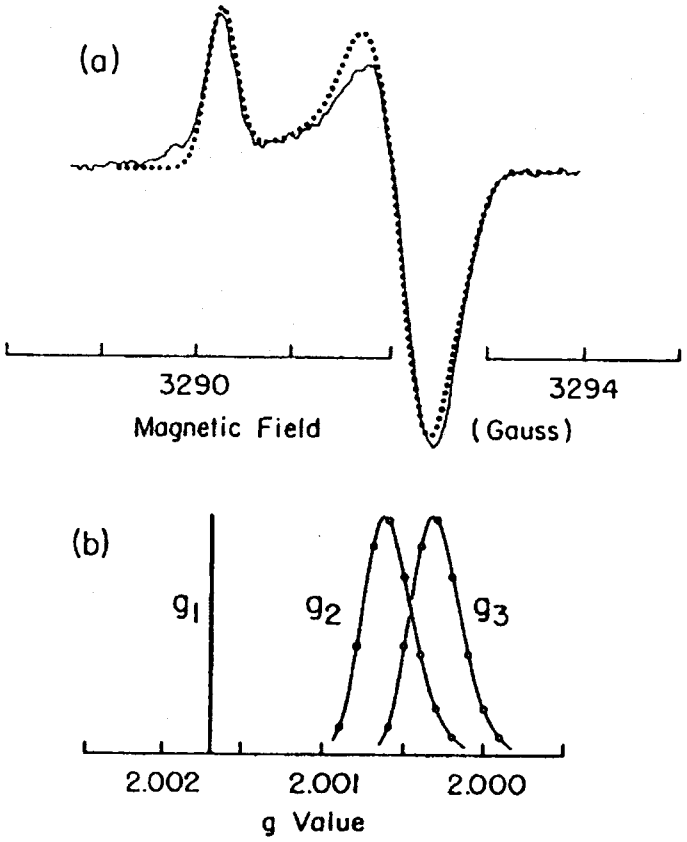

Figure 4-1. ESR spectrum of the E′ center in glassy quartz.
(a) Solid line is an experimental ESR spectrum of the E′ center in glassy quartz. Dotted line is a simulated spectrum considering the distribution of g-factors in (b) (Griscom 1979).

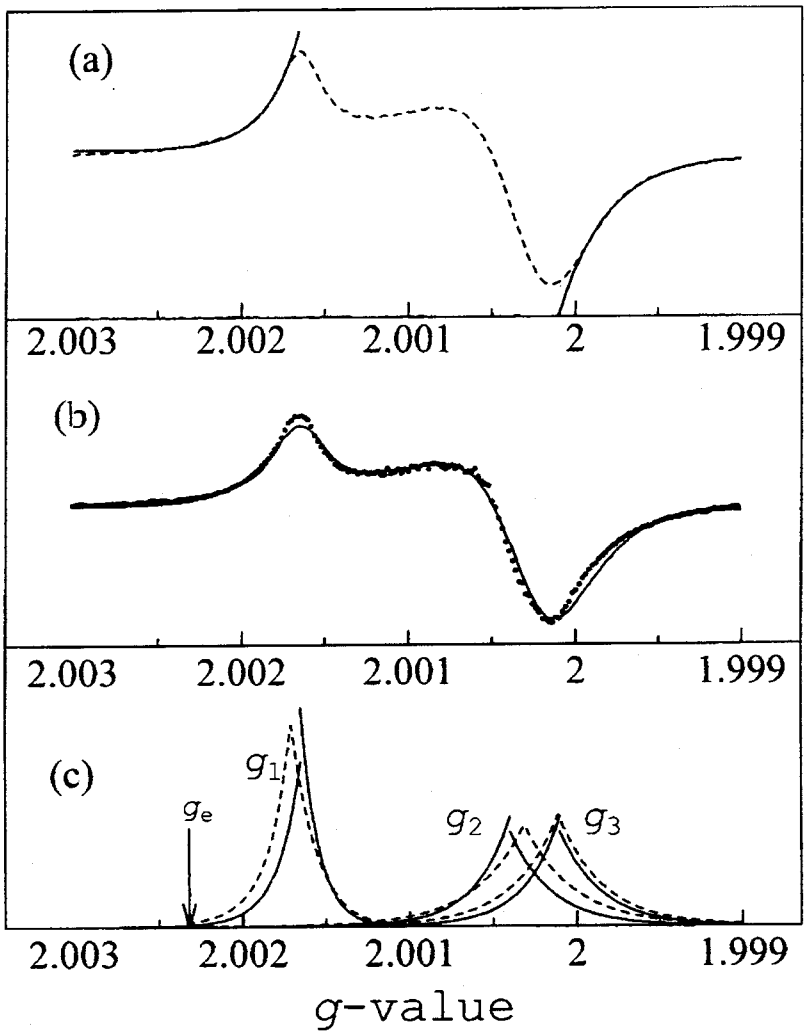

Figure 4-2. ESR spectrum of the E′ center in crushed quartz.
(a) The broken line is the spectrum of the E′ center in irradiated crushed quartz. The solid lines are exponential functions fit to the spectrum. (b) The spectrum (dotted line) was simulated with statistical distribution of the principal values, g_1, g_2 and g_3 in (c). The experimental spectrum was also displayed together (Hirai & Ikeya 1998).

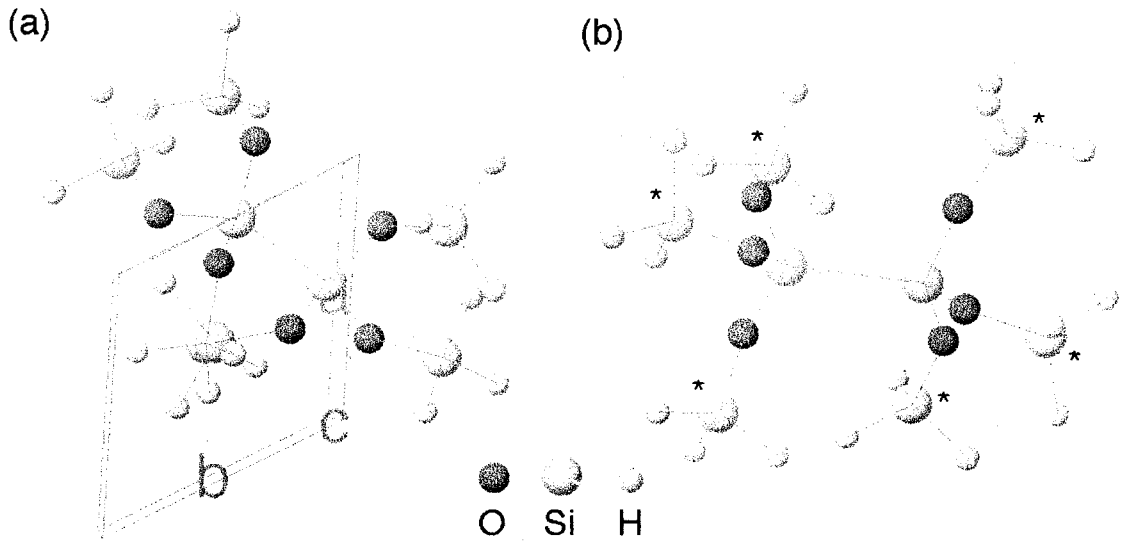

Figure 4-3. The model of the E′ center for MO calculations.
(a) The projection onto (001). (b) Oxygen vacancy after rotaion. Bonded line is drown for convenience.

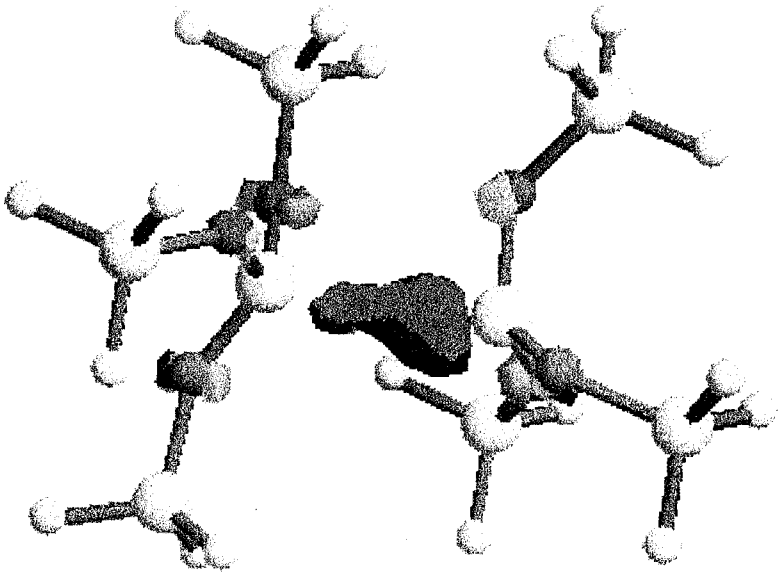

Figure 4-4. SOMO of the E′ center under no strain.

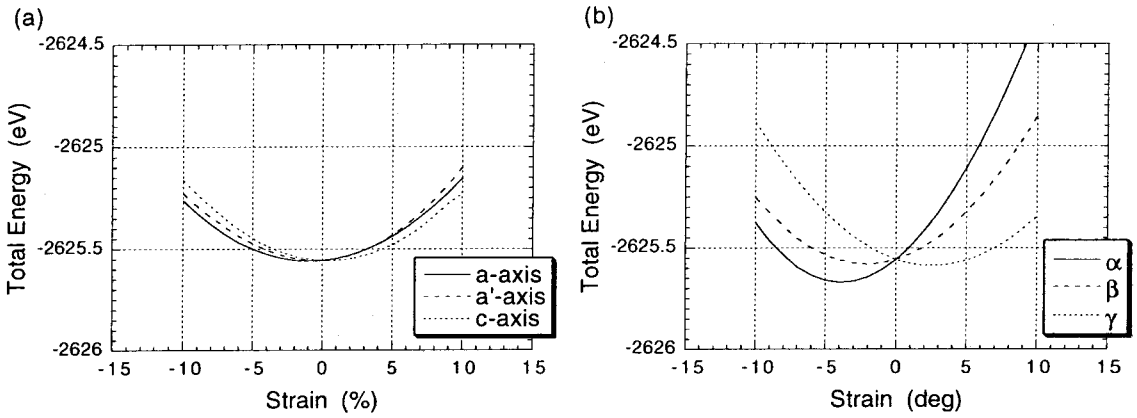

Figure 4-5. Total energy of the cluster for different strain on each axis or angle.

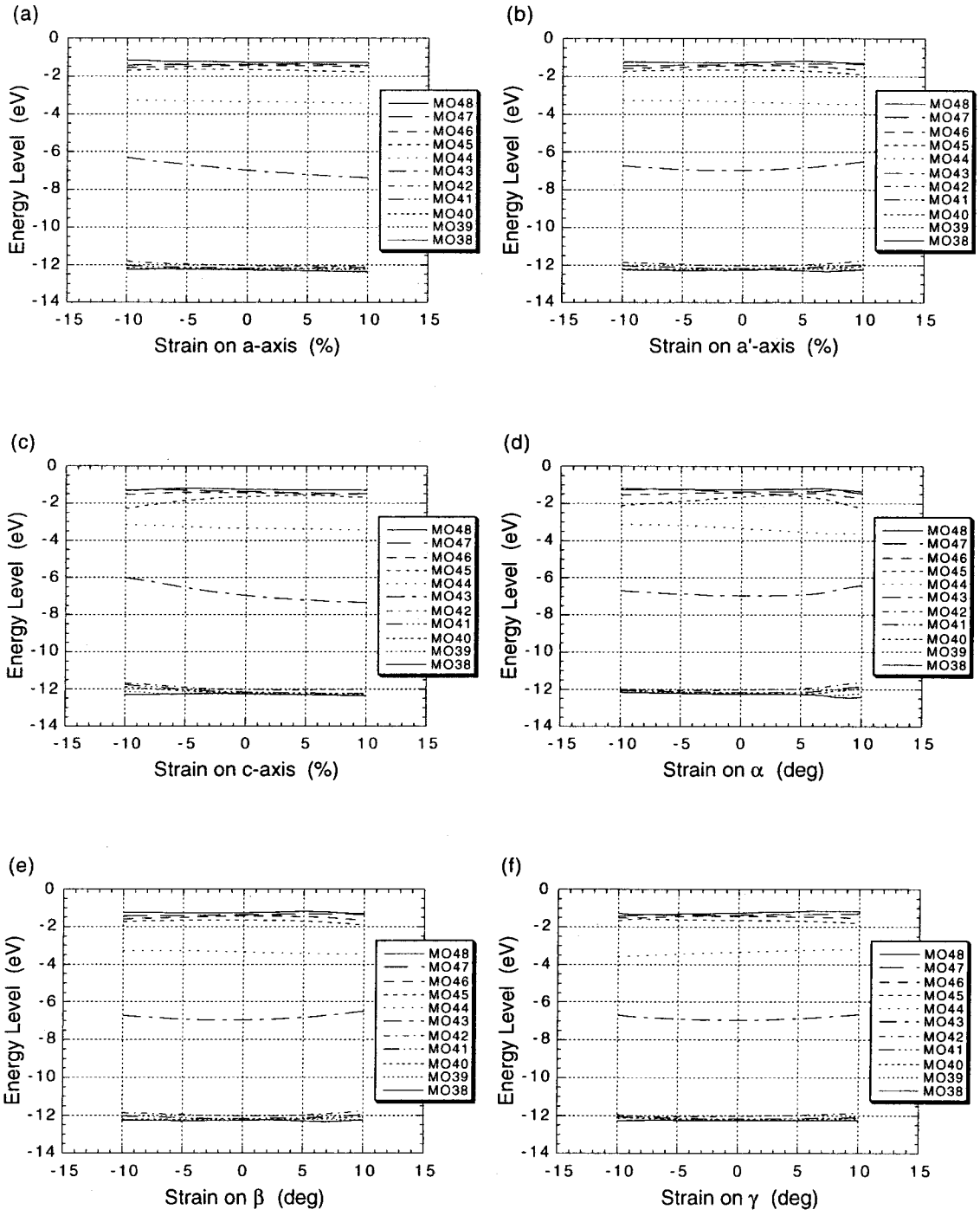

Figure 4-6. Energy level changes for different strain on each axis and angle.

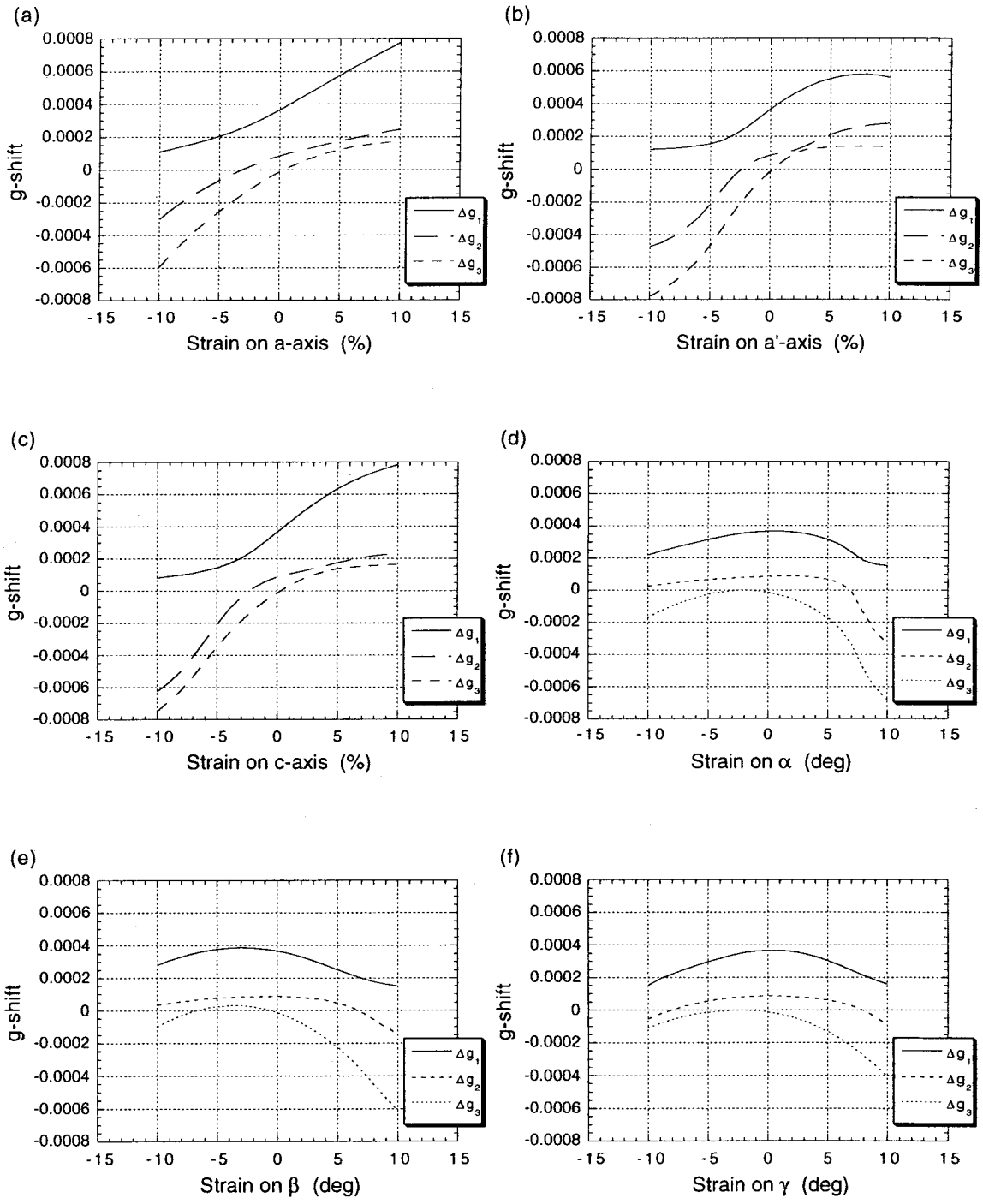

Figure 4-7. Changes of *g*-shift for different strain on each axis and angle.

CHAPTER 5

Quaternary Geological Studies on Drilling Core

ESR signals of radiation-induced centers accumulated in quartz can tell geological or geographical information in Quaternary because some of those centers have been accumulated for a few million years under an annual dose of 0.1-1 mGy/a. This chapter includes two studies on drilling core samples by ESR. The first study revealed the thermal history, cooling rate and denudation rate of the young intrusive granite in Great Caucasus, Russia. It also indicated that the ratio of signal intensities of the E′ center before and after heating around 250 °C had good correlation to storage temperature in the host rock. The latter study is a survey of thermal disturbance in the drilling core penetrating the Nojima geological fault at 625 m in depth that was moved at the Kobe earthquake in 1995, Japan.

5.1 Signal growth of radiation-induced centers in cooling system

Orogenic belts can be seen where the crusts are uplifted due to tectonic movements of the plates. The uplift rate is around a few mm/a in active places. The host rock in such regions cools down at a particular cooling rate determined by the geothermal gradient and the uplift rate. A growth of ESR signal intensity can be easily calculated on the assumption of the constant cooling rate, though several cooling systems were proposed (see Dodson 1973).

As described in chapter 1, radiation-induced centers are not stable thermally and disappear typically in the manner of the first or second order decay kinetics.

$$\frac{dn}{dt} = a\dot{D} - \nu n \quad \text{(for the first order)}, \tag{5-1}$$

$$\frac{dn}{dt} = a\dot{D} - \lambda n^2 \quad \text{(for the second order)}, \tag{5-2}$$

where the rate constant ν and λ are defined as

$$\nu = \frac{1}{\tau} = \nu_0 \exp\left(-\frac{E_a}{k_B T}\right), \tag{5-3}$$

$$\lambda = \lambda_0 \exp\left(-\frac{E_a}{k_B T}\right), \tag{5-4}$$

where E_a is activation energy for the center, k_B is Boltzman constant and ν_0 and λ_0 are called pre-exponential factors for the first and second kinetics. The equations (5-1) and

(5-2) can be transferred to

$$\frac{d}{dt}\left(\frac{n}{a\dot{D}}\right) = 1 - \frac{1}{\tau}\frac{n}{a\dot{D}} \quad \text{(for the first order),} \tag{5-5}$$

$$\frac{d}{dt}\left(\frac{n}{a\dot{D}}\right) = 1 - \lambda a\dot{D}\left(\frac{n}{a\dot{D}}\right)^2 \quad \text{(for the second order).} \tag{5-6}$$

As $a\dot{D}$ is a production rate of defects, $n/a\dot{D}$ has a dimension of time and shall be called apparent age t_a. Then, these equations are expressed with t_a as

$$\frac{dt_a(t)}{dt} = \left(1 - \frac{t_a}{\tau}\right) \quad \text{(for the first order),} \tag{5-7}$$

$$\frac{dt_a(t)}{dt} = (1 - \lambda a\dot{D}t_a^2) \quad \text{(for the second order).} \tag{5-8}$$

Here it was assumed that the signal intensity was not saturated and that the annual dose was constant for the whole storage time. The equation (5-8) contains production efficiency of the center a while the equation (5-7) contains only the lifetime τ, so that the apparent age for the first order can be calculated using only the parameters of thermal stability of the center; activation energy E_a and frequency factor ν_0.

The numerical calculation was made for the constant cooling system with the first order decay kinetics to know how radiation-induced centers were accumulated in quartz. The reported parameters of thermal stability of the impurity centers in quartz were summarized in Table 5-1 but not close to each other for the same impurity center. Therefore, thermal stability of the center was assumed as activation energy of 1.5 eV and frequency factor of 2.6×10^{11} s^{-1}. The growth curves of signal intensity for different cooling rates were shown in Figure 5-1. For comparison, two other models of the center having different thermal stability ($E_a = 1.7$ eV or $\nu_0 = 2.6 \times 10^{10}$ s^{-1}) were also calculated for 20 °C/Ma and show in the Figure 5-1. The results indicate that the

Table 5-1. Thermal stability of the impurity centers in quartz.
This is the list of the reported thermal stability of the Ti and Al centers. The results indicate that each sample has own thermal stability of the center.

Center	Activation energy E_a (eV)	Frequency factor ν_0 (s^{-1})	Reference
Ti	1.0	2.9×10^7	(Fukuchi 1992)
Ti	1.7	4.1×10^{11}	(Toyoda & Ikeya 1991)
Al	2.4	3.0×10^{12}	(Imai *et al.* 1985)
Al	1.7	1.1×10^7	(Toyoda & Ikeya 1991)
Al	1.5	9.0×10^{12}	(Ikeya & Toyoda 1991)
Al	1.3	1.0×10^9	(Melnikov *et al.* 1989)

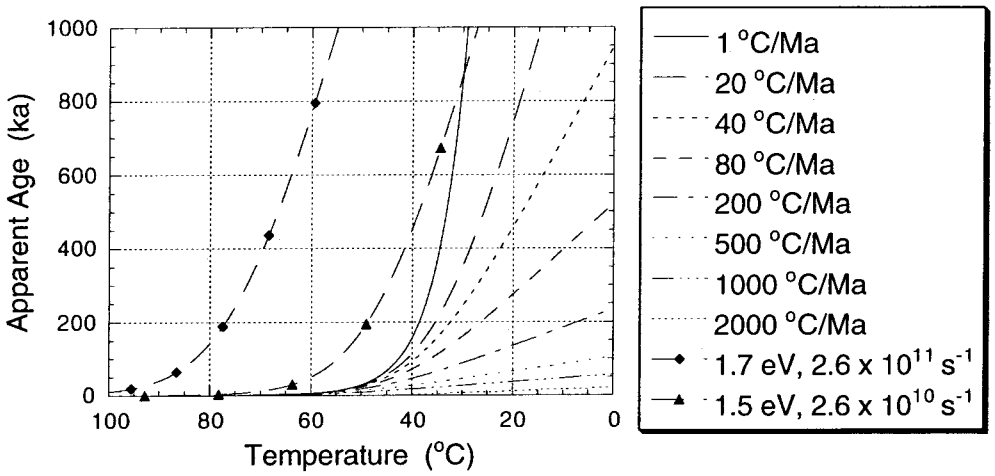

Figure 5-1. Signal growth at typical cooling rates.
Thermal activation energy and frequency factor of the center were assumed as 1.5 eV and 2.6 x 1011 s-1 for no marker lines, respectively. The lines with markers displayed the signal growth for the center of different thermal stability as shown in the legend. Start of accumulation of the radiation-induced defects is dependent on the thermal stability. Below a typical temperature, the curve gets close to the line reflecting the cooling rate.

temperature where the signal starts to be accumulated is dependent on the thermal parameters, activation energy and frequency factor. The curve become a line below a certain temperature (*e.g.* about 30 °C for the center of $E_a = 1.5$ eV or $\nu_0 = 2.6 \times 10^{11}$ s^{-1}) and the slope is referred to the cooling rate.

5.2 Assessment of denudation and cooling rates in Quaternary

(i) The intrusive Eldzhurtinskiy granite in Great Caucasus

The Eldzhurtinskiy granite is located in the Great Caucasus, Russia between the Caspian Sea and the Black Sea (Figure 5-2). This area is very active orogenic belt due to the collision of the Arabian Plate moving to the north into the Eurasian Plate, which causes the high mountain ranges in the Great Caucasus. The highest mountain is a volcanic Mt. El'brus (5642 m) located in the middle of the Caucasus. The Eldzhurtinskiy granite is one of about a dozen small plutonic intrusions into the crystalline basement of the central part of the Caucasus and appears in the northwest of the Chegem caldera that produced rhyolitic to dacitic welded tuff in Pliocene (around 2.8 Ma) (Gazis *et al.* 1995). This is very young intrusive granite and the age of intrusion was reported as 1.9 and 2.5 Ma determined by K/Ar (Borsuk 1979) and ^{40}Ar/^{39}Ar (Hess *et al.* 1993) methods, respectively.

Figure 5-3 shows the geological environment around the Eldzhurtinskiy granite and the cross section of the granite on the line of two boreholes. The Baksan River starts at the foot of the Mt. El'brus and have created a deep valley on the granite due to denudation erosion. The two drilling cores were obtained; one was from the top of the

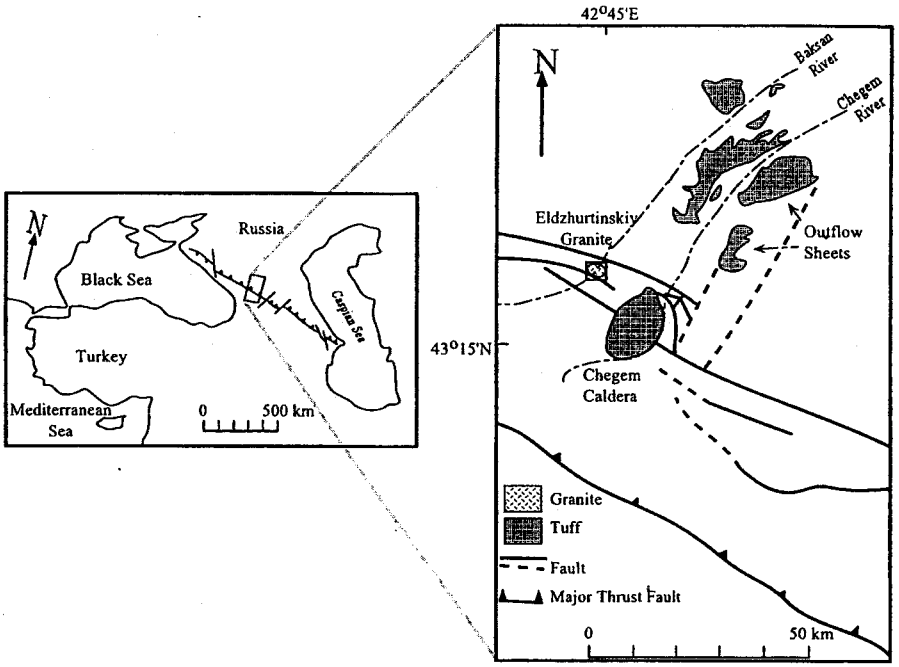

Figure 5-2. Location of the Great Caucasus and the Eldzhurtinskiy granite. The Great Caucasus is located between the Caspian Sea and the Black Sea. The Eldzhurtinskiy granite is one of intrusive granite in this region.

mountainside and the other was beside the Baksan River. For later reference, I shall call upper core for the mountainside and lower core for the riverside. The granite is described as I-type biotite granite and consists of mainly quartz, plagioclase, potassium feldspar and biotite as well as zircon, monazite and sphene as accessory minerals (< 1%). A share zone at 3850 m in depth separates the Eldzhurtinskiy granite from more leucocratic two-mica granite. Temperature was measured continuously in the lower borehole (Figure 5-4).

(ii) Samples and experimental

Rock samples were taken from the both cores and summarized in Table 5-2. Each piece was crushed and sieved, and quartz was separated using heavy liquid and magnetic separation. Only the piece at 637 m in upper core contained much chloride, suggesting that hydrothermal alteration occurred locally in the past.

Quartz samples were measured on ESR spectrometer (Bruker ECS 106). The E′ center was detected at room temperature under a microwave power of 0.005 mW and a modulation magnetic field of 0.05 mT. As the natural signal intensity of the E′ center was very weak, the spectra were accumulated 1500 times for 8.75 hours. The Al and Ti centers were detected at 77 K under 10 mW and 0.1 mT. Each measurement took 4.5 min and the average value of the signal intensities for five times was calculated for analysis. After both measurements, samples were heated at 270 °C for 1 hour to increase the signal intensity of the E′ center. Irradiation source of γ-rays was ^{137}Cs.

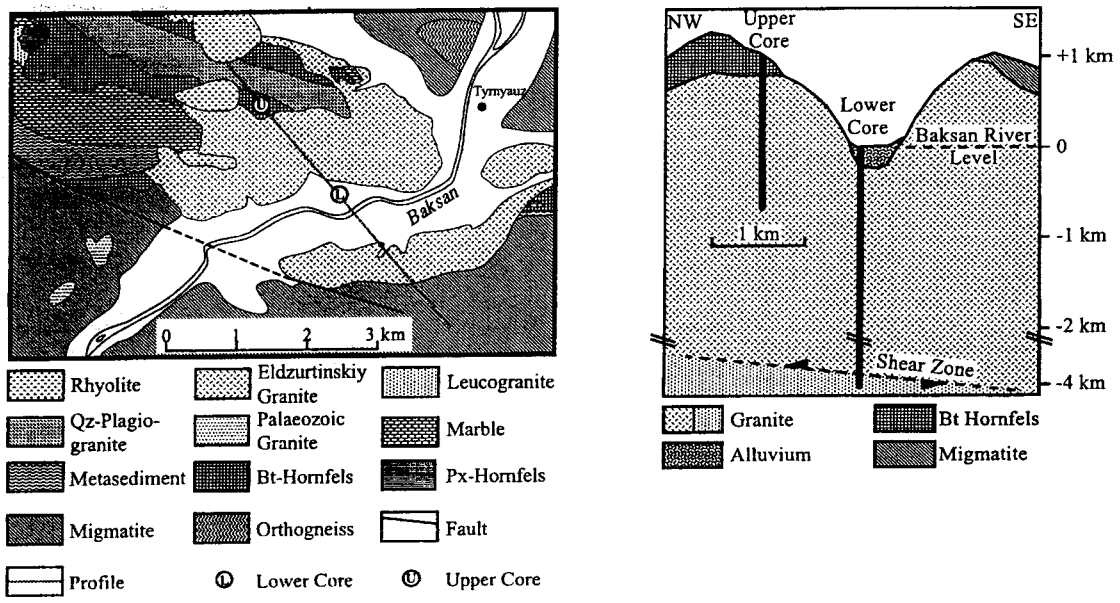

Figure 5-3. Geological map and cross section on the indicated line.
The Baksan River eroded the Eldzhurtinskiy granite. The upper core was obtained in mountainside and the lower core was beside the river.

(iii) Storage temperature and the ratio I_1/I_2 of E′ center intensities

The intensity of the E′ center increases on heating. McMorris (1970) suggested that this behavior could be used for palaeo-thermometry. The isochronal annealing experiment (Figure 1-7) by heating for 15 min steps showed that the intensity of the E′ center started to increase around 180 °C, gave the maximum around 270 °C, decreased and then disappear around 400 °C (Toyoda & Ikeya 1991). The ratio of the intensity of the unheated sample (I_1) to the maximum intensity around 250 °C (I_2) is dependent on

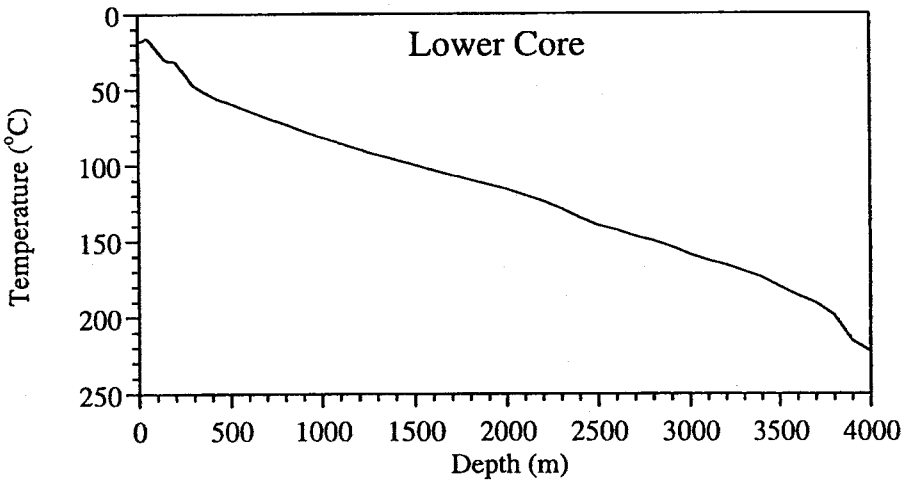

Figure 5-4. Measured temperature on the lower borehole.
It almost monotonically decreased along the depth.

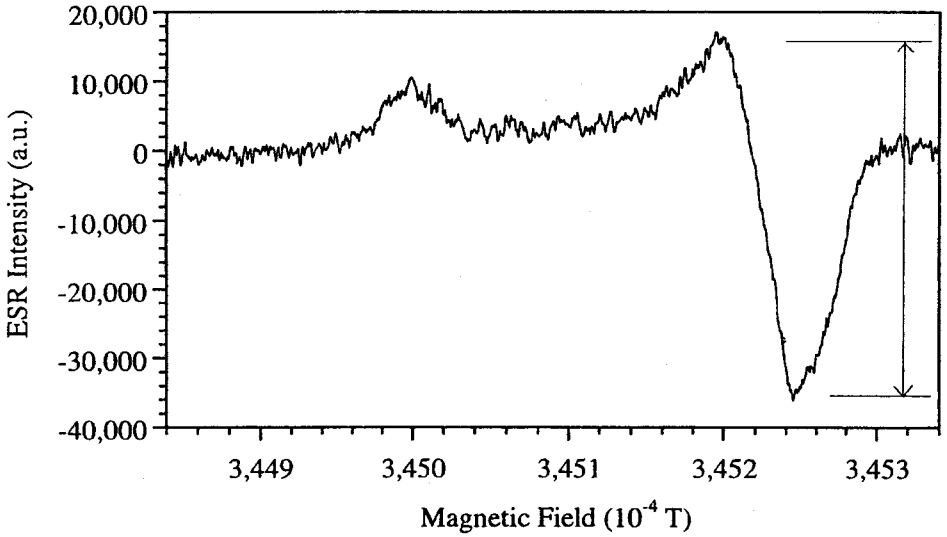

Figure 5-5. ESR spectrum of the E′ center.
The spectrum of the E′ center was obtained for 8.75 hour measurements. The arrow height was evaluated as the signal intensity.

the storage temperature of the sample (Toyoda *et al.* 1993a). The drilling core samples into oil-bearing sandstone in eastern China has been tested to check that the ratio of I_1/I_2 is closely associated with recent storage temperatures (Chen *et al.* 1997).

ESR spectrum of the E′ center in the most upper sample of the lower core is

Table 5-2. Great Caucasus core samples.
Temperature for the upper core '*' was estimated with the ratio I_1/I_2. The annual dose was calculated with the concentration of natural isotope, ^{238}U, ^{232}Th and ^{40}K obtained by neutron activation analysis.

Sample	Field	Depth (m)	Temperature (°C)	Annual dose (mGy/a)
		Upper core		
1373	96/85	338	36.7*	5.64 ± 0.33
1474	97/85	448	43.7*	5.99 ± 0.37
1374	99/85	637	84.3*	5.77 ± 0.38
1375	101/85	848	48.3*	6.09 ± 0.41
1376	104/85	1148	56.1*	5.45 ± 0.33
1377	106/85	1336	61.6*	4.77 ± 0.29
1378	107/85	1620	79.3*	4.89 ± 0.28
1379	108/85	1697	76.6*	4.37 ± 0.27
		Lower core		
1380	1/90	258	40.6	6.39 ± 0.35
1381	2/90	385	53.7	6.35 ± 0.32
1382	3/90	562	62.2	6.70 ± 0.37
1383	4/90	660	66.8	6.89 ± 0.34
1475	5-2/90	792	72.6	7.43 ± 0.49
1476	10-4/90	1334	94.4	6.57 ± 0.59
1477	17-1/90	1835	111	7.79 ± 0.44

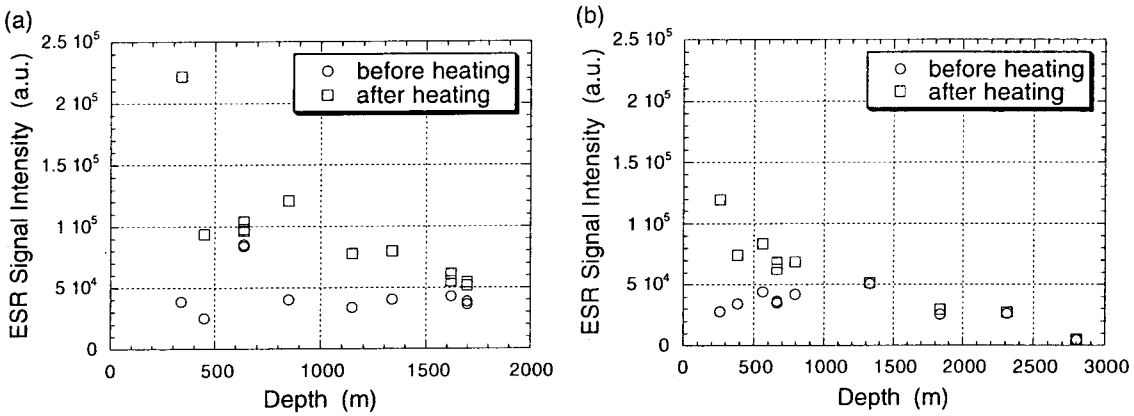

Figure 5-6. The E′ center for both the cores.

The behavior for the upper core is in (a) and for the lower core in (b). The intensity before heating I_1 'O' is almost constant for all samples except for the sample at 637 m in the upper core. The intensity after heating I_2 '□' shows the relation with the depth.

shown in Figure 5-5. The signal intensity was taken by peak to peak as shown in Figure 5-5 because the spectral shapes did not change for all experiments.

Figure 5-6 shows the signal intensity of the E′ center before and after heating against the depth of the drilling cores. The amazing result is that the intensity I_1 was nearly constant for the most samples above 2500 m. However, once sample was heated at 270 °C, the signal intensity I_2 showed clear relation to the depth.

This can be explained as follows. A precursor of the E′ center is oxygen vacancy. The oxygen vacancy has two electrons, which is the most thermally stable but not detectable by ESR. It can be produced much slowly by natural radiation in comparison with the electron or hole trapped centers (Odom 1982, Grün 1982), so that the number of oxygen vacancy may be constant for all samples. The result of the constant E′ center indicates almost no growth by natural radiation for about 1 Ma. Although the E′ center increases by heating, the Al center decreases at the same time. Once a hole is released from the Al center by heating and trapped by the oxygen vacancy, an unpaired electron appears and the E′ center is formed. Therefore, the behavior of the intensity I_2 after heating may be due to the increase of the hole-trapped center like the Al center. This model is concordant with the result of the Al center as discussed later.

The ratio of I_1/I_2 was plotted in Figure 5-7. This ratio increased monotonically up to 1 and almost saturated around 1500 m. A sample at 637 m in upper core deviated from the line because the sample was already heated by hydrothermal process.

The temperature was measured only in the lower borehole. The ratio for the lower core was plotted against the temperature in Figure 5-8. The result was in very good correlation to storage temperature and indicates that the ratio I_1/I_2 can be used for estimation of storage temperature. The line obtained by least square fitting was shown together in Figure 5-8. The storage temperature was estimated from the ratio

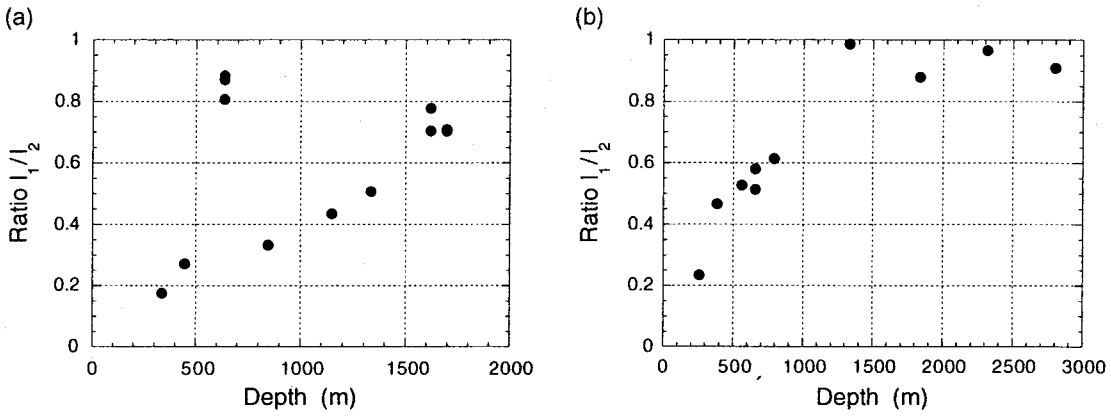

Figure 5-7. The ratio I1 / I2 for both the core.
The ratio increased to 1 except for the sample at 637 m in the upper core. The upper core is in (a) and the lower one is in (b).

I_1/I_2 for the upper core where no temperature data were available (Figure 5-9). The temperature gradually decrease except for the sample 637 m, indicating that the ratio I_1/I_2 can be useful for a survey of local unknown thermal events in Quaternary.

(iv) Assessment of denudation rate and cooling rate by ESR

ESR spectrum of the Al and Ti centers was shown in Figure 5-10. The Ti centers with a compensator of Li^+ and H^+ were detected. One series of the signal intensity for each center, indicated in the Figure 5-10, was used for analysis because of lower measurement errors. The signal intensities of the Al and Ti center were shown in Figure 5-11. The sample of the upper core at 637 m showed the smaller intensity than

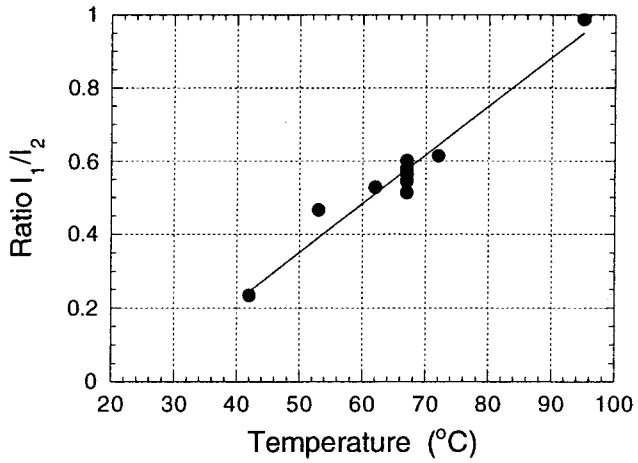

Figure 5-8. The ratio I_1/I_2 against the temperature for the lower core.
This is a good correlation between the ratio and the storage temperature. The line was obtained by least square fitting and used for estimating the storage temperature for the upper core.

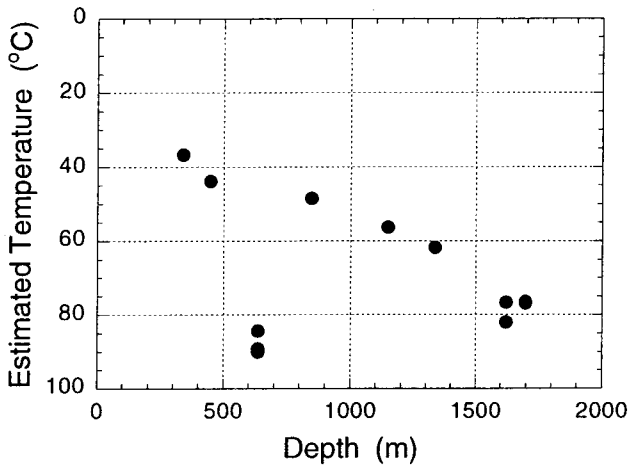

Figure 5-9. Estimated temperature for the upper core.
The temperature monotonically increased. The sample at 637 m was deviated from the envelope due to hydrothermal effect on the ESR signals.

the value expected from the curve due to the thermal effect. This point was omitted for the later discussions.

The apparent age t_a was obtained by the regeneration method described in chapter 1 and shown in Figure 5-12. The slope of the sample in the upper samples should be close to the cooling rate and the denudation rate as shown in the section 5.1. The denudation rates estimated with the two data set of the upper samples were 5.5 ± 0.5 mm/a (Al center) and 5.6 ± 1.1 mm/a (Ti center) for the lower core and were 2.7 ± 0.5 mm/a (Al center) and 2.4 ± 0.6 mm/a (Ti center) for the lower core. The denudation rate for the lower core is much higher because the Baksan River beside the lower borehole erodes the granite. The cooling rates were estimated in the same way

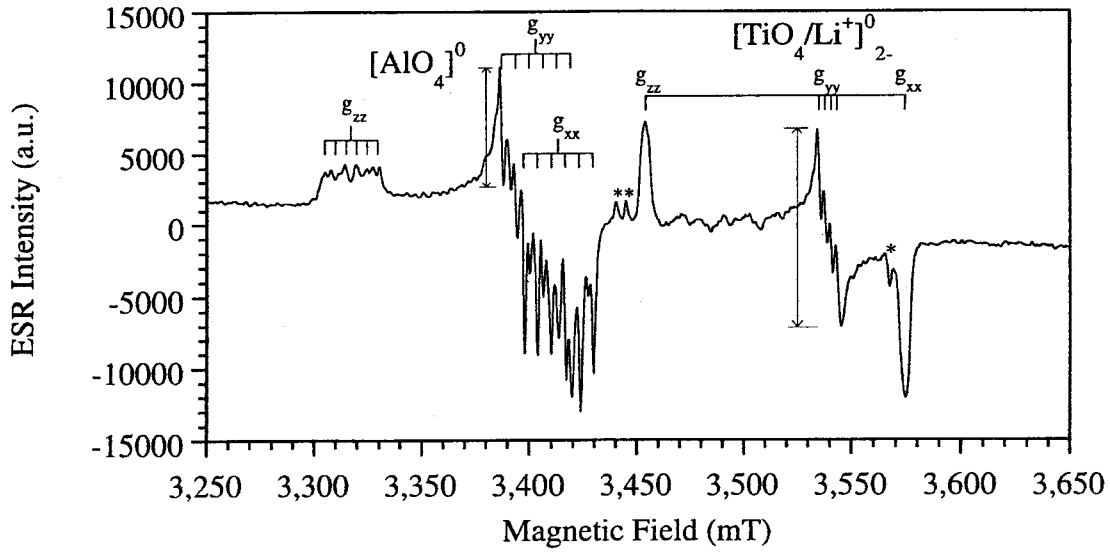

Figure 5-10. ESR spectrum of Al and Ti centers.

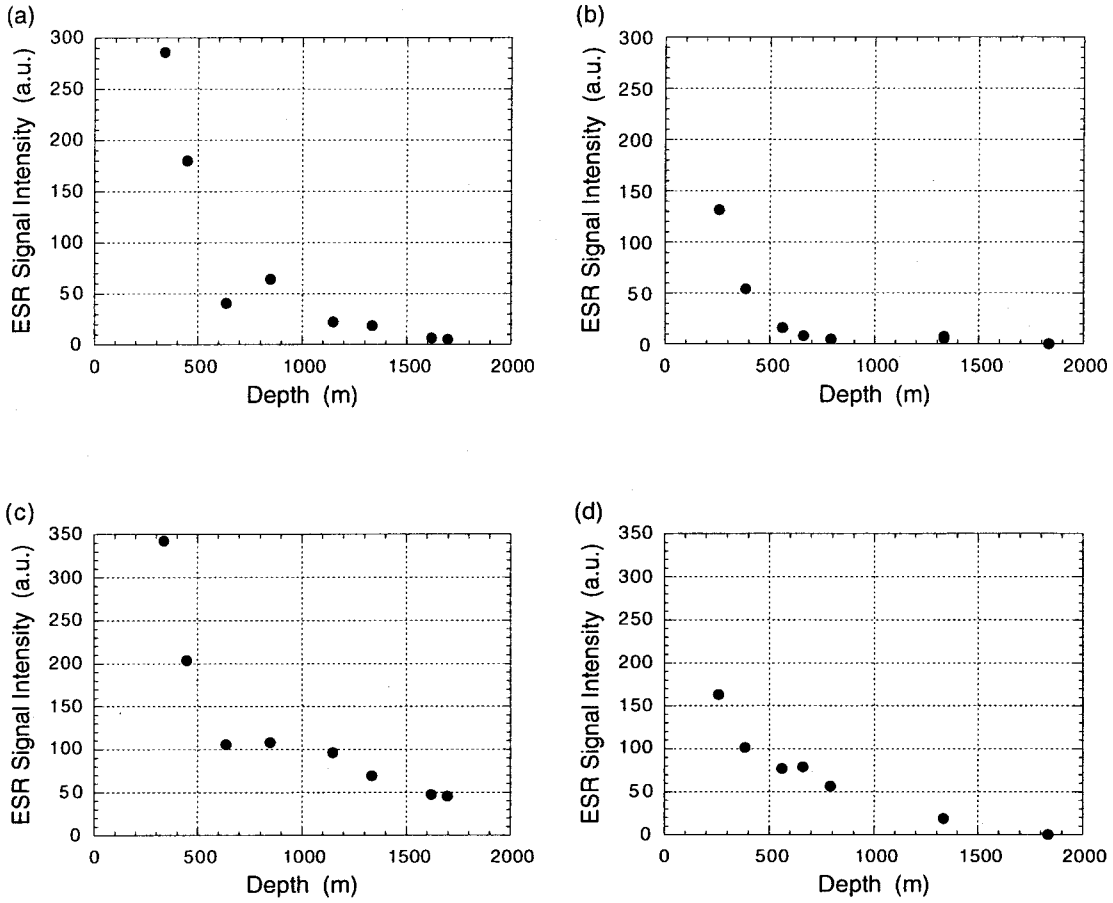

Figure 5-11. Al & Ti centers.
(a) Al centers for the upper core. (b) Al center for the lower core. (c) Ti center for the upper core. (d) Ti center for the lower core.

as 570 ± 55 °C/Ma (Al center) and 600 ± 120 °C/Ma (Ti center) for the lower core. For the upper core, the cooling rates were obtained with the estimated temperature from the ratio I_1/I_2 as 180 ± 35 °C/Ma (Al center) and 160 ± 40 °C/Ma (Ti center). The difference on both the cores is also due to denudation erosion by the Baksan River. One can estimate cooling rate and denudation rate using the curves calculated in the section 5.1 if lifetime of the center, *i.e.* activation energy and frequency factor, is known.

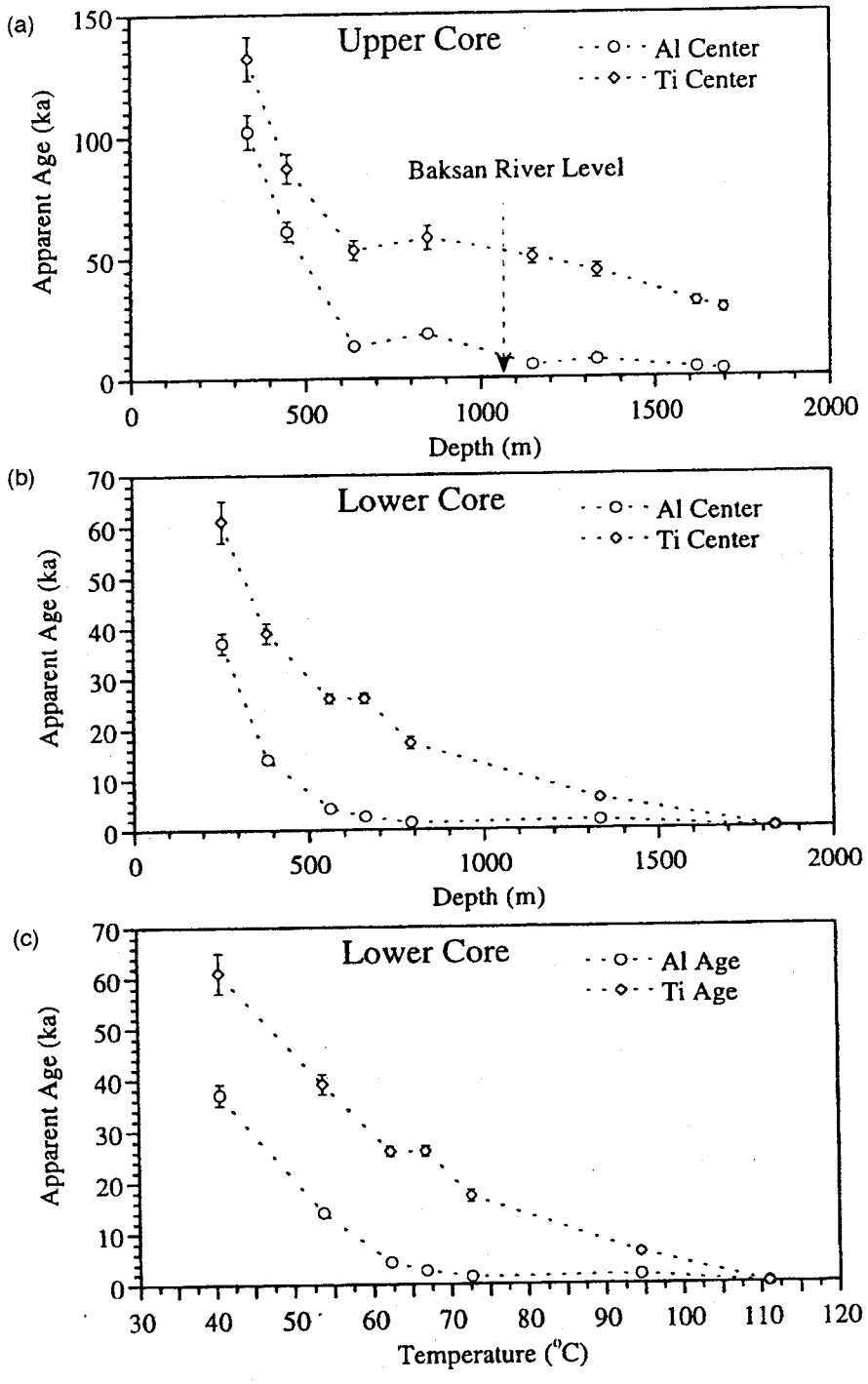

Figure 5-12. Apparent ages for the Al and Ti centers.
The obtained apparent ages were shown in (a) for the upper core and in (b) for the lower core. The same data were plotted in (c) with temperature.

5.3 A survey of local thermal events on the Nojima fault zone

The ESR study of fault material was started by Ikeya *et al.* (1982) for dating the latest fault activity. After that, several groups have investigated fault material by ESR (*e.g.* Buhay *et al.* 1988, Fukuchi 1991, Lee and Schwarcz 1993). The recent drilling core projects in the Nojima fault, Japan gave the first opportunity to get the fresh fault sample at a depth of several hundred meters. ESR studies were already reported using fault gouge on the Nojima core to discuss the possibility to make ESR signals reset by fault activity (Yamanaka *et al.* 1998; Fukuchi, 1998). This section is a short report about changes of ESR signal intensities in the whole Nojima core samples to investigate local unknown thermal events.

(i) Nojima fault and drilling core projects

The Nojima fault is located in the Awaji island, Hyogo prefecture, Japan

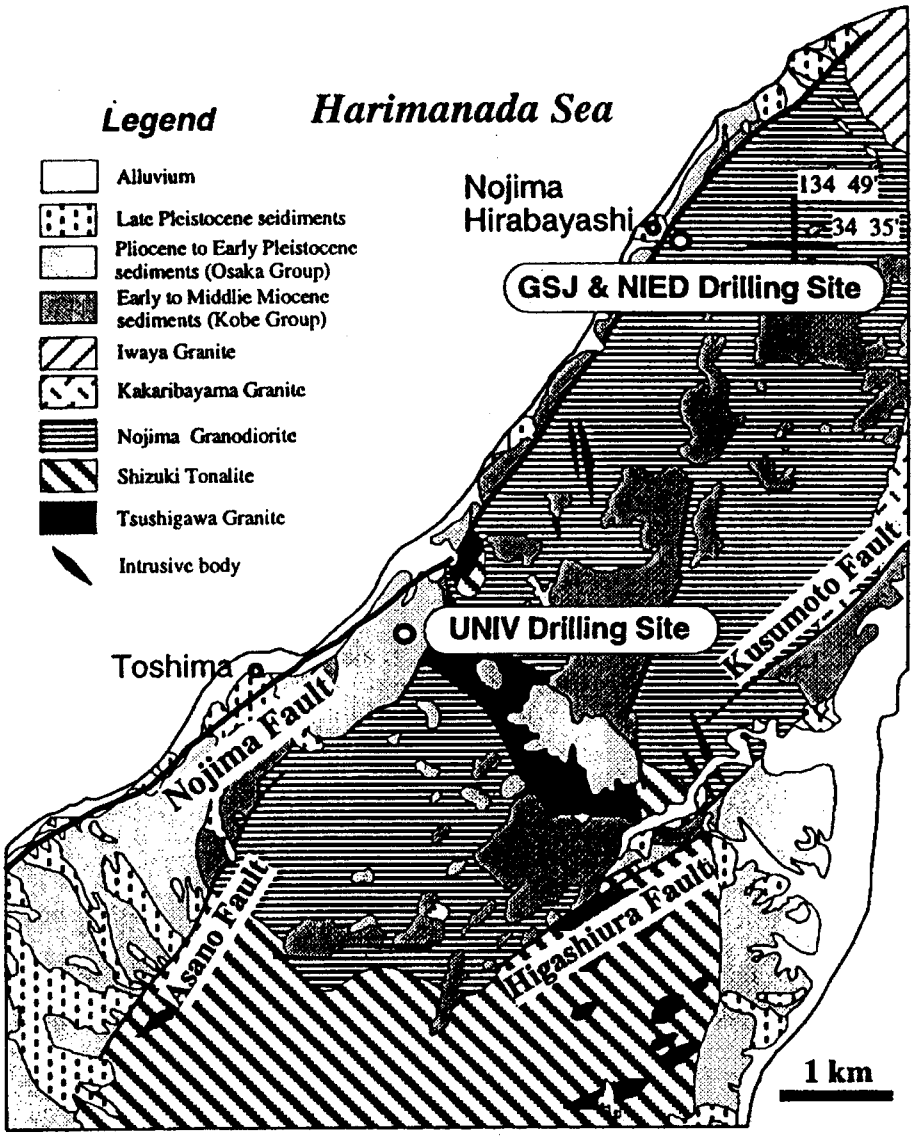

Figure 5-13. Location of the Nojima fault and the GSJ borehole

(Figure 5-13) and caused the Kobe earthquake (the Hyogoken-Nambu earthquake), M = 7.2 on January 17, 1995. The boreholes were drilled in the vicinity of the epicenter by university group [Ando], Geological Survey of Japan [GSJ: ~Ito] and National Research Institute for Earth Science and Disaster Prevention [NIED: ~Ikeda]. The core samples were obtained to study physical and chemical properties of the fault rock while the boreholes were used for *in-situ* seismic and material analysis like permeability and heat flow. The uniqueness of these core projects is the first obtained fresh material around the geological fault from deep places, especially just after the intense earthquake.

(ii) Sample and Experimental

The GSJ Nojima core was analyzed in this study. The whole core description is shown in Figure 5-14 (Ito *et al.* 1996, Tanaka, Ohtani). The fault zone is characterized by altered and deformed granodiorite from 426.1 m to 746.7 m with fault core of fault gouge at 623.3-625.1 m and 707.8-707.9 m and cataclasite at 525.5-525.7 m and 669.5-672.7 m. The host rock is the Nojima granodiorite formed in late Cretaceous, about 84 Ma by Rb-Sr dating and classified as ilmenite-series granitoid [kinki-book]. All core pieces used for ESR measurements were indicated in the Figure 5-14 with a marker '◀' and summarized in Table 5-3. Most samples are granodiorite or weakly altered and deformed granodiorite. The samples near the fault gouge at 625 m are mostly deformed and do not remain the original structure of granodiorite at all.

Table 5-3. GSJ core samples.
The samples with marker '*' contains resin but no contaminant signals were overlapped to the radiation-induced centers in quartz.

Core & Sample No.	Depth (m)	Description	etc.
#1	156	Granodiorite	
#11	203	Granodiorite	
#21	251	Granodiorite	
#32	303	Granodiorite	
#42	347	Granodiorite	
#53	402	Granodiorite	
#65	459	Granodiorite	
#75-7A	507	Weakly altered and deformed granodiorite	
#84-11	550	Weakly altered and deformed granodiorite	
#97-14	617	Fault breccia	
#99-06	625	Light grayish green fault gouge	*
#99-22	625	Weakly altered and deformed granodiorite	*
#100-08	630	Weakly altered and deformed granodiorite	
#103-17	656	Weakly altered and deformed granodiorite	*
#105-24	669	Weakly altered and deformed granodiorite	*
#106-13	676	Granodiorite	
#111-15	696	Weakly altered and deformed granodiorite	
#121-16	743	Weakly altered and deformed granodiorite	

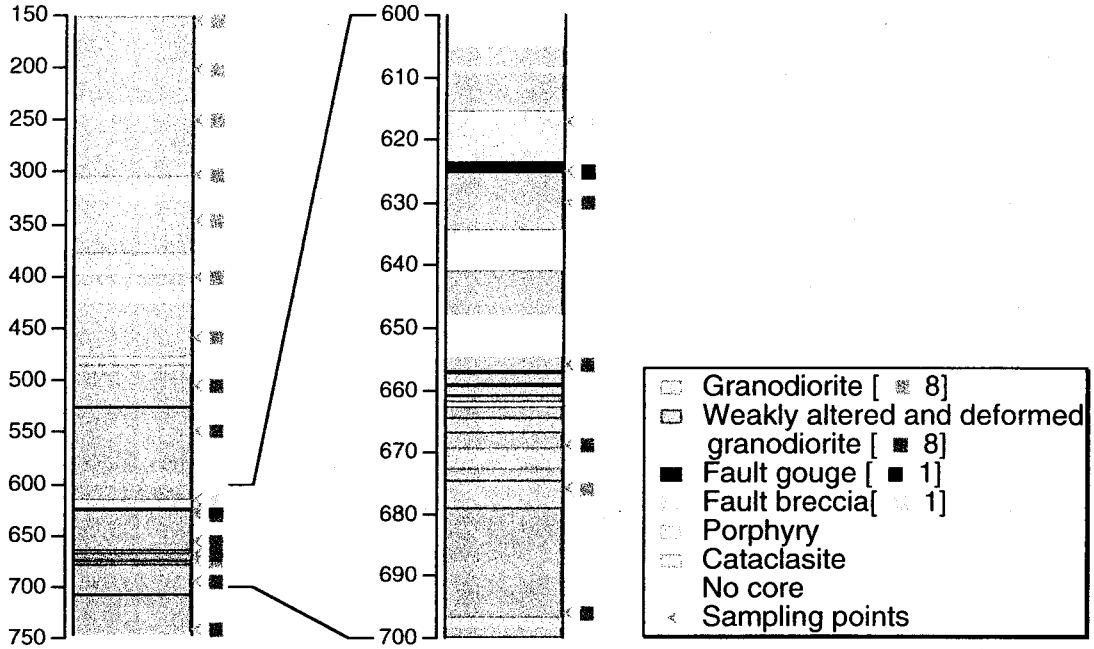

Figure 5-14. GSJ core description.
The marker '◄' indicates the sampling points for ESR analysis.

Thermochronological study was carried out on the same drilling core with fission tack method [(open book FT)]. The results in Figure 5-15 shows that shortened tracks were found in two regions; one is upper place from 150 m to 350 m and the other is in the fault zone around 650 m, which indicating that any thermal events occurred in those regions. They got the quite similar results on the other Nojima core samples [iland ark].

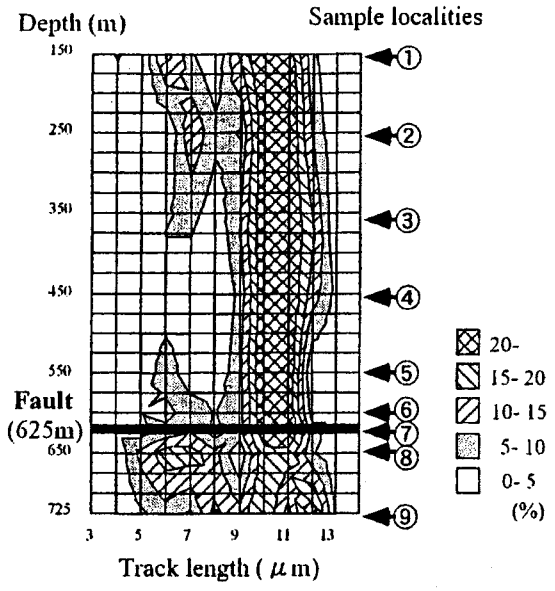

Figure 5-15. FT study of the GSJ Nojima core.

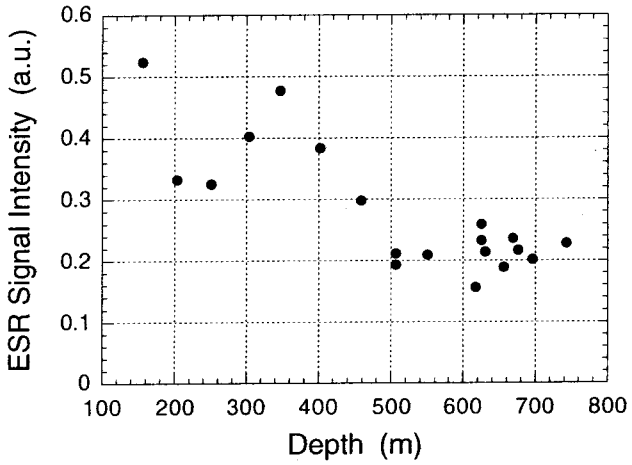

Figure 5-16. Ti center on GSJ core sample.

A piece of about 1 cm in thickness was taken out by saw in the middle of each full or half-cut core. The surface of the piece was cut off about 3-5 mm to remove resin that was used for keeping the core structure. The obtained piece was gently crushed into small grains in an alumina mortar and sieved into four aliquots based on grain size of 0-100, 100-250, 250-500 and more than 500 μm. Only the aliquot of 100-250 μm was used because the smaller grains were easily dissolved in HF acid and the larger grains gave a huge angular dependence on ESR spectra. Those samples were washed with 35 % HCl to dissolve carbonate and some other minerals and put in 10 % HF solution for 30-90 minutes to remove other minerals like feldspar and biotite. This solution can also remove surface of quartz grains that were damaged by external α-rays.

Samples were measured with ESR spectrometer (JEOL RE-2X) with a 100 kHz field modulation of 0.1 mT for the Al and Ti centers and of 0.05 mT for E′ center. The Al and Ti centers were detected at 77 K with a finger Dewar while the E′ center was at room temperature. Magnesium oxide with Mn^{2+} impurity was also measured simultaneously for calibration of signal intensities. Microwave power was 5 mW for the Al and Ti centers and 0.001 mW for the E′ center. After measurements, all were heated in an oven at 250 °C for 30 minutes. A ^{60}Co source of the γ-rays was used for irradiation.

(iii) Results and Discussions: Ti Center

The trend of the Ti center shown in Figure 5-16 is close to the results on the previous study of the intrusive granite. The Ti center decreased around the deformed granodiorite zone below 500 m. This may be due to the thermal effects. However, clear change was not observed around the fault gouge. The samples around 200-300 m also showed small intensities. In conclusion, the Ti center indicates that unknown local thermal events were happened in 200-300 m and the fault zone. This is concordant with the results of fission-track study as shown in Figure 5-15.

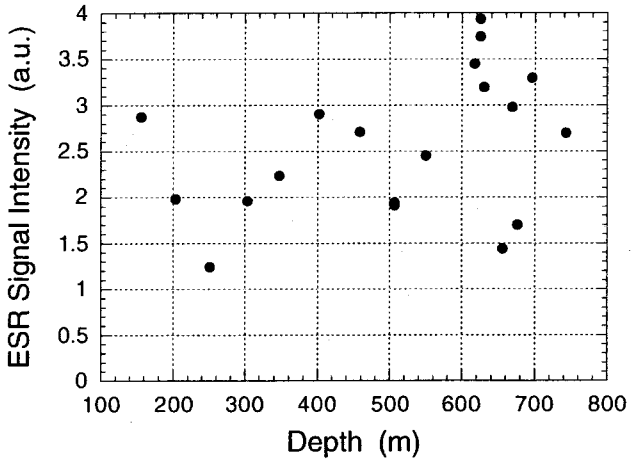

Figure 5-17. Al center on the GSJ core sample.

(iv) Results and Discussions: Al Center

The behavior of the Al center was plotted in Figure 5-17. The Al center decreased around 250 m, which is in good agreement with the results of the Ti center and the FT. However, the intensity did not decrease in the fault zone below 500 m but even increased in the heavily deformed region around 625 m.

The Al center in this samples may be more stable than the Ti center, so that the thermal event in the fault zone may not be sufficient to anneal out the Al center. The similar relation of thermal stability for those centers was reported by Toyoda and Ikeya (1991) in quartz samples taken from the Mannari granite, Japan (Figure 1-7 and Table 5dd-1). This granite was formed in late Cretaceous and classified as ilmenite-series granitoid, which is quite similar to the Nojima granodiorite.

As the Al center in the samples near 625 m did not increase by artificial γ-ray irradiation, those signals have been already saturated and the intensity may be related

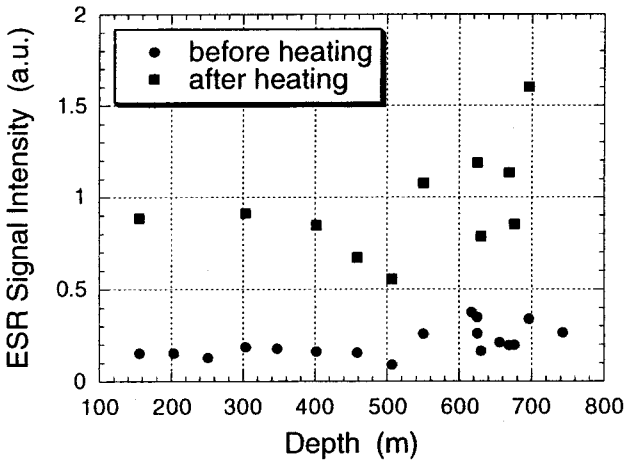

Figure 5-18. E′ center on the GSJ core.

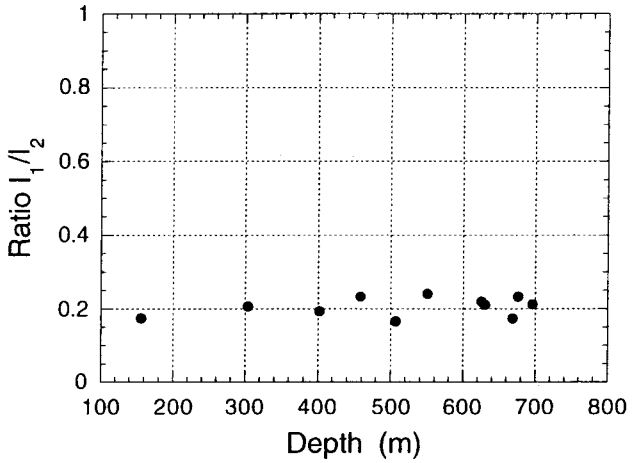

Figure 5-19. Ratio of I_1/I_2 on the GSJ core.

to aluminum content. Quartz in fault zone is crushed by fault activity and many cracks should be involved into quartz grains. Water containing aluminum ions dissolved from feldspar or clay minerals will surround quartz grains. Those aluminum ions may be attached on fresh surface or go into cracks in quartz grains. Silica in water will precipitate at the surface of the grains and rearrangement of SiO_2 network may include such aluminum atoms inside. This model might be the reason why the intensity of Al center increased in the region of fault zone.

(v) Results and Discussions: E′ Center

Signal intensity of the E′ center is almost constant for all samples except for a few samples near fault gouge around 625 m as shown in Figure 5-18. This is so similar to the case of the Eldzhurtinskiy granite in the previous section and indicates that the E′ center does not increase continuously by natural radiation as well.

The data of the E′ center in several samples after heating were also measured (Figure 5-18) to study whether unknown thermal events occurred locally or not. The ratio of the E′ center before (I_1) and after (I_2) heating was plotted in Figure 5-19. The all obtained ratio I_1/I_2 were around 0.2. Although the study in the previous section was tested above 40 °C, the storage temperature of the Nojima core was reported below 40 °C. Chen *et al.* (1997) investigated the relation between the ratio I_1/I_2 and the storage temperature up to 20 °C but the result did not show the clear relation in low temperature regions. This study indicates that there is no relation between the ratio I_1/I_2 and the storage temperature below about 40 °. The different intensities of the E′ center may depend on the number of the precursor, oxygen vacancy due to the similar ratio I_1/I_2 for all samples. No thermal effect could be observed with the E′ center.

5.4 Summary

The core samples of the intrusive Eldzhurtinskiy granite in Grate Caucasus, Russia were investigated to reveal thermometry and to assess the cooling rate and

denudation rate in Quaternary. The estimated cooling and denudation rates were 170 oC/Ma and 2.5 mm/Ma for mountainside and 580 oC/Ma and 5.5 mm/Ma for riverside. The riverside has much larger cooling rate and denudation rate due to high erosion by the Baksan River. In addition, the ratio I_1/I_2 of the E′ center before and after heating was tested for temperature assessment successfully.

The GSJ Nojima drilling core sample penetrating the main Nojima fault at 625 m was analyzed by ESR. No high thermal event occurred around the fault gauge during the Kobe earthquake in 1995 because the radiation-induced centers of the Al, Ti and E′ centers in quartz were not annealed out. However, thermal event happened possibly in Quaternary around the depth of 200-300 m in the host rock, the Nojima granodiorite due to the decrease of the Ti and Al centers.

CHAPTER 6

Conclusion

Radiation-induced centers in quartz and stishovite were investigated with both of experimental and theoretical methods. This thesis revealed the followings. (1) Two unidentified electron centers having orthorhombic g-tensors ($g_1 = 1.9764$, $g_2 = 1.9527$ and $g_3 = 1.9370$; $g_1 = 1.9749$, $g_2 = 1.9572$ and $g_3 = 1.9331$) were found in synthetic stishovite and identified as an electron trapped by the impurity of titanium ion (the Ti center) due to the relatively large g-shift. Two possible models of the Ti center (interstitial and substitutional) were considered. The analogue of the symmetry on the g-factors of the interstitial Ti center in rutile implies that the latter center may be interstitial Ti center in stishovite. (2) The g-factors of the impurity centers in stishovite were calculated by the discrete variational (DV)-Xα method and qualitatively in good agreement with the experimental results. (3) The OSL of synthetic stishovite was observed for the first time under infrared laser (830 nm) and blue light emitting diodes (470 nm). The blue light stimulated luminescence (BLSL) was still measurable after heating up to 450 °C. The centers related to BLSL are very stable and may be useful for geochronology of impact craters. (4) The g-shift changes of the E′ center in strain-introduced quartz were evaluated by semi-empirical molecular orbital calculation with MOPAC. It was confirmed that the changes of molecular orbital caused the distribution of g-factors in crushed quartz rather than the distribution of energy splitting. (5) The centers induced by sudden pressure release were found in stishovite. One signal appears at axial g-factors ($g_{//} = 2.00181$ and $g_{\perp} = 2.00062$) and the other appears at isotropic g-factor (2.00305). These centers may be formed in amorphous region produced by sudden pressure drop because the similar centers were found in crushed quartz. (6) The core samples of the intrusive Eldzhurtinskiy granite in Grate Caucasus, Russia were investigated to reveal thermometry and to assess the cooling rate and denudation rate in Quaternary. The estimated cooling and denudation rates were 170 °C/Ma and 2.5 mm/Ma for mountainside and 580 °C/Ma and 5.5 mm/Ma for riverside. The riverside has much larger cooling rate and denudation rate due to high erosion by the Baksan River. (7) The GSJ Nojima drilling core sample penetrating the main Nojima fault at 625 m was analyzed by ESR. No high thermal event occurred around the fault gauge during the Kobe earthquake in 1995 because the radiation-induced centers in quartz were not annealed out. However, thermal event happened possibly in Quaternary around the depth of 200-300 m in the host rock, the Nojima granodiorite.

APPENDIX A

The Stone Tool from the Paleolithic Kami-Takamori Site in Japan[†]

The radiation-induced defects can be annealed out by heat. As this means that the accumulated age can be reset to zero, ESR and luminescence dating can be applied to an archaeological lithic tool heated at a particular time. The yellow stone tool with a reddish edge was discovered at the paleolithic site in Kami-takamori, northern Japan and was investigated by ESR to make sure of the thermal history and to determine the archaeological age. The Kami-takamori site is one of the oldest paleolithic sites in Japan. It may be one of the oldest stone tools in Japan and might be evidence that ancient men used fire to heat the stone or stone tool.

A.1 Introduction

In dating the burnt material, the heating temperature should be studied to ensure that all defects used for dating were annealed completely by heating. It can be estimated by ESR with signals of Fe^{3+} ion or radiation-induced centers (e.g. Warashina *et al.* 1981; Toyoda *et al.* 1993a), which was applied to soil investigation to distinguish between burnt and unburnt soil (Bartoll *et al.* 1996). Thermoluminescence (TL) dating was frequently applied to burnt stones, heated chert and burnt flint (Aitken 1985). ESR dating of heated chert and burnt flint, mainly composed of SiO_2, was reported (Garrison *et al.* 1981; Griffiths *et al.* 1983; Porat & Schwarcz 1991), while a burnt stone tool of the other material has not been studied by ESR.

The stone tool (7 cm x 4 cm x 1 cm) was discovered at the Kami-takamori site, northern Japan (Figure A-1), which Japanese archeologists consider to be possibly the oldest paleolithic site in Japan. The yellow stone tool is made of silicified tuff (Tsuchiyama 1995) and has a red belt at the edge (Figure A-2). It was collected under a tephra layer called Ks-1 (Figure A-3) which was dated by paleomagnetism as 560 ka (Hirooka *et al.* 1995). The other scientific methods of ESR and TL gave the age of a tephra layer called Tm-1 above the Ks-1 layer as 430-610 ka and 406-484 ka, respectively (Toyoda 1993; Nagatomo *et al.* 1995). In the present work, we have tried to reveal the thermal history of the stone tool and to date the stone tool directly using signals of Fe^{3+} ion and radiation-induced centers in SiO_2 by ESR.

[†] This is modified from a part of the master thesis (Tani 1997).

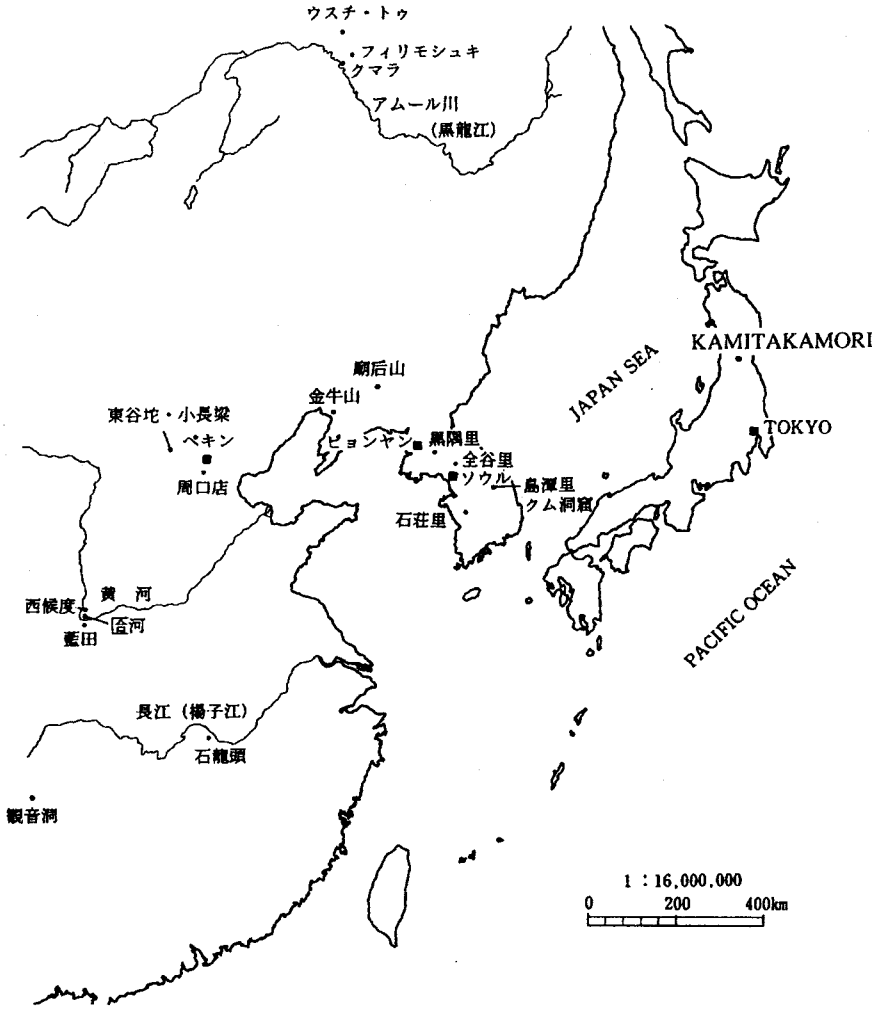

Figure A-1. The paleolithic sites in east Asia.

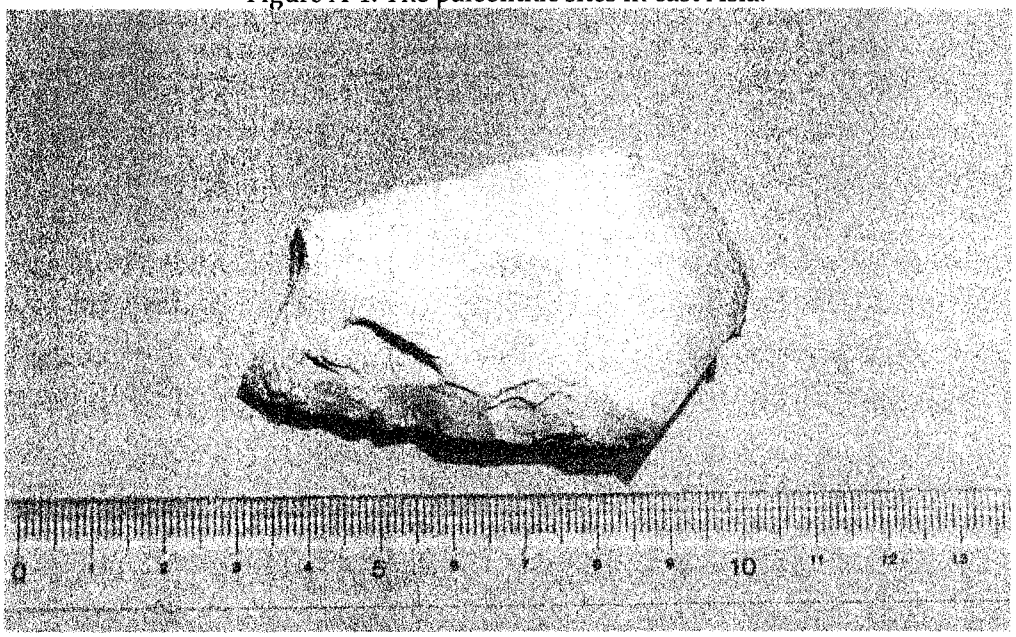

Figure A-2. The stone tool found at the Kami-takamori site.

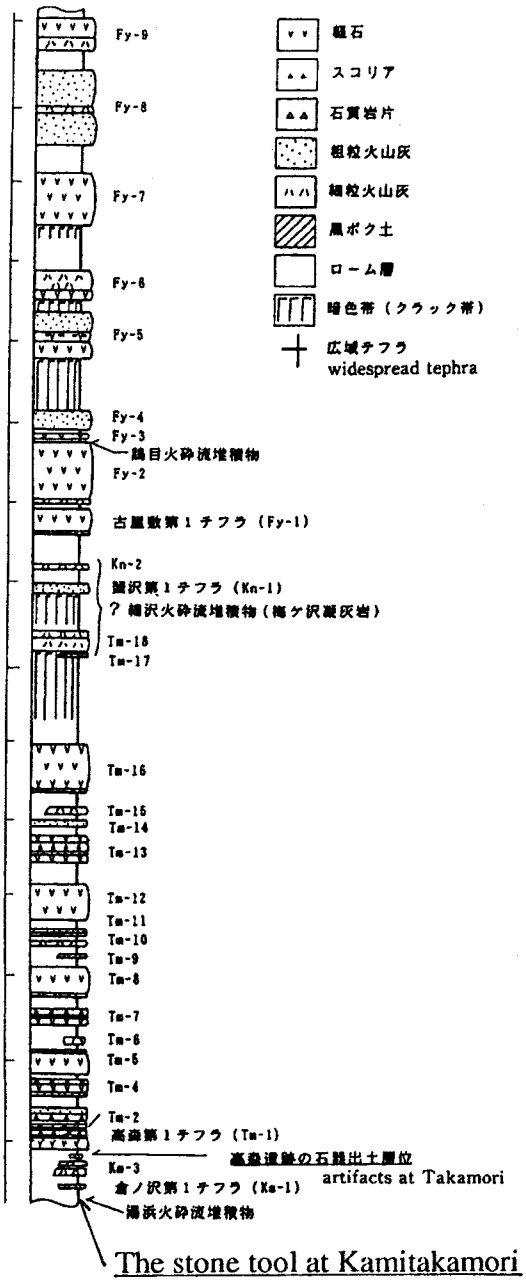

Figure A-3. The stratigraphical map at the Takamori site.
This was modified from (Soda 1993).

A.2 Experimental

Samples for ESR measurement were taken from both color parts of the stone tool using a diamond drill or saw. The diameter of each sample grain was approximately 1 mm. Some pieces were put in a cup and heated for 15 minutes in a furnace to study changes in the ESR spectrum and the color. A source of ^{60}Co was used in γ-ray irradiation to determine the equivalent dose, D_E. The samples were measured with a commercial X-band ESR spectrometer using a cylindrical cavity at a 100 kHz modulation field of 0.1 mT at room temperature and 77 K. ESR spectra in wide magnetic fields under 1 mW of microwave power were used for observing Fe^{3+} ion and radiation-induced centers. E', peroxy and Al centers in SiO_2 were measured under

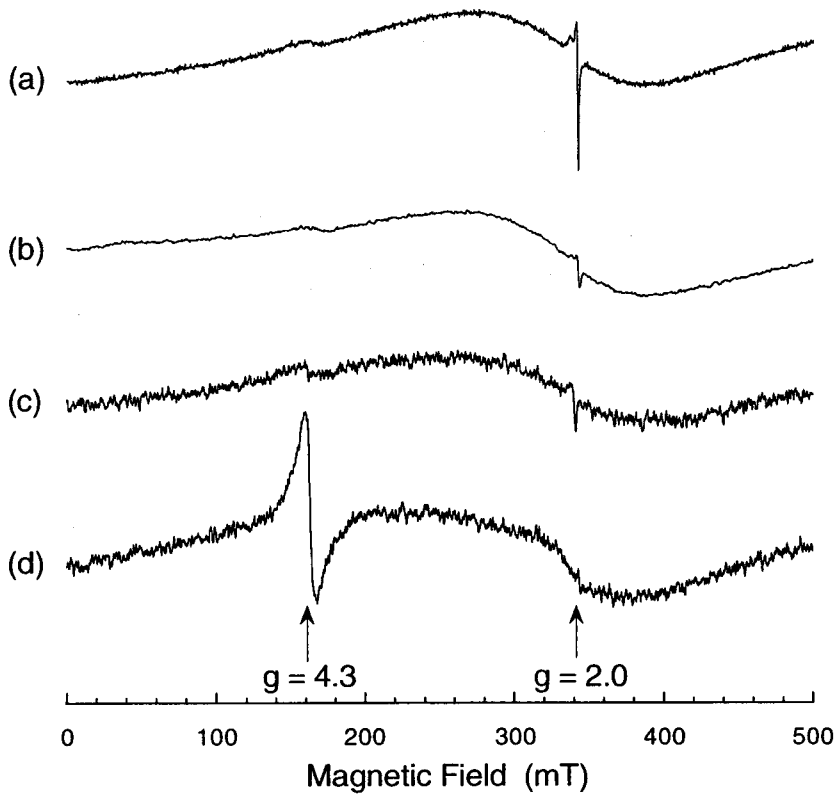

Figure A-4. ESR wide spectra.

0.01 mW, 1 mW and 5 mW, respectively.

A γ-ray spectrum of the stone was measured using γ-ray spectrometer with a 93.5 % low background co-axial Ge detector installed in Ogoya Underground Laboratory in order to estimate contents of ^{238}U, ^{232}Th and ^{40}K in the stone tool (Komura & Yamazaki 1996) before the stone tool was broken to take samples for ESR measurement. A mockup source made with potter's clay containing known amounts of ^{238}U, ^{232}Th and ^{40}K was measured under the same counting conditions to calibrate the counting efficiency of the Ge detector (Yokoyama & Nguyen 1981).

The material making up the yellow part was ground into fine powder for X-ray diffraction. X-rays emitted from a copper plate were used in the measurement. In addition, a thin section of the yellow part was prepared for observation by a light microscope.

A.3 Results and Discussions

A micro photograph of the thin section of the yellow part indicates that the stone consists of fine material and larger white or transparent grains of about 50 μm in diameter. The X-ray powder diffraction pattern shows that the crystalline component of the stone is mainly quartz (SiO_2). The white or transparent material on the micro photograph may be quartz grains. Fine material is not amorphous but may contain a

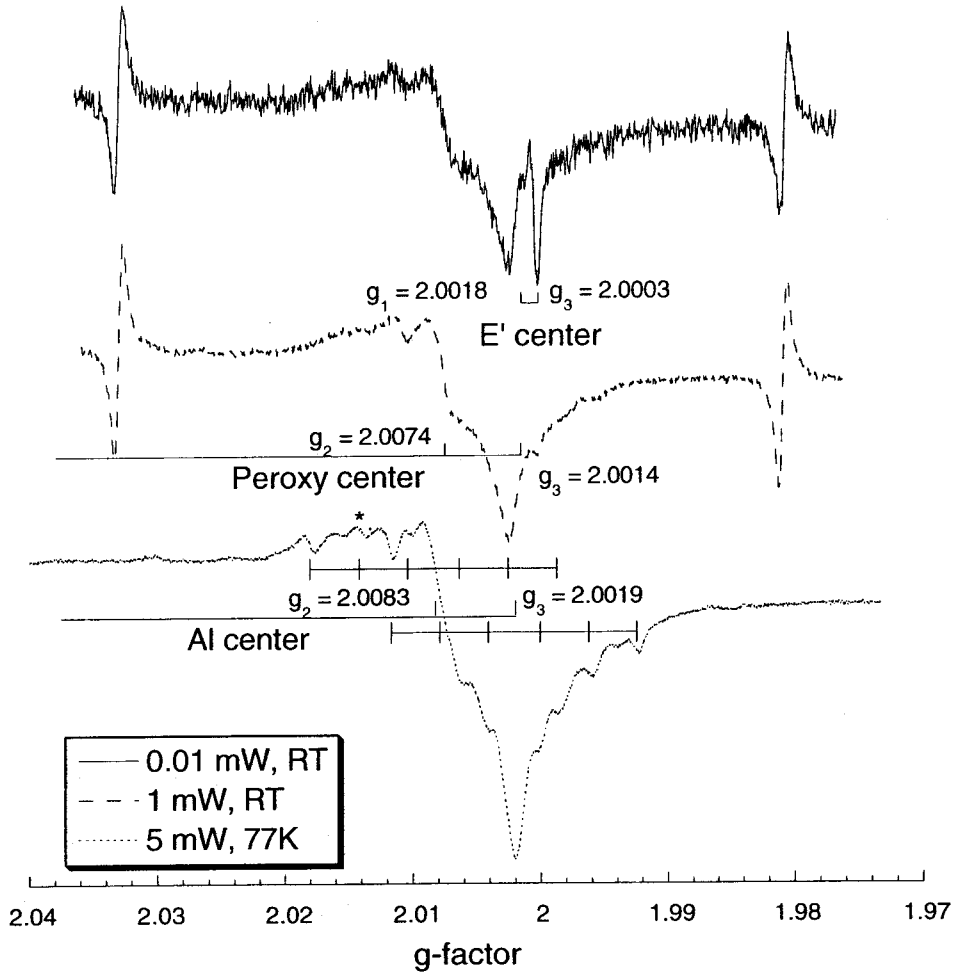

Figure A-5. ESR spectra around $g = 2.0$.

lot of SiO_2.

(i) Thermal history of the stone tool

ESR spectra of four samples measured at magnetic fields of between 0 and 500 mT are shown in Figure A-4. The ESR spectrum of the yellow part (Figure A-4-a) has large signals of radiation-induced centers around $g = 2.0$. The signals at the same g-value in the spectrum of the red part (Figure A-4-b) are smaller than that of the yellow part. The spectrum of the sample heated at 450 °C for 15 minutes (Figure A-4-c) is quite similar to that of the red part. These three spectra indicate that more defects in the red part might be annealed out than those in the yellow part due to heating.

The spectrum of the sample heated at 600 °C (Figure A-4-d) is different from the others. It has a large signal at $g = 4.3$ which is due to Fe^{3+} ion in an orthorhombic environment because a significant lattice change might occur at a temperature between 450 °C and 600 °C. It may be concluded that the stone was not heated to more than 600 °C. In addition, the color of the material changed from yellow to red at 240 °C, probably due to formation of hematite (Fe_2O_3) following dehydration.

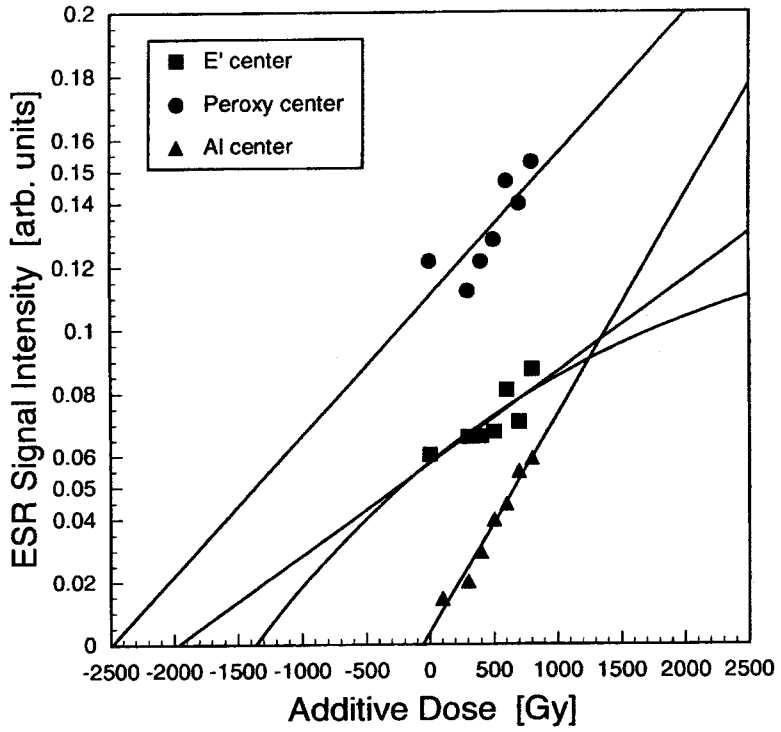

Figure A-6. The DRC of the radiation-induced centers.

I conclude that the red part of the stone tool was heated at a temperature between 240 °C and 600 °C and that the yellow part was not heated or heated below 240 °C. This means that only the red part can be used for ESR dating.

(ii) Dating of the burnt stone tool

ESR spectra of the yellow part around $g = 2.0$, measured at different microwave powers and temperatures, are shown in Figure A-5. ESR signals of the E', peroxy and Al centers in quartz were identified. The Al center has a hyperfine splitting because its nuclear spin, I is 5/2.

Figure A-6 shows growth curves for the E' center, the peroxy center and the second peak of the Al center using the additive dose method on the red part of the stone tool. The peak height was used for evaluation of signal intensity. The equivalent dose, DE was obtained by fitting with a linear or a saturation function and the results are shown in Table A-1. The equivalent dose for the peroxy center is largest and that for the Al center is much smaller than the others. The error in the equivalent doses is very large because only a few milligrams of the red part were available.

An analysis by γ-ray spectroscopy shows that the contents of ^{238}U, ^{232}Th and ^{40}K in the stone tool are 1.31 ± 0.05 ppm, 3.99 ± 0.14 ppm and 4.69 ± 0.03 %, respectively, after the shape of the stone tool was taken into account to calibrate the counting efficiency of the Ge detector. An inner dose rate for the stone tool was calculated to be 5.6 mGy/a, assuming radioactive equilibrium of the 238U-series nuclides and an a-ray defect formation efficiency (k-value) of 0.1 (Grun 1989; Ikeya 1993). An annual dose of

3.1 ± 0.5 mGy/a at the edge where the red part had been sampled was calculated, considering the shape of the stone tool and a dose rate of the soil surrounding the stone tool of 0.5 mGy/a (Hashimoto *et al.* 1993). A cosmic dose rate of 0.26 mGy/a is included in the calculation of the dose rate (Hashimoto *et al.* 1993). The converted age for each center is summarized in Table A-1.

Isochronal annealing experiments with 10 kGy-irradiated sample were carried out to study the thermal stability of E', peroxy and Al center in this sample. The results are shown in Figure A-7. Figure A-7-a shows that the E' center was annealed around 360 °C. Figure A-7-b shows that the peroxy center was overlapped with broad signals (g = 2.0086) which were not destroyed below 450 °C, and the age for the peroxy center may be overestimated. Figure A-7-c shows that the Al center in the stone tool is less stable than that in crystalline quartz studied by Toyoda and Ikeya (1991). That may be the reason why the equivalent dose for the Al center is relatively small and the estimated age in this case is too young. Therefore, only the E' center can be used for ESR dating but it is noted that the estimated age is just a maximum because it is not certain that the heating temperature was sufficiently high for the E' center in the stone tool to be destroyed completely at the time of heating.

(iii) A trial of dating burnt material using unburnt material by ESR

In this study, a large amount of unburnt material and only a small amount of burnt material are available for ESR measurement. Assuming that the formation efficiency of unburnt material which is heated in a laboratory at a particular temperature is the same as that of the burnt material, we can obtain a growth curve starting from the origin as a model for the original growth curve in the burnt material. Theoretically, the equivalent dose of the burnt material can be estimated using both the ESR signal intensity of the burnt material without any irradiation and the growth curve of the unburnt material heated in the laboratory. The deviation on the growth curve could get much smaller because enough material can be used for ESR measurement.

This method was applied to the unburnt yellow material. The material was heated at 450 °C for 30 minutes to anneal the E' center completely. A new growth curve for the E' center from the origin was obtained with the ordinary additive dose method and is shown in Figure A-8. Most data points are nearly on a line and the slope of the line is almost the same as that of the linear growth curve using the red part

Table A-1. The results of ESR dating.

ESR signal	DE (Gy)	Age (ka)	Fitting function
E' center	1970 ± 740	340-1040	Linear function
	1340 ± 460	240-690	Saturation function
Peroxy center	2490 ± 980	420-1330	Linear function
Al center	54 ± 44	2.8-38	Linear function
E' center	1940 ± 70	520-770	Regeneration method

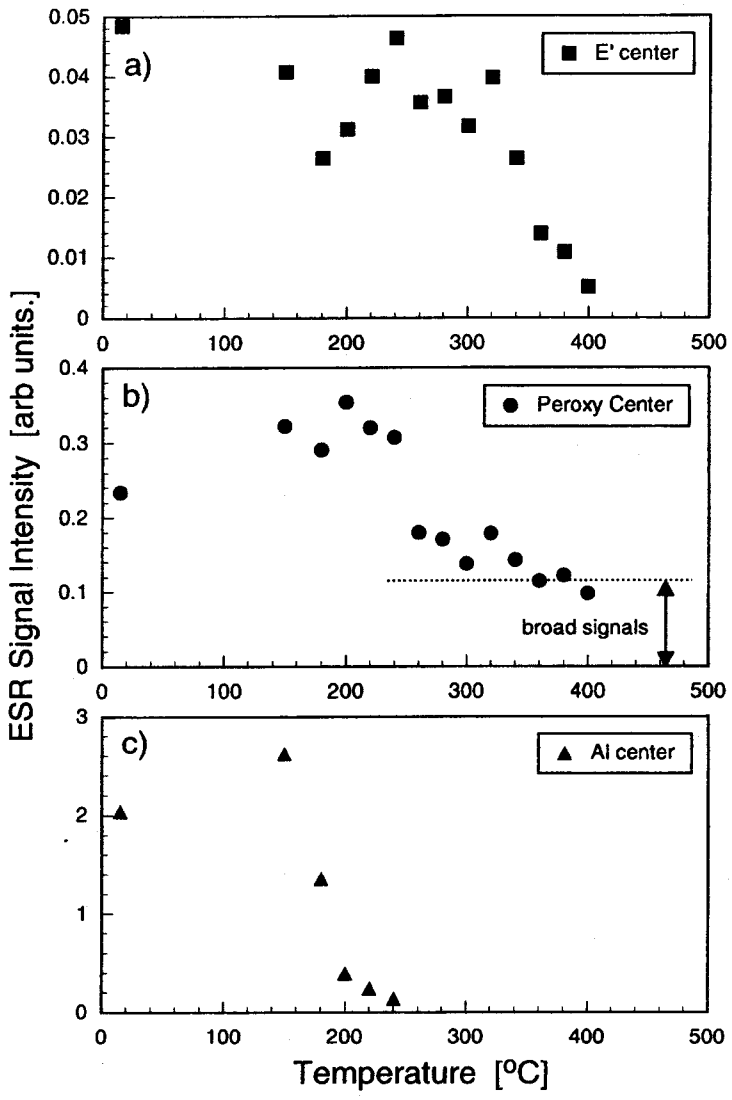

Figure A-7. Isochronal annealing experiments for the centers.

of the sample. This may mean that the signal intensity of the red part is in the linear region of the growth curve. In this work, all data points were used to find an average of the equivalent dose. The equivalent dose for the E' center was obtained as 1940 ± 70 Gy. An estimated maximum age was calculated as 520-770 ka. The error is mainly due to uncertainty of the dose rate at the edge of the stone tool.

A.4 Summary

ESR signals of Fe^{3+} ion and radiation-induced centers and the color change of the material indicated that the red part of the stone was heated at a temperature between 240 °C and 600 °C and that the yellow part was heated below 240 °C or was not heated. Only the red part can be used for ESR dating, but it must be remembered that an age estimated by ESR is a maximum age because heating temperatures in the past are not known exactly and it is not certain that the signal intensity was zero when the radiation-induced centers started to accumulate in the SiO_2.

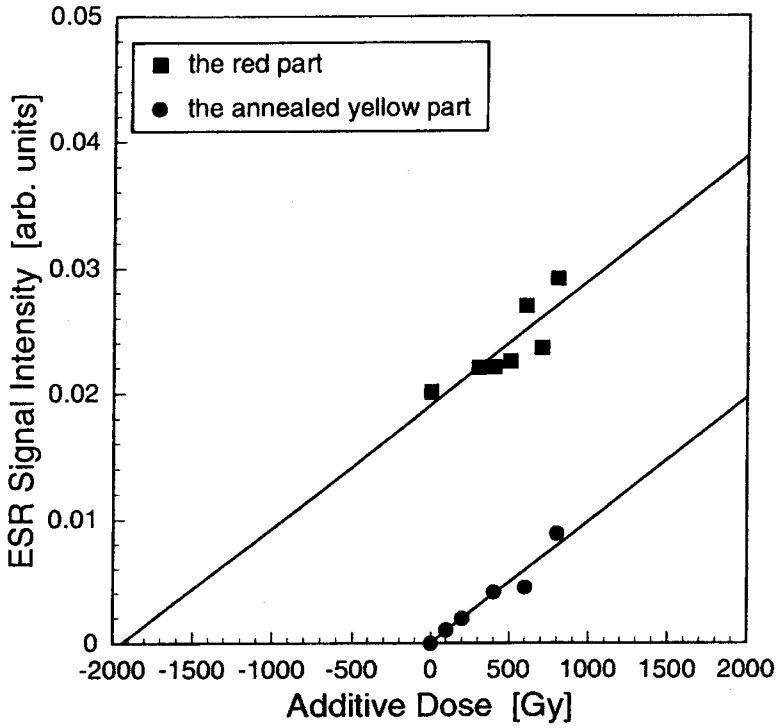

Figure A-8. Regenerated DRC.

The age of the red part of the burnt stone, 340-1040 ka, was estimated by ESR dating for the E' center. The difficulty of calculation of the dose rate at the edge of the stone and the small amount of burnt material caused huge errors in the age calculation. Assuming that the growth curve which was obtained using the unburnt material heated in a laboratory could be used to date the burnt part, the age might be 520-770 ka. This age is quite similar to the age of the marker-tephras dated by ESR, TL and paleomagnetism (Hirooka *et al.* 1995; Toyoda 1993; Nagatomo *et al.* 1995).

The age obtained by ESR is not necessarily the age of the stone tool or of human activity but the age of the burning event. This ambiguity cannot be avoided using only ESR studies. However, if the estimated age is a real archaeological age, the result may support that the ancient men used fire in a paleolithic age in Japan, and this stone tool may be the oldest in Japan.

APPENDIX B

Other topics

These are useful table and list for the *g*-shift calculation.

B.1 D_{2h} symmetry

D_{2h}	E	C_{2z}	C_{2y}	C_{2x}	i	σ_{xy}	σ_{zx}	σ_{yz}
A_g	1	1	1	1	1	1	1	1
B_{1g}	1	1	-1	-1	1	1	-1	-1
B_{2g}	1	-1	1	-1	1	-1	1	-1
B_{3g}	1	-1	-1	1	1	-1	-1	1
A_u	1	1	1	1	-1	-1	-1	-1
B_{1u}	1	1	-1	-1	-1	-1	1	1
B_{2u}	1	-1	1	-1	-1	1	-1	1
B_{3u}	1	-1	-1	1	-1	1	1	-1

Symmetry of points

(0,0,0) at the origin	A_g
(x,0,0) in the x-axis	A_g, B_{3u}
(0,y,0) in the y-axis	A_g, B_{2u}
(0,0,z) in the z-axis	A_g, B_{1u}
(x,y,0) on the xy-plane	A_g, B_{1g}, B_{2u}, B_{3u}
(0,y,z) on the yz-plane	A_g, B_{1u}, B_{2u}, B_{3g}
(x,0,z) on the zx-plane	A_g, B_{1u}, B_{2g}, B_{3u}
(x,y,z) in space	all

Atomic orbitals

s	A_g	d_{xy}	B_{1g}
p_x	B_{3u}	d_{yz}	B_{3g}
p_y	B_{2u}	d_{zx}	B_{2g}
p_z	B_{1u}	d_{x2-y2}	A_g
		d_{3z2-r2}	A_g

B.1 Table of *p*- and *d*-orbital functions with orbital angular momentum

	p_x^m	p_y^m	p_z^m
$< p_i^t \mid L_x \mid p_j^m >$			
p_x^t	0	$i < p_x^t \mid p_z^m >$	$-i < p_x^t \mid p_y^m >$
p_y^t	0	$i < p_y^t \mid p_z^m >$	$-i < p_y^t \mid p_y^m >$
p_z^t	0	$i < p_z^t \mid p_z^m >$	$-i < p_z^t \mid p_y^m >$
$< p_i^t \mid L_y \mid p_j^m >$			
p_x^t	$-i < p_x^t \mid p_z^m >$	0	$i < p_x^t \mid p_x^m >$
p_y^t	$-i < p_y^t \mid p_z^m >$	0	$i < p_y^t \mid p_x^m >$
p_z^t	$-i < p_z^t \mid p_z^m >$	0	$i < p_z^t \mid p_x^m >$
$< p_i^t \mid L_z \mid p_j^m >$			
p_x^t	$i < p_x^t \mid p_y^m >$	$-i < p_x^t \mid p_x^m >$	0
p_y^t	$i < p_y^t \mid p_y^m >$	$-i < p_y^t \mid p_x^m >$	0
p_z^t	$i < p_z^t \mid p_y^m >$	$-i < p_z^t \mid p_x^m >$	0

$< d^t_{ij} \mid L_x \mid d^m_{kl} >$	d^m_{xy}	d^m_{yz}	d^m_{zx}	$d^m_{x^2-y^2}$	$d^m_{z^2}$
d^t_{xy}	$i < d^t_{xy} \mid d^m_{zx} >$	$\sqrt{3}i < d^t_{xy} \mid d^m_{z^2} > + i < d^t_{xy} \mid d^m_{x^2-y^2} >$	$-i < d^t_{xy} \mid d^m_{xy} >$	$-i < d^t_{xy} \mid d^m_{yz} >$	$-\sqrt{3}i < d^t_{xy} \mid d^m_{yz} >$
d^t_{yz}	$i < d^t_{yz} \mid d^m_{xz} >$	$\sqrt{3}i < d^t_{yz} \mid d^m_{z^2} > + i < d^t_{yz} \mid d^m_{x^2-y^2} >$	$-i < d^t_{yz} \mid d^m_{xy} >$	$-i < d^t_{yz} \mid d^m_{yz} >$	$-\sqrt{3}i < d^t_{yz} \mid d^m_{yz} >$
d^t_{zx}	$i < d^t_{zx} \mid d^m_{yz} >$	$\sqrt{3}i < d^t_{zx} \mid d^m_{z^2} > + i < d^t_{zx} \mid d^m_{x^2-y^2} >$	$-i < d^t_{zx} \mid d^m_{xy} >$	$-i < d^t_{zx} \mid d^m_{yz} >$	$-\sqrt{3}i < d^t_{zx} \mid d^m_{yz} >$
$d^t_{x^2-y^2}$	$i < d^t_{x^2-y^2} \mid d^m_{zx} >$	$\sqrt{3}i < d^t_{x^2-y^2} \mid d^m_{z^2} > + i < d^t_{x^2-y^2} \mid d^m_{x^2-y^2} >$	$-i < d^t_{x^2-y^2} \mid d^m_{xy} >$	$-i < d^t_{x^2-y^2} \mid d^m_{yz} >$	$-\sqrt{3}i < d^t_{x^2-y^2} \mid d^m_{yz} >$
$d^t_{z^2}$	$i < d^t_{z^2} \mid d^m_{zx} >$	$\sqrt{3}i < d^t_{z^2} \mid d^m_{z^2} > + i < d^t_{z^2} \mid d^m_{x^2-y^2} >$	$-i < d^t_{z^2} \mid d^m_{xy} >$	$-i < d^t_{z^2} \mid d^m_{yz} >$	$-\sqrt{3}i < d^t_{z^2} \mid d^m_{yz} >$
$< d^t_{ij} \mid L_y \mid d^m_{kl} >$					
d^t_{xy}	$-i < d^t_{xy} \mid d^m_{yz} >$	$i < d^t_{xy} \mid d^m_{xy} >$	$-\sqrt{3}i < d^t_{xy} \mid d^m_{z^2} > +i < d^t_{xy} \mid d^m_{x^2-y^2} >$	$-i < d^t_{xy} \mid d^m_{zx} >$	$\sqrt{3}i < d^t_{xy} \mid d^m_{zx} >$
d^t_{yz}	$-i < d^t_{yz} \mid d^m_{xz} >$	$i < d^t_{yz} \mid d^m_{xy} >$	$-\sqrt{3}i < d^t_{yz} \mid d^m_{z^2} > +i < d^t_{yz} \mid d^m_{x^2-y^2} >$	$-i < d^t_{yz} \mid d^m_{zx} >$	$\sqrt{3}i < d^t_{yz} \mid d^m_{xz} >$
d^t_{zx}	$-i < d^t_{zx} \mid d^m_{yz} >$	$i < d^t_{zx} \mid d^m_{xy} >$	$-\sqrt{3}i < d^t_{zx} \mid d^m_{z^2} > +i < d^t_{zx} \mid d^m_{x^2-y^2} >$	$-i < d^t_{zx} \mid d^m_{zx} >$	$\sqrt{3}i < d^t_{zx} \mid d^m_{zx} >$
$d^t_{x^2-y^2}$	$-i < d^t_{x^2-y^2} \mid d^m_{yz} >$	$i < d^t_{x^2-y^2} \mid d^m_{xy} >$	$-\sqrt{3}i < d^t_{x^2-y^2} \mid d^m_{z^2} > +i < d^t_{x^2-y^2} \mid d^m_{x^2-y^2} >$	$-i < d^t_{x^2-y^2} \mid d^m_{zx} >$	$\sqrt{3}i < d^t_{x^2-y^2} \mid d^m_{zx} >$
$d^t_{z^2}$	$-i < d^t_{z^2} \mid d^m_{yz} >$	$i < d^t_{z^2} \mid d^m_{xy} >$	$-\sqrt{3}i < d^t_{z^2} \mid d^m_{z^2} > +i < d^t_{z^2} \mid d^m_{x^2-y^2} >$	$-i < d^t_{z^2} \mid d^m_{zx} >$	$\sqrt{3}i < d^t_{z^2} \mid d^m_{zx} >$
$< d^t_{ij} \mid L_z \mid d^m_{kl} >$					
d^t_{xy}	$-2i < d^t_{xy} \mid d^m_{x^2-y^2} >$	$-i < d^t_{xy} \mid d^m_{xz} >$	$i < d^t_{xy} \mid d^m_{yz} >$	$2i < d^t_{xy} \mid d^m_{xy} >$	0
d^t_{yz}	$-2i < d^t_{yz} \mid d^m_{x^2-y^2} >$	$-i < d^t_{yz} \mid d^m_{yz} >$	$i < d^t_{yz} \mid d^m_{xz} >$	$2i < d^t_{yz} \mid d^m_{xy} >$	0
d^t_{zx}	$-2i < d^t_{zx} \mid d^m_{x^2-y^2} >$	$-i < d^t_{zx} \mid d^m_{zx} >$	$i < d^t_{zx} \mid d^m_{yz} >$	$2i < d^t_{zx} \mid d^m_{xy} >$	0
$d^t_{x^2-y^2}$	$-2i < d^t_{x^2-y^2} \mid d^m_{x^2-y^2} >$	$-i < d^t_{x^2-y^2} \mid d^m_{zx} >$	$i < d^t_{x^2-y^2} \mid d^m_{yz} >$	$2i < d^t_{x^2-y^2} \mid d^m_{xy} >$	0
$d^t_{z^2}$	$-2i < d^t_{z^2} \mid d^m_{x^2-y^2} >$	$-i < d^t_{z^2} \mid d^m_{zx} >$	$i < d^t_{z^2} \mid d^m_{yz} >$	$2i < d^t_{z^2} \mid d^m_{xy} >$	0

LIST OF PUBLICATIONS

Refereed Papers in Journals

1. Ikeya, M., Tani, A. & Yamanaka, C. (1995) Electron spin resonance isochrone dating of fracture age: grain-size dependence of dose rates for fault gouge. *Jpn. J. Appl. Phys.* **34**, L334-L337.
2. Tani, A., Kohno, H., Yamanaka, C. & Ikeya, M. (1996) ESR dating of geological fault with a new isochrone method: granite fractured on the earthquake in 1995. *Appl. Radiat. Isot.* **47**, 1423-1426.
3. Bartoll, J., Tani, A., Ikeya, M. & Inada, T. (1996) ESR investigation of burnt soil. *Appl. Magn. Reson.* **11**, 577-586.
4. Oka, T., Grün, R., Tani, A., Yamanaka, C., Ikeya, M. & Huang, H.P. (1997) ESR microscopy of fossil teeth. *Radiat. Meas.* **27**, 331-337.
5. Ikeya, M., Ochiai, H. & Tani, A. (1997) Total dose (TD) formula for uranium saturation-uptake model for ESR and TL dating. *Radiat. Meas.* **27**, 339-343.
6. Grün, R., Kohno, H., Tani, A., Yamanaka, C., Ikeya, M. & Huang, H.P. (1997) Pulsed ESR measurements on fossil teeth. *Radiat. Meas.* **27**, 425-431.
7. Tani, A., Bartoll, J., Ikeya, M., Komura, K., Kajiwara, H., Fujimura, S., Kamada, T. & Yokoyama, Y. (1997) ESR study of thermal history and dating of a stone tool. Appl. *Magn. Reson.* **13**, 561-569.
8. Ikeya, M., Takaki, S., Matsumoto, H., Tani, A. & Komatsu, T. (1997) Pulsed charge model of fault behavior producing seismic electric signals (SES). *J. Circuits, Systems and Computers* **7**, 153-164.
9. Ikeya, M. & Tani, A. (1997) Dating of ancient lithic tool factory and geological fault: electron spin resonance (ESR) of fractured grains. *Anthropos* **13**, 65-69.
10. Bartoll, J. & Tani, A. (1998) Thermal history of archaeological objects, studied by electron spin resonance. *Naturwissenschaften* **85**, 474-481.
11. Grün, R., Tani, A., Gurbanov, A., Koshchug, D., Williams, I. & Braun, J. (1999) A new method for the estimation of cooling and denudation rates using paramagnetic centers in quartz: a case study on the Eldzhurtinskiy Granite, Caucasus. *J. Geophys. Res.* **104**, 17531-17549.

Refereed Papers in Journals (in Press)

12. Tani, A. & Ikeya, M. (in press) ESR study of a new electron centre in synthesised stishovite, a high-pressure phase of SiO_2. *Appl. Radiat. Isot.*

Non-Refereed Papers

13. Tani, A., Yamanaka, C. & Ikeya, M. (1995) ESR dating of Rokko fault gouge: new method considering the quality factor of a radiation. *Isotope News* no. 5, 11-13 (in Japanese).
14. Tani, A., Bartoll, J., Ikeya, M., Inokuchi, H., Morinaga, H. & Inada, T. (1996) Scientific investigation of an ancient heated site by ESR. *The Proceeding on the 4th Meeting of Development of Advanced Archaeological Prospecting Methods* 116-120 (in Japanese).

15. Tani, A., Bartoll, J., Ikeya, M., Komura, K. & Kajiwara, H. (1996) ESR study of thermal history and dating on a burnt stone. *Monthly Ionics* **22**, 3-7 (in Japanese).
16. Tani, A. & Ikeya, M. (1996) ESR dating. *Chikyu Monthly* **18**, 326-330 (in Japanese).
17. Tani, A., Grün, R., Gurbanov, A. & Koshchug, D. (1999) Thermal history of intrusive granite: another application of ESR to quaternary geology. *Chikyu Monthly Special Ed.* **26**, 88-94 (in Japanese).
18. Tani, A. (1999) Molecular orbital and g-tensor calculations of paramagnetic centers of stishovite by DV-Xα method. *Bull. Soc. Discrete Variational Xα* **12**, 71-75 (in Japanese).
19. Tani, A., Matsumoto, H. & Ikeya, M. (2000) A survey of thermal disturbance on the GSJ Nojima core sample by electron spin resonance (ESR). *The Proceeding of the Workshop on Nojima Core and Borehole Data Analysis* xx-xx.

BIBLIOGRAPHY

Adachi, H. (1991) *Introduction of quantum material chemistry: approach by the DV-Xa method.* Tokyo, Sankyo Press. (ISBN: 4-7827-0261-2).

Adachi, H., Kowada, Y., Tanaka, I., Nakamatsu, H. & Mizuno, M. (1998) *Introduction to electronic state calculation by DV-Xa molecular orbital method.* Tokyo, Sankyo Press. (ISBN: 4-7827-0392-9).

Adachi, H., Tsukuda, M. & Satoko, C. (1978) Discrete variational Xa cluster calculations. I. application to metal clusters. *J. Phys. Soc. Jpn.* **45**, 875-883.

Aitken, M.J. (1985) *Thermoluminescence dating.* London, Academic Press. (ISBN: .

Aitken, M.J. (1990) *Science-based dating in archaeology.* New York, Longman. (ISBN: 0-582-49309-9).

Aitken, M.J. (1998) *An introduction to optical dating: the dating of Quarternary sediments by the use of photon-stimulated luminescence.* New York, Oxford University Press. (ISBN: 0-19-854092-2).

Akaogi, M., Yusa, H., Shiraishi, K. & Suzuki, T. (1995) Thermodynamic properties of a-quartz, coesite, and stishovite and equilibrium phase relations at high pressures and high temperatures. *J. Geophys. Res.* **100**, 22337-22347.

Akizuki, M. (1993) *Crystal in mountain: mineralogy of rock crystal.* Tokyo, Shokabo. (ISBN: 4-7853-8587-1).

Arends, J., Dekker, A.J. & Perdok, W.G. (1963) . *Phys. Status Solidi B* **3**, 2275.

Bartoll, J., Tani, A., Ikeya, M. & Inada, T. (1996) ESR investigations of burnt soil. *Appl. Magn. Reson.* **11**, 577-586.

Bohlen, S.R. & Boettcher, A.L. (1982) The quartz-coesite transformation: a precise determination and the effects fo other components. *J. Geophys. Res.* **87**, 7073-7078.

Borsuk, A.M. (1979) *The mesozoic and cenozoic magmatic formations of the Great Caucasus.* Moscow, Akad. Nauk SSSR. (ISBN: .

Chao, E.C.T., Fahey, J.J., Littler, J. & Milton, D.J. (1962) Stishovite, SiO_2, a very high pressrue new mineral from meteor crater, Arizona. *J. Geophys. Res.* **67**, 419-421.

Chen, Y., Feng, J., Gao, J. & Grün, R. (1997) Investigation of the potential use of ESR signals in quartz for palaeothermometry. *Quat. Sci. Rev.* **16**, 495-499.

Chester, P.F. (1961) Electron spin resonance in semiconducting rutile. *J. Appl. Phys.* **32**, 2233-2236.

Daniels, F., Boyd, C.A. & Saunders, D.F. (1953) Thermoluminescence as a research tool. *Science* **117**, 343-349.

Devine, R.A.B. & Hübner, K. (1989) Radiation-induced defects in dense phases of crystalline and amorphous SiO_2. *Phys. Rev. B* **40**, 7281-7283.

Dodson, M., H. (1973) Closure temperature in cooling geochronological and petrological systems. *Contr. Min. Petrol.* **40**, 259-274.

Faure, G. (1986) *Principles of isotope geology.* New York, John Wiley & Sons. (ISBN: 0-471-86412-9).

Foresman, J.B. & Frisch, Æ. (1996) *Exploring chemistry with electronic structure methods.* Pittsburgh, Gaussian, Inc. (ISBN: 0-9636769-3-8).

Fukuchi, T. (1992) ESR studies for absolute dating of fault movements. *J. Geol. Soc. London* **149**, 265-272.

Garrison, E.G., Rowlett, R.M., Cowan, D.L. & Holroyd, L.V. (1981) ESR dating of ancient flints. *Nature* **290**, 44-45.

Gazis, C.A., Lanphere, M., Taylor, H.P., Jr. & Gurbanov, A. (1995) $^{40}Ar/^{39}Ar$ and $^{18}O/^{16}O$ studies of the Chegem ash-flow caldera and the Eldjurta Granite: cooling of two late Pliocene igneous bodies in the Greater Caucasus Mountaines, Russia. *Earth Planet. Sci. Lett.* **134**, 377-391.

Gobsch, G., Haberlandt, H., Weckner, H.-J. & Reinhold, J. (1978) Calculation of the *g*-tensor and

^{29}Si hyperfine tensors of the E'_1 center in silicon dioxide. *Phys. Status Solidi B* **90**, 309-317.

Griffiths, D.R., Seeley, N.J., Chandra, H. & Symons, M.C.R. (1983) ESR dating of heated chert. *PACT* **9**, 399-409.

Griscom, D.L. (1979) E' center in glassy SiO_2: Microwave saturation properties and confirmation of the primary ^{29}Si hyperfine structure. *Phys. Rev. B* **20**, 1823-1834.

Griscom, D.L. (1980) E' center in glassy SiO_2: ^{17}O, ^{1}H, and "very weak" ^{29}Si superhyperfine structure. *Phys. Rev. B* **22**, 4192-4202.

Grun, R. (1989) Electron spin resonance (ESR) dating. *Quat. Int.* **1**, 65-109.

Hashimoto, T., Koyanagi, A., Yokosaka, K., Hayashi, Y. & Sotobayashi, T. (1986) Thermoluminescence color images from quartz of beach sands. *Geochem. J.* **20**, 111-118.

Hashimoto, T., Notoya, S. & Shirai, N. (1993). Red thermoluminescence dating of Takamori pre-historical sites using quartz inclusion method. In *Takamori Site II*, Tagajo, Tohoku Historical Museum, 43-51.

Hess, J.C., Lippolt, H.J., Gurbanov, A.G. & Michalski, I. (1993) The cooling history of the late Pliocene Eldzhurtinskiy garanite (Caucasus, Russia) and the thermochronological potential of grain-size/age relationships. *Earth Planet. Sci. Lett.* **117**, 393-406.

Hirai, M. (1997) *Effects of radiation and annealing on E' center in crushed quartz.* Ph. D., Osaka University, Toyonaka, JAPAN.

Hirai, M. & Ikeya, M. (1998) Narrowing of ESR spectra of the E' center in crushed quartz by thermal annealing. *Phys. Status Solidi B* **209**, 449-462.

Hirai, M. & Matsumoto, H. (1999) ESR of the E' center in crushed quartz (personal communication).

Hirooka, K., Tanaka, A. & Yamada, A. (1995). Magnetostratigraphic study of the middle Pleistocene sediments at Kuranosawa, Miyagi, northeast Japan. In *Takamori Site III*, Tagajo, Tohoku Historical Museum, 33-40.

Hochstrasser, G. & Antonini, J.F. (1972) . *Surface Science* **32**, 644.

Huntley, D.J., Godfrey-Smith, D.I. & Thewalt, M.L.W. (1985) Optical dating of sediments. *Nature* **313**, 105-107.

Hutt, G., Jaek, I. & Tchonka, J. (1988) Optical dating: K-feldspars optical response stimulation spectra. *Quat. Sci. Rev.* **7**, 381-385.

Ikeya, M. (1975) Dating a stalactite by electron spin resonance. *Nature* **225**, 48-50.

Ikeya, M. (1993) *New applications of electron spin resonance: dating, dosimetry and microscopy.* Singapore, World Scientific. (ISBN: 981-02-1199-6).

Ikeya, M., Miki, T. & Tanaka, K. (1982) Dating of faults by electron spin resonance on intra-fault material. *Science* **215**, 1392-1393.

Ikeya, M. & Toyoda, S. (1991) Thermal effect in metamorphic rock around an intrusion zone with ESR studies. *Appl. Magn. Reson.* **2**, 69-91.

Imai, N., Shimokawa, K. & Hirota, M. (1985) ESR dating of volcanic ash. *Nature* **314**, 81-83.

Isoya, J., Tennant, W.C. & Weil, J.A. (1988) EPR of the TiO_4/Li center in crystalline quartz. *J. Magn. Reson.* **79**, 90-98.

Ito, H., Kuwahara, Y., Miyazaki, T., Nishizawa, O., Kiguchi, T., Fujimoto, K., Ohtani, T., Tanaka, H., Higuchi, T., Agar, S., Brie, A. & Yamamoto, H. (1996) Structure and physical properties of the Nojima Fault by the active fault drilling. *BUTSURI-TANSA* **49**, 522-535.

Jani, M.G., Bossoli, R.B. & Halliburton, L.E. (1983) Further characterization of the E'_1 center in crystalline SiO_2. *Phys. Rev. B* **27**, 2285-2293.

Kaneoka, I. (1998) *Numerical dating: from a decade to 46 hundred million yeas ago.* Tokyo, University of Tokyo Press. (ISBN: 4-13-060722-7).

Kanosue, K., Hirai, M. & Ikeya, M. (1996) Preliminary study for future ESR dating of solid SO_2. *Appl. Radiat. Isot.* **47**, 1433-1436.

Kingsbury, P.I., Jr., Ohlsen, W.D. & Johnson, O.W. (1968) Defects in rutile. I. Electron paramagnetic resonance of interstitiall doped n-type rutile. *Phys. Rev.* **175**, 1091-1098.

Komura, K. & Yamazaki, S. (1996). Ogoya underground laboratory for the measurement of extremely low-level radioactivity. In *Todai International Symposium on Cosmochronology and*

Isotope Geoscience, Tokyo, Tokyo University, 119-122.

Li, Y.P. & Ching, W.Y. (1985) Band structures of all polycrystalline forms of silicon dioxide. *Physcal Review B* **31**, 2172-2179.

Marfunin, A.S. (1979) *Spectroscopy, luminescence and radiation cetners in minerals*. Berline, Springer-Verlag. (ISBN: 3-540-09070-3).

McKeever, S.W.S. (1985) *Thermoluminescence of solids*. Cambridge, Cambridge University Press. (ISBN: 0-521-24520-6).

McMorris, D.W. (1970) ESR detection of fossil alpha damage in quartz,. *Nature* **226**, 146-148.

McMorris, D.W. (1971) Impurity color centers in quartz and trapped electron dating: Electron spin resonance, thermoluminesscence studies. *J. Geophys. Res.* **76**, 7875-7887.

Melnikov, P.V., Moiseev, B.M. & Shekhvatov, D.B. (1989) Natural radiatoin parameters of Al-center in quartz. *Geokhimiya* 7, 1015-1020.

Moiseyev, B.M. & Rakov, L.T. (1977) Paleodosimetry properties of E' centers in quartz. *Dokladi Akad. Nauk SSSR* **223**, 679-683.

Nagatomo, T., Uno, M. & Fujimoto, K. (1995). TL age of a tephra layer: Tm-1. In *Takamori Site III*, Tagajyo, Tohoku Historical Museum, 17-21.

Navrotsky, A. (1994) *Physics and chemistry of earth materials*. Cambridge, Cambridge University Press. (ISBN: 0-521-35378-5).

Norizawa, K., Kanosue, K. & Ikeya, M. (2000) Radiation effects of dry ice - models for a bump in Arrhenius curve --. *Applied Radiation and Isotopes* **xx**, xx-xx.

Nuttall, R.H.D. & Weil, J.A. (1981) The magnetic properties of the oxygen-hole aluminum centers in crystalline SiO_2. I. $[AlO_4]^0$. *Can. J. Phys.* **59**, 1696-1708.

Odom, A.L. & Rink, W.J. (1988) Natural accumulation of Schottky-Frenkel defects: Implications for a quartz geochronometer. *Geology* **17**, 55-58.

Ogoh, K. (1996c) *Radiation-induced paramagnetic defects in coesite and stishovite, high pressure phases of SiO_2*. Ph. D., Osaka University, Toyonaka, JAPAN.

Ogoh, K., Takaki, S., Yamanaka, C., Ikeya, M. & Ito, E. (1996b) Thermoluminescence and electron spin resonance of atomic hydrogens in coesite and stishovite, high pressure phases of SiO_2. *J. Phys. Soc. Jpn.* **65**, 844-847.

Ogoh, K., Yamanaka, C., Ikeya, M. & Ito, E. (1995a) Hyperfine interaction of electron at oxygen vacancy with nearest and next-nearest ^{29}Si in high-pressure-phase SiO_2: Stishovite. *J. Phys. Soc. Jpn.* **64**, 4109-4112.

Ogoh, K., Yamanaka, C., Ikeya, M. & Ito, E. (1996a) Two-center model for radiation induced aluminum hole center in stishovite. *J. Phys. Chem. Solids* **57**, 85-88.

Ogoh, K., Yamanaka, C., Toyoda, S., Ikeya, M. & Ito, E. (1994) ESR studies on radiation induced defects in high pressure phase SiO_2. *Nucl. Instr. Meth. Phys. Res. B* **91**, 331-333.

Okada, M., Rinneberg, H., Weil, J.A. & Wright, P.M. (1971) EPR of Ti^{3+} centers in α-quartz. *Chem. Phys. Lett.* **11**, 275-276.

Porat, N. & Schwarcz, H.P. (1991) Use of signal subtraction methods in ESR dating of burned flint. *Nucl. Tracks Radiat. Meas.* **18**, 203-212.

Price, P.B. & Walker, R.M. (1962) Observation of fossile particle tracks in natural micas. *Nature* **196**, 732.

Rink, W.J. (1997) Electron spin resonance (ESR) dating and ESR applications in Quaternary science and archaeolmetry. *Raidat. Meas.* **27**, 975-10225.

Rinneberg, H. & Weil, J.A. (1972) EPR studies of Ti^{3+}-H^+ centers in X-irradiated α-quartz. *J. Chem. Phys.* **56**, 2019-2028.

Rodes, E. (1999) IRSL of quartz (personal communication).

Ross, N.L., Shu, J.-F., Hazen, R.M. & Gasparik, T. (1990) High-pressure crystal chemistry of stishovite. *Am. Min.* **75**, 739-747.

Rudra, J.K. & Fowler, W.B. (1987) Oxygen vacancy and the E'_1 cetner in crystalline SiO_2. *Phys. Rev. B* **35**, 8223-8230.

Silk, E.C.H. & Barnes, R.S. (1959) Examination of fission fragment tracks with an electron microscope. *Phil. Mag.* **4**, 970.

Soda, T. (1993). Tephrochronological study on Takamori site. In *Takamori Site II*, Tagajo, Tohoku Historical Museum, 25-37.

Stapelbroek, M., Griscom, D.L., Friebele, E.J. & Sigel, G.H., Jr. (1979) Oxygen-associated trapped-hole centers in high-purity fused silicas. *J. Non-Cryst. Solids* **32**, 313-326.

Stewart, J.J.P. (1989) . *J. Comp. Chem.* **10**, 209.

Stishov, S.M. & Popova, S.V. (1961) New dense polymorphic modification of silica. *Geokhimiya* **10**, 837-839.

Szabo, A. & Ostlund, N.S. (1982) *Modern quantum chemistry: Introduction to advanced electronic structure theory*, Macmillan Publishing. (ISBN: 0486691861).

Tani, A. (1997) *Application of electron spin resonance to archaeology*. Master, Osaka University, Toyonaka, JAPAN.

Tossell, J.A. & Vaughan, D.J. (1992) *Theoretical geochemistry: applications of quantum mechanics in the earth and mineral sciences*. New York, Oxford University Press. (ISBN: 0-19-504403-7).

Toyoda, S. (1992) *Production and decay characteristics of paramagnetic defects in quartz: Applications to ESR dating*. Ph. D., Osaka University, Toyonaka, JAPAN.

Toyoda, S. (1993). ESR dating applied to tephra layers associated with Takamori site. In *Takamori Site II*, Tagajo, Tohoku Historical Museum, 53-55.

Toyoda, S. & Ikeya, M. (1991) Thermal stabilities of paramagnetic defect and impurity centers in quartz: Basis for ESR dating of thermal history. *Geochem. J.* **25**, 437-445.

Toyoda, S., Ikeya, M., Dunnel, R.C. & McCutcheon, P.T. (1993a) The use of electron spin resonance (ESR) for the determination of prehistoric lithic heat treatment. *Appl. Radiat. Isot.* **44**, 227-231.

Toyoda, S., Kohno, H. & Ikeya, M. (1993b) . *Appl. Radiat. Isot.* **44**, 215.

Tsuchida, Y. & Yagi, T. (1989) A new, post-stishovite high-pressrue polymorph of silica. *Nature* **340**, 217-220.

Tsuchiyama, A. (1995) The thin section analysis of the stone tool (personal communication).

Ugumori, T. & Ikeya, M. (1980) Luminescence of $CaCO_3$ under N_2 laser excitation and application to archaeological dating. *Jpn. J. Appl. Phys.* **19**, 459-465.

Warashina, T., Higashimura, T. & Maeda, Y. (1981) Determination of the firing temperature of ancient pottery by means of ESR spectrometry. *Br. Mus. Occ. Pap.* **19**, 117-128.

Weil, J.A. (1971) Germanium-hydrogen-lithium center in α-quartz. *J. Chem. Phys.* **55**, 4685-4698.

Weil, J.A. (1984) A review of electron spin spectroscopy and its application to the study of paramagnetic defects in crystalline quartz. *Phys. Chem. Min.* **10**, 149.

West, J.K., West, D.J. & Hench, L.L. (1998) Molecular orbital models of AM1 and PM3 multi-ring silica clusters and their infrared spectra. *Phys. Chem. Glasses* **39**, 301-304.

Wintle, A.G. (1990) A review of current research on TL dating of loess. *Quat. Sci. Rev.* **9**, 385-397.

Xu, Y.-N. & Ching, W.Y. (1991) Electronic and optical properties of all polymorphic forms of silicon dioxide. *Phys. Rev. B* **44**, 11048-11059.

Yokoyama, Y. & Nguyen, H.V. (1981) Datation directe de l'Homme de Tautavel par la spectrometrie gamma nondestructive du crane humain fossil Arago XXI. *Comptes rendus a l'Academie des Science* **292**, 741-744.

Zhang, J., Li, B., Utsumi, W. & Liebermann, R.C. (1996) In situ X ray observations of the coesite-stishovite phase transition: reversed phase boundary and kinetics. *Phys. Chem. Min.* **23**, 1-10.